[redacted]

(NASA-CR-120615) LASER SPACE RENDEZVOUS AND DOCKING TRADEOFF Quarterly Progress Report, 8 Mar. - Dec. 31 1974 (United Aircraft Corp.) 134 p HC $5.75 CSCL 17I

N75-17546

Unclas
G3/32 12197

Norden

UA

DIVISION OF UNITED AIRCRAFT CORPORATION

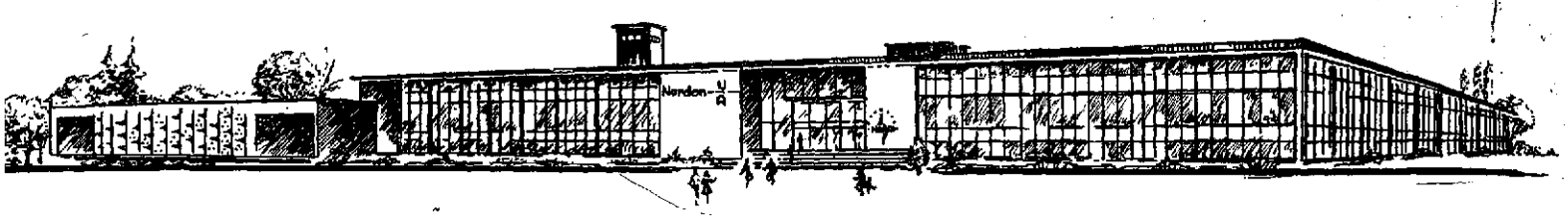

NORWALK, CONNECTICUT

LASER SPACE RENDEZVOUS AND DOCKING TRADEOFF

Report for the Period
8 March through 31 December 1974

1247 R 0004

Written by:

S. Adelman
S. Levinson
P. Raber
F. Weindling

Prepared for:

George C. Marshall Space Flight Center
Marshall Space Flight Center, Alabama
Contract No. NAS8-30738

Prepared by:

Norden Division of United Aircraft Corp
Norwalk, Connecticut

31 December 1974

ABSTRACT

Under contract NAS8-30738 with NASA/Marshall Space Flight Center (MSFC), Norden Division of United Aircraft Corporation has configured a spaceborne laser radar (LADAR) to meet the requirements for rendezvous and docking with a cooperative object in synchronous orbit. The ladar, configurated using existing pulsed CO_2 laser technology and a 1980 system technology baseline, is well suited for the envisioned Space Tug Missions.

The performance of a family of candidate ladars has been analyzed. Tradeoff studies as a function of size, weight, and power consumption have been accomplished. Maximum ranges of 50, 100, 200, and 300 nautical miles were considered.

The investigation supports the original contention that a rendezvous and docking ladar can be constructed to offer a cost effective and reliable solution to the envisioned space missions. In fact, the CO_2 ladar system offers distinct advantages over other candidate systems.

TABLE OF CONTENTS

LIST OF ILLUSTRATIONS

LIST OF ILLUSTRATIONS (Continued)

1. SUMMARY

1.1 Study Definition

The effort under this contract has concentrated on the following specific areas:

a. The identification of detailed requirements for rendezvous and docking with cooperative objects in geosynchronous or near geosynchronous orbit.

b. The configuration of a ladar which, utilizing a pulsed CO_2 laser as the transmitter, will be responsive to the Tug rendezvous and docking requirements.

c. The identification of the various technologies which are involved in the construction of the required system.

1.2 Study Results

In the course of configuring the rendezvous and docking ladar, as well as performing the necessary design and performance tradeoffs, progress has been as follows:

a. A baseline system which is responsive to the mission requirements has been configured and can be constructed with available or 1980 technology.

b. A reflective optical design has been configured and analyzed. The design permits rapid and efficient beam scanning required for search.

c. Search, acquisition, track, and docking are accomplished with a single four-quadrant detector array in the receiver.

d. The performance of the system has been calculated and tradeoff studies have been made to ensure that the system is optimum with respect to size, weight, and power consumption.

e. A measurements program has been designed which will permit the basic assumptions regarding target characteristics and their relation to the ladar parameters.

f. The performance of the pulsed CO_2 ladar has been compared to the equivalent performance of a GaAs laser transmitter using an image dissector as the receiver.

g. A novel technique for accomplishing the final docking maneuver has been developed. The unique technique permits complete autonomous docking to be accomplished easily and reliably.

Weights have been determined for the family of systems considered in the tradeoff analysis. The weight estimate for each of the main components and the total system weights are as follows.

CO_2 Ladar Weight Breakdown

MAIN COMPONENTS	WEIGHT (grams)
Case and Hardware	5800
Radiation Cooler	1360
Optical Train	536
Mounts	268
Local Oscillator	450
LOPS	100
Circuitry	1000
LVPS	425
Main Laser and Power Supply	
2 watt	2232
4 watt	2965
10 watt	4113
20 watt	5831
TOTAL SYSTEM WEIGHT	
2 watt	12,171
4 watt	12,904
10 watt	14,052
20 watt	15,770

2. SYSTEM REQUIREMENT

2.1 Mission Definition

The CO_2 rendezvous ladar that is being configured under the present contract is intended to supply control inputs to a space vehicle in order to permit autonomous rendezvous and docking with a cooperative object in geosynchronous or near geosynchronous orbit. In order to provide a meaningful interface with the space vehicle and its related avionics, the functional capabilities of the ladar are broken down into:

a. Acquisition
b. Track
c. Docking

2.1.1 Acquisition

The ladar will be directed to the general location of the target, and will initiate a search pattern that will have a sufficiently high probability of intercepting the target. The ladar will have the capability of being directed to any point within a 30 by 30° sector with respect to its axis on the spacecraft, and will scan a 5 by 5° pattern in 10 seconds, assuming a range uncertainty of 5% of the maximum range.

2.1.2 Track

The target will be directed and tracked in angle and range with sufficient accuracy to permit the spacecraft to be maneuvered into position for a final docking maneuver. Angle and range information will be available to the spacecraft in order to effect the necessary dynamic control.

2.1.3 Docking

The ladar will have the capability of supplying control inputs to the spacecraft propulsion system, which will permit the spacecraft to perform a docking maneuver, and thereby physically to secure to the object.

2.2 Technology Baseline

Although the technology developed is applicable to the general technique of using a ladar for surveillance, search, acquisition, and tracking, the study is specifically oriented towards the rendezvous and docking mission envisioned for a Space Tug.

The Space Tug is tentatively scheduled to be deployed within the early 1980s. Therefore, the technology related to various components and software is baselined as 1980. The components and technology required to deploy the sensor either are presently available or will be available by 1980, provided that the impetus for the necessary development is established.

2.3 Tradeoff Analysis

The purpose of the study, within the constraints relative to the available definition of the requirements, is to perform a tradeoff analysis that will define the anticipated size, weight, and power consumption of a family of ladars. The parameters being considered follow.

2.3.1 Environmental Considerations

The environment is considered to be typical of that encountered on other spacecraft. The temperature will vary from -55°F to +60°F. Vibration is 17 g white from 20 to 2000 Hz.

2.3.2 Range

Since the range will affect size, weight, power consumption, and interface with other on-board avionics, it will be treated as a parameter. Maximum ranges of 50, 100, 200, and 300 nautical miles are considered. The salient system characteristics are presented in a form permitting a system tradeoff to be made with range as the critical parameter. The range uncertainty is taken to be 5% of the maximum range of each configuration. The relative range rate uncertainty is between 0 and 200 feet per second.

2.3.3 Prime Power

The prime power is 28 V dc. The power consumption is a parameter that will be a function of the maximum range, and is intended to be estimated for each system configuration. The system configuration is to be optimized for minimum overall power consumption.

2.3.4 Docking

Docking is to be accomplished via a docking ring on the cooperative satellite, and clamps on the Tug. The clamps are matched to the ring configuration, and are to be dedicated to the docking maneuver. Tests of a least one docking ring configuration have established the position tolerances as one foot offset and 20° in angle, in order to ensure a successful latching.

2.3.5 Computation Facilities

It is assumed that the Tug will contain on-board computation facilities which may be utilized, on a time shared basis, for such functions as signal processing and the various control functions.

3. DESIGN CONSIDERATIONS

3.1 Operation

The sequential operation of the Ladar Space Rendezvous and Docking System is as follows:

a. Search

The system is pointed to the most probable target position and a search is initiated over a 5 by 5° sector.

b. Discrimination

The target of interest is separated from spurious targets and debris.

c. Acquisition

The target is acquired in angle and range.

d. Track

The target is tracked in angle and range, as the vehicle maneuvers into position for rendezvous.

e. Docking

The vehicle maneuvers into position to mate with the target.

3.2 Basic Configuration

The system is configured to utilize a passively Q-switched CO_2 laser as the transmitter and a four-quadrant photodiode detector array operated as a coherent receiver element. The laser, as well as the receiver configuration are similar to equipment which presently exists in a deployable form for airborne applications. The electronics, logic, and computer interface are similar to equipment which is associated with most coherent pulse Doppler radar sets.

3.3 Block Diagram

A block diagram of the system is shown in Figure 3-1. The functional system operation is controlled by the on-board vehicle computer. The computer programs the modes of operation and performs calculations, such as ambiguity resolution, necessary for target tracking. The vehicle computer is also assumed to be available for several minor functions, such as closing the control loops for angle and range tracking, as well as for spurious target target rejection.

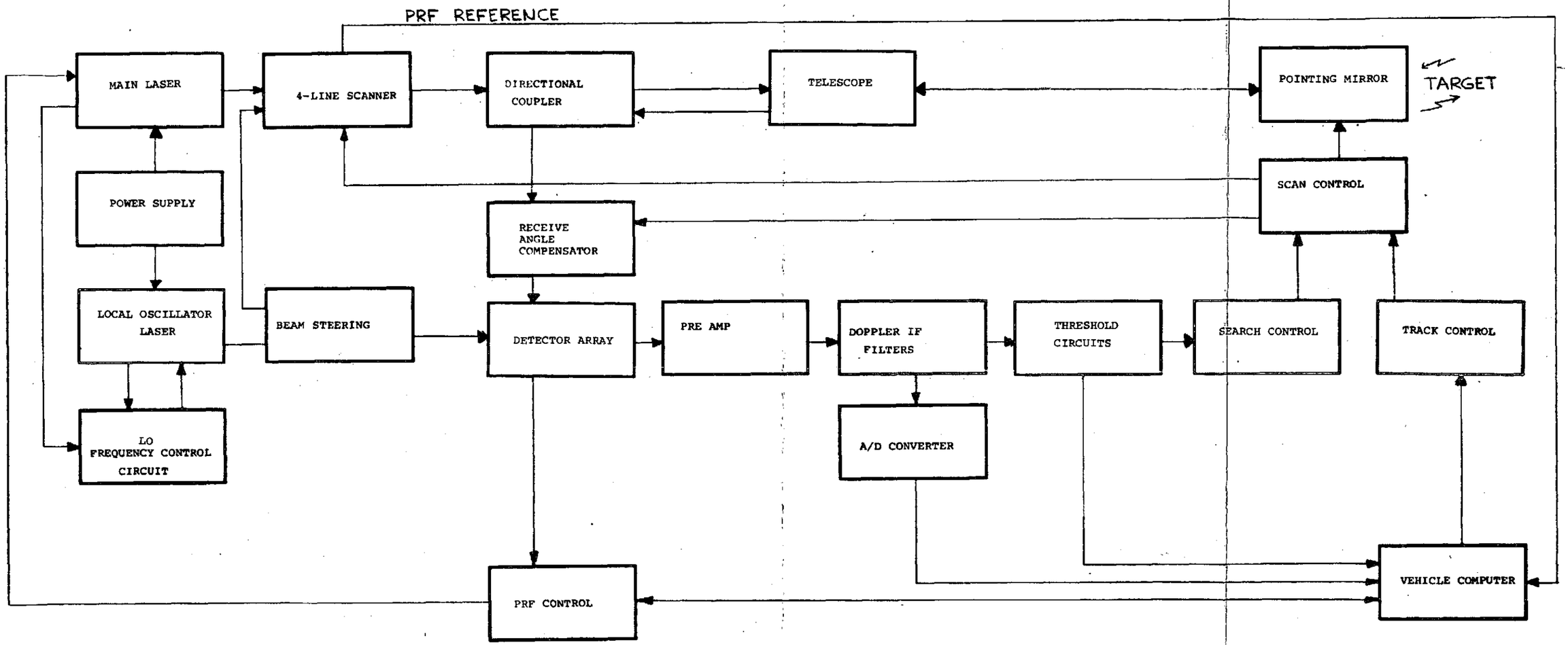

Figure 3-1. System Block Diagram

FOLDOUT FRAME 1

FOLDOUT FRAME 2

3.4 Laser Control Loop

The design for the rendezvous ladar sensor is configured around the main Q-switch laser and the local oscillator (LO) minilaser. As shown in Figure 3-2 the local oscillator provides a reference for the main laser control. The main laser cavity is frequency-locked to the minilaser which is used as the cw local oscillator for the heterodyne detection. The shorter cavity of the LO laser is easier to control as a result of its wider resonant line spacing.

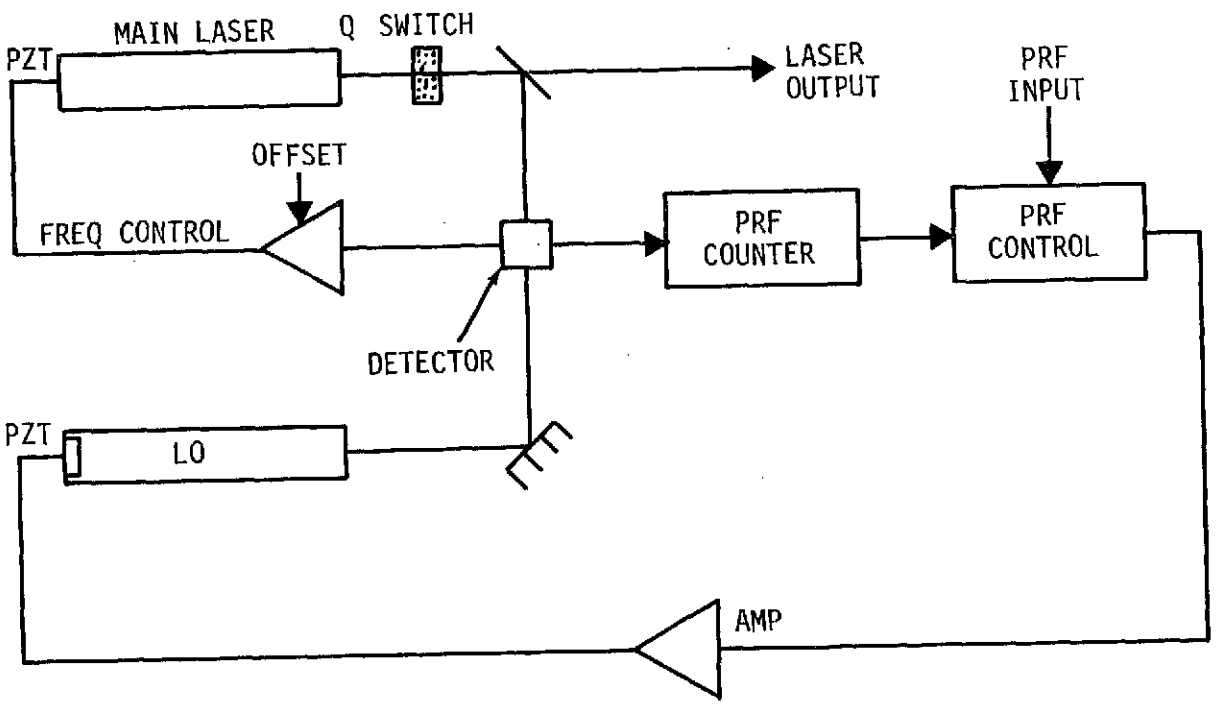

Figure 3-2. Laser Control Diagram

3.4.1 Transmitter

The main laser will contain a CO_2 mixture continuously excited by a switching regulator power supply operated in a current limiting mode, which will result essentially in a constant current discharge through the plasma tube.

The resonator is of a confocal configuration for the purposes of maintaining ease of alignment and immunity to vibration, as well as to thermal distortion. This is important, since the system will be subject to a launch environment and may be in an unattended space vehicle for a protracted period of time.

The laser will be optimized to oscillate on the P-20 line of the CO_2. A bleachable Q-switch is employed for operation in a pulse mode. The pulse intervals will be between 20 and 35 microseconds.

The pulse repetition frequency (PRF) and the wavelength of the laser will be controlled by piezoelectrically driven cavity mirrors in both the transmitter and the LO. The mirrors will be capable of varying the cavity lengths approximately 1 micron depending on the strength of an applied electric field. Since the piezoelectric transducers are essentially capacitors, they will consume little or no power; they are electrostatic devices which use a high voltage with microscopic leakage currents. (In the various modes of operation of the rendezvous ladar, care has been taken to ensure that rapidly gated voltages will not be applied to the piezoelectric transducers since this would generate dielectric loss.)

3.4.2 Local Oscillator

When a PRF has been selected, the minilaser will operate at a wavelength determined by its cavity characteristics. The Q-switched transmitter will be controlled via the feedback loop to maintain a frequency offset of 11.5 MHz. The PRF is controlled, as shown in Figure 3-2, by varying the cavity length of the LO. At each new PRF setting and its resultant wavelength change, the main laser will be brought into the desired frequency offset with respect to the LO.

The LO laser will operate cw at a fixed frequency and will have a power output of approximately 60 milliwatts. Approximately 8 milliwatts will be used for the LO function in the receiver; i.e., to excite the receiver detectors for heterodyne detection. The remaining power will be extracted via a Brewster angle beam splitter for use as a low power transmitter for close approach operation where the main laser power would be excessive. This is discussed below and in the section on docking.

The LO laser, because of its small size, will be less efficient than the main laser. Whereas the main laser will have better than 10% efficiency, the LO laser is expected to have only 3% efficiency. The LO laser will use a confocal cavity configuration, the same as the main laser, for the same reasons of freedom from vibration and induced misalignment difficulties.

The power output of the LO laser will go through a beam splitter and, as mentioned earlier, part of the power will be sent directly to the heterodyne detector element. The other fraction of the LO output power will either be absorbed in a black body or steered by means of mechanically indexed mirrors into the telescope for service as the transmitted beam for medium and close range operation.

3.5 Output Beam Scanning

The laser output beam is directed to an oscillating mirror which covers an angle of ±0.125 milliradian generating a beam deflection of ±0.25 milliradian. The scanner provides master synchronization for the PRF and gives the effect of synthesizing four simultaneous scan lines when the large pointing mirror is scanned across a 5° wide field of view.

Since the PRF of the main laser is phase locked to the sinusoidally scanning mirror of 8333 Hz, the transmitted pulse occurs four times per mirror cycle at relative phase angles of 18° 26' and every 90° thereafter. Thus, four equally spaced transmissions are generated in the Y direction.

Coincidentally, the large pointing mirror moves the beam in the X direction at a constant speed proportional to the PRF. Thus, a four-line scan pattern is generated with each elemental area equally covered in both the X and Y directions.

At the end of each scan line group, the large pointing mirror is indexed four line widths in the Y direction and the scan traverses in the reverse X direction as illustrated in Figure 3-3. The process is repeated until the entire field of view is covered.

The entire field of view is covered uniformly, with only 6% pointing mirror turnaround time. The pointing mirror requires 1.2 watts drive power, and the sinusoidal scan mirror uses an additional 0.2 watts.

3.6 Directional Coupler

After the four-line scanner, the beam is directed into a directional coupler (optical combiner) which superimposes the

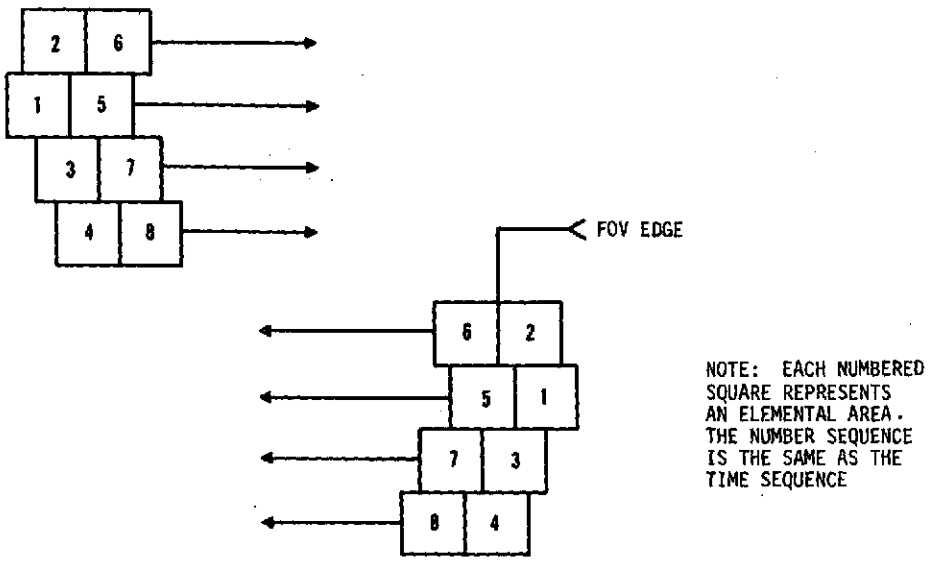

Figure 3-3. Four-line Scan Pulse Sequence

path of the transmitted beam and the received beam through the same telescope optics. The directional coupler permits the transmitted beam to go outwards and the received beam to travel in the reverse direction with minimum interaction.

3.6.1 Main Bang

The backscatter of the transmitted beam from the optical combiner surfaces will be on the order of 1 part in 10^{10}, giving essentially a signal feedback of -100 dB with respect to main beam power. The backscatter of the main beam will generate a detectable pulse which will be used to define t=0 (main bang) timing pulses. The pulses will be used for both PRF control and ranging to the target.

3.6.2 Design

The directional coupler will consist of a Brewster angle window and a quarter-wave plate. The Brewster angle window will receive the transmitted signal orthogonally polarized to its direction of transmission and will reflect it into the telescope angle window. The reflection process will be approximately 70% efficient. The linearly polarized beam reflected off the Brewster angle plate will then enter the quarter-wave plate where it is converted into a circularly polarized wave. After the quarter-wave plate it will enter the telescope.

3.7 Telescope

The telescope consists of a series of mirrors which will expand the beam to a diameter of 77 millimeters and point it in the desired direction. The telescope design is essentially the same as that described in the interim progress report.

3.7.1 Efficiency

The telescope optical efficiency will be improved over the values computed in the previous progress report. In the earlier design, the field of view of the telescope was 1° peak-to-peak. In the improved configuration the field of view of the telescope is less than 0.65°, with a corresponding reduction in off-axis aberrations and the size of the holes in certain elements. The reduction in hole size in the mirrors will result in an optical efficiency improvement of about 20%.

3.8 Pointing

3.8.1 Transmitting

After the beam has been expanded it is steered by the pointing mirror. The pointing mirror serves the functions of both scanning and pointing. The mirror will be driven from side to side at approximately 1.4 radians per second in the form of a fast scan, when used to search a designated 5 by 5° field of view within an overall 30 by 30° field of view capability.

The mirror will have a 2-axis drive and will use a torque motor in each axis. The angle of deflection is limited to ±15° (the mirror movement is only half the angle of the field of view because of ray geometry). The torque motors will have capability adequate for both the rapid scan as well as the slow positioning functions. The position of the mirror will be controlled with resolvers through a feedback loop. The resolvers will require an accuracy of 0.005° or 18 seconds of arc.

After the beam leaves the telescope it will go out to the target which may be as far away as 300 nmi (555.6 km).

3.8.2 Receiving

The target will be cooperative, i.e., the transmitted beam will strike a corner reflector optimized for 10.6 micron reflection. The corner reflector will have an equivalent mean cross section of up to 64.4 dB above a square meter and a peak cross section of up to 70 dB above a square meter.

The returned echo will arrive back at the pointing mirror where it will be redirected through the telescope in a reverse path into the directional coupler. The received beam will be circularly polarized in a reverse sense to the transmitted beam. In going through the quarter-wave plate it will become linearly polarized orthogonally to the direction in which the transmitted beam was polarized. Hence, it will then be in the preferred direction for transmission through the Brewster angle plate.

The beam passes through the Brewster angle plate with minimum loss and into an angle compensating mirror. The angle compensating mirror compensates for the off-axis angle between the transmitted beam and the received beam, which is caused by the finite round trip time of the laser energy.

The beam angle, external to the telescope, will be a maximum of 5 milliradians. After going through the telescope which has a magnification of 10, the angle will be magnified to 50 milliradians. The angle compensating mirror will essentially insert an angular correction in the beam and direct it onto the detector array.

3.9 Detector

The detector will consist of four square chips in a quadrantal array to define azimuth and elevation. The detector chips will be closely spaced to minimize losses because of beam spot falling on the inter-chip space.

The detector array will be simultaneously illuminated by the LO and the received signal. Approximately 2 milliwatts of LO power per detector chip will be used. Thus, a total of 8 milliwatts will be applied to the detector array for heterodyne detection. The detector will have a quantum efficiency of 50%.

Each element of the detector array will be connected to a wide-band low-noise preamplifier with 30 dB of gain. Each of the four preamplifiers will pass frequencies from 0 to 12 MHz.

3.10 Receiver

At the output of the preamplifiers there will be a group of differential amplifiers which will combine the four amplified signals into sum and difference groups, corresponding to elevation and azimuth. The sum signal will be the sum of the four pre-amplifier outputs. The difference signals will be further amplified with an additional 60 dB of gain in log IF amplifiers, followed by video detection and filtering to derive orthogonal error oorrecting signals for use in target angle tracking.

3.10.1 Signal Processing

The sum channel will be processed by a bank of eight doppler filters. Each doppler filter will have a 2 MHz wide Gaussian bandpass IF amplifier. The filters are designed to be optimally matched for the Gaussian shapped 0.35 microsecond wide transmitted pulse to ensure an optimum detection probability for the low-level received target echo. The IF output is applied through threshold circuits to a series of interconnected latches to identify which filter was closest to the center frequency of the received signal.

3.10.1.1 Emitter Coupled Logic

Each IF filter output has its own independent threshold circuit which will use emitter coupled logic for minimum time delay and maximum range accuracy. The emitter coupled logic will have typical propagation delays of about three nanoseconds per gate. The variability is expected to be on the order of 1/5 to 1/10 of three nanoseconds, thereby preserving ranging accuracy.

3.10.1.2 IF Filters

Each of the 2 MHz wide Gaussian IF amplifiers will have a logarithmic characteristic. Each one will be gain matched to close limits with respect to the other IF filter amplifiers. This is to permit valid relative amplitude measurements to be made both for identifying which IF filter had the strongest signal and to permit derivation of a digital 6-bit word with each of the 64 levels representing 1 dB in order to supply the vehicle computer memory with amplitude information on the target size. The information will be used in false target elimination.

3.10.2 Target Identification

When a signal above the detection threshold is received (i.e., a signal whose strength implies that it is a significantly sized target or one that is likely to be a desired target) then it will be recorded as three 16-bit digital words. Two of the 16-bit words will describe the angle coordinates of the pointing mirror. The third 16-bit word will use 6 bits for target size and 10 bits for address and control functions.

The vehicle computer will store these individual returns and correlate them, especially those that are adjacent in angle and range, to determine it if is a true or false target. The computer will also initiate a program involving changes in the PRF once it is decided specifically to analyze the status of a particular target.

When the computer has ascertained that a detected target is a valid target (as well as the target of interest) and has tracked and positioned the vehicle in proximity to the target, the docking maneuver is initiated.

3.11 Docking

Docking consists of both preliminary approach and positioning, followed by a maneuver which ensures accurate alignment of the two spacecraft prior to final approach.

The required maneuvering consists of the following three phases which may be accomplished simultaneously and/or sequentially:

a. The reduction to an acceptable value of the radial misalignment

b. The reduction to an acceptable value of the angle between the axes of the two spacecraft

c. The reduction to zero of the distance between the mating faces

The low power transmitter (see Section 3.4.2) located on the Tug is utilized. By means of the scanning mechanism the beam is allowed to describe a cone, centered about the Tug axis.

A special circular target is centered on the mating face of the satellite. The target consists of two concentric sections. The main section is an annulus whose reflectivity depends only on the distance from the center of the target, being a maximum for small distances and a minimum for large distances.

The variable reflectivity can be achieved by a series of narrow concentric annular zones, alternating between very high and very low reflectivity. The ratio of the widths of two adjacent zones is appropriately tapered as a function of distance from the center. The maximum width of a zone is small compared to the diameter of the beam on the target.

The second section is a small circular area whose surface has a backscatter pattern of low amplitude. The backscatter pattern, which is a function of the angle of incidence only, is sharply peaked about normal incidence. Such a surface is being experimentally investigated.

4. PERFORMANCE SUMMARY AND CALCULATIONS

The baseline ladar system described in this report uses a 76-mm optical aperture with a transmitted average power of between 2 and 20 watts. A performance analysis is evaluated herein for operation at various ranges and for satellite-mounted retroreflectors of various sizes (cooperative targets). A figure of merit is evaluated that indicates the extent to which the system meets the required detection and false alarm criteria.

The figure of merit is the ratio of signal power to noise power (S/N) available at the input to the threshold detector stage. When compared to the S/N required to satisfy the system specifications, the calculated figure of merit is an indication of the available safety margin in the system design. It is also useful as a basis for comparison with other system designs. In the analysis a S/N value of 12 dB is used as a bench mark (minimum safety margin).

4.1 Figure of Merit, S/N

The signal-to-noise ratio is expressed in the form of the conventional radar equation, which is derived in Appendix A as

$$\frac{S}{N} = 10 \log_{10}\left[\frac{P_T G_T G_R \lambda^2 \sigma}{(4\pi)^3 R^4 P_n L}\right] \text{ dB},$$

where:

P_T is the laser transmitter peak power in watts

P_n is the minimum detectable received signal power, in watts, numerically equal to the received noise power

G_T, G_R are the transmitter and receiver antenna gains, respectively

λ is the wavelength of the laser, 10.6×10^{-6} m

σ is the retroreflector equivalent cross section relative to an isotropic radiator, in m^2

R is the range to target in m

L is a composite loss factor, accounting for several effects, which are discussed.

The above parameters are discussed further in some detail.

4.1.1 Peak Power (P_T) equals the average power divided by the duty cycle which, in turn, equals the product of the pulse width and the PRF. Thus, for an average power of 1 watt:

$$P_T = \frac{P_{ave}}{T \times PRF} = \frac{1}{0.35 \times 10^{-6} \times 3.33 \times 10^4} = 85.8 \text{ watts.}$$

4.1.2 Minimum Detectable Power (P_n) for a photodiode heterodyne detector is given by

$$P_n = \frac{hf\Delta f}{\eta} = \frac{hc\Delta f}{\lambda \eta}$$

where:

h is Planck's constant, 6.6×10^{-34} watts

c is the velocity of light, 3×10^8 ms^{-1}

Δf is the noise bandwidth, or bandwidth of the IF filter, 2×10^6 Hz

η is the quantum efficiency, 0.5.

The calculated value of P_n is 7.7×10^{-14} watts.

4.1.3 Transmitter Antenna Gain (G_T) is defined as the ratio of the far field power density on the optic axis of the transmit aperture to that of a hypothetical isotropic radiator radiating over a full sphere, or 4π steradians. This quantity is approximated by $4\pi/\beta^2$ where β is the beamwidth in radians between 1/2 power points. In the system the transmitted beamwidth β equals 0.33 milliradian, (see Appendix A) which yields

$$G_T = \frac{4\pi}{(0.33 \times 10^{-3})^2} = 1.15 \times 10^8.$$

4.1.4 Receiver Antenna Gain (G_R) is calculated in a similar manner. Here, however, because of the fact that on receive the optics are uniformly illuminated, the effective receive beamwidth is less, and equals 0.167 milliradian. This yields

$$G_R = \frac{4\pi}{(0.167 \times 10^{-3})^2} = 4.51 \times 10^8.$$

4.1.5 Target Cross Section In the radar equation, σ is the cross section in m^2 of an istropic scatterer, equivalent to the actual target in that it backscatters the same power density.

Here σ is the cross section of a triangular-face corner reflector, calculated according to the following formula:*

$$\sigma = 4\pi \left(\frac{0.289\ell^2}{\lambda}\right)^2 m^2$$

- - - - - - -

*Robertson, Sloan D., "Targets for Microwave Radar Navigation: *Bell System Tech. Journal*, Vol. 26, pp. 852-869, October 1947.

where ℓ is the length of the edge of a triangular face of the corner reflector, in meters.

The above value of σ holds on the optic axis of the corner reflector.

4.1.6 Miscellaneous Losses (L). Grouped in this factor are a number of miscellaneous system losses as follows:

a. Optical Losses. Revised optical efficiencies for components listed in Appendix B yield the optical loss factor 3.56.

b. Scanning Loss. This factor is caused by the discrete raster scan and results from the fact that a target, when illuminated, is not always on the optic axis, i.e., on the peak of the beam. The loss factor from this effect, as computed in Appendix C, is 1.15.

c. Geometric Loss of Detector Efficiency. The four-quadrant detector has a nonactive cross-shaped section, resulting from separation of the four individual quadrants. The effective signal used for detection is the sum of the four individual output signals. The sum is reduced by the presence of the nonactive area. The loss factor corresponding to this effect, as computed in Appendix C, is 1.03.

d. Mismatch of Frequency Filter. A situation arises similar to that which causes the scanning loss, in that the doppler shift of the target echo wavelength may cause the signal frequency, after heterodyning, to fall somewhere off the center frequency of any of the frequency filters. The loss factor from filter mismatch (cited in Section 6.4 as 0.5 dB for the worst case and 0 dB at best) is averaged to 0.25 dB, corresponding to a loss factor of 1.06.

e. The Retroreflector is, in General, Not Viewed Along Its Optic Axis. In Appendix D a particular configuration of fourteen corner reflectors is described. Since, in general, a target will not be aligned with a reflector axis, an average degradation of 5.2 dB is derived with respect to operation along the optic axis. This corresponds to a loss factor of 3.31.

f. Imperfections in the Construction of the Corner Reflectors This effect was estimated at 3 dB, or a loss factor of 2.

g. Allowance for Degradation of Overall Performance 2 dB was allowed for degradation of performance in the field. This corresponds to a loss factor of 1.58.

h. The Focal Spot and the LO Wave Are Not Perfectly Matched in Phase. The central bright spot, or Airy disc, contributes the main fraction of the detected signal energy. The first bright ring surrounding the central spot is 180° out of phase with the central spot and its contribution will subtract In the worst case, the first bright ring entirely falls on the detector area (the effect of higher order rings will be neglected). The calculated values of the energy contained in the central spot and the first bright ring are 0.838 and (0.91-0.838),* respectively.

The product of all the above factors, as listed in the following table, is 61.2.

SYSTEM LOSS FACTORS

Optical losses	3.56
Scanning loss	1.15
Geometric loss, detector inactive area	1.03
Frequency filter mismatch	1.06
Corner reflector nonalignment	3.31
Corner reflector imperfections	2.00
Performance degradation in the field	1.58
Heterodyne phase mismatch	1.31
Overall loss factor:	61.2

4.2 Operation at Medium Range

The analysis of the medium range operation, where the LO laser is used as the transmitter, is identical to the previous analysis. The changed parameters are listed below.

* Born & Wolf, *Principles of Optics* p.398 MacMillan, 1964

a. The Transmit Power 52 milliwatts instead of 1 watt resulting in a decrease in performance of 12.8 dB.

b. The Contributions of the Optical Losses to the Total Loss Factor In transmit, the following additional elements are included:

	Efficiency
Half-wave plate	0.96
Lens	0.96
4 Folding mirrors	$(0.99)^4$
Additional loss in hole of pointing mirror, due to nonuniform illumination	0.50
Total additional optical loss:	3.5 dB

c. The lesser effectiveness of homodyne, as compared to heterodyne detection, causes the minimum detectable power to increase by about 10 dB.

d. The use of a narrow-band (100 Hz) post-envelope detection filter reduces the noise power by the ratio of the bandwidths.

The new effective bandwidth equals 34.7 kHz (see 4.4.2).
The previous bandwidth was 2×10^6 Hz.

The ratio represents an improvement of 17.6 dB.

The overall effect of the changes is a penalty of 8.7 dB with respect to the performance curves of Figure 4-1, based on a 1-watt pulsed laser operation.

4.3 Signal Strength Considerations

4.3.1 Far Field

After the target is acquired, which may be as far as 300 nmi (555.6 km), the received signal strength to the rendezvous ladar will vary as R^{-4}. The R^{-4} relationship holds until the target is in the near field. The near field occurs when range to a point target is less than

$$R = \frac{2D^2}{\lambda}$$

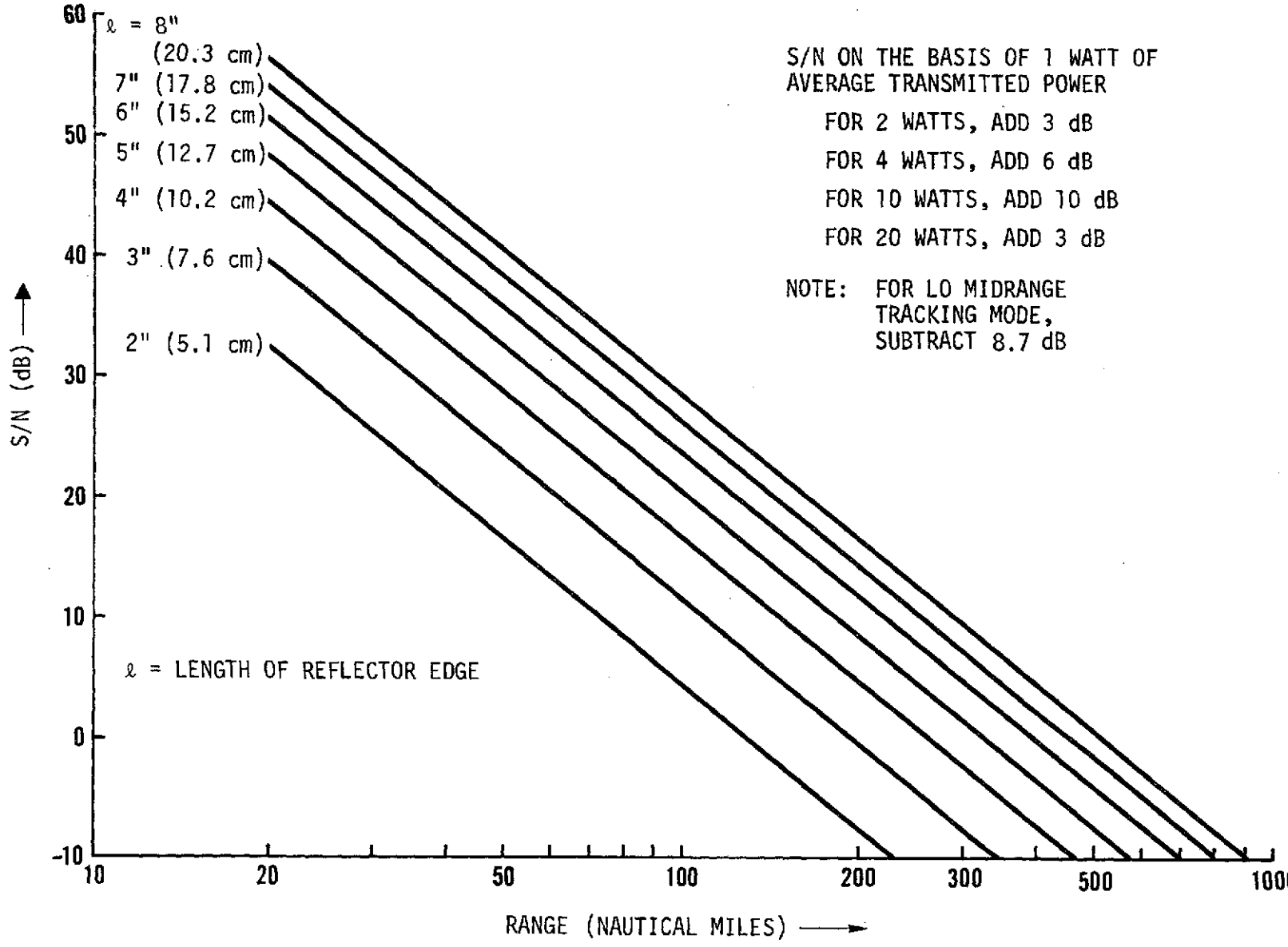

Figure 4-1. Ladar Performance

where D is the diameter of the primary mirror of the optical system.

In the case of the nonpoint targets, the dimensions of the target must also be taken into account. Since our target, in this case, is a mirror in the configuration of a cube corner, the relationships are somewhat different. A cube corner is essentially equivalent to a plane mirror. A plane wave is reflected as a plane wave in the reverse direction, whereas a point target reflects a spherical wavefront. The apparent range of a corner reflector is the distance to its vertex, i.e., where all three corners of the corner cube come together at a point.

4.3.2 Near Field

The behavior of the echo signal strength to a point target has been studied mathematically and is illustrated in Figure 4-2. Note, that after rising to a peak at approximately $0.25D^2/\lambda$, deep fading occurs and the echo (theoretically) goes to zero at $0.125D^2/\lambda$. An analysis for the near field behavior of a corner cube relfector target has not been published. Since it acts as a rctrodirective mirror, however, and the echo is a plane wave at all ranges, the echo strength behavior should monotonically increase without fading.

4.3.3 Close-In Approach

It is planned that the corner reflectors on the target may be as large as 20 cm on edge. The 7.76 cm diameter optics could fit as an inscribed circle within the projected equilateral triangular cross section of the corner reflector. As a result, it is conceivable for 100% of the transmitted beam to be returned to the receiver detectors, subject only to the losses in the optical train, which are approximately 6 dB. For a 6 watt average power laser transmitter,this represents about 1.25 watt on the detectors which would be considerably above the threshold of damage.

As a practical matter, the system is designed for 80 dB of dynamic range. It is possible to build 90 dB dynamic range amplifiers. These are more difficult to build, however, and more costly than an 80 dB dynamic range amplifier which is readily realizable. The rendezvous ladar system needs four such amplifiers which must be matched in order to permit signal strength comparison for angle tracking and the resolution of false targets.

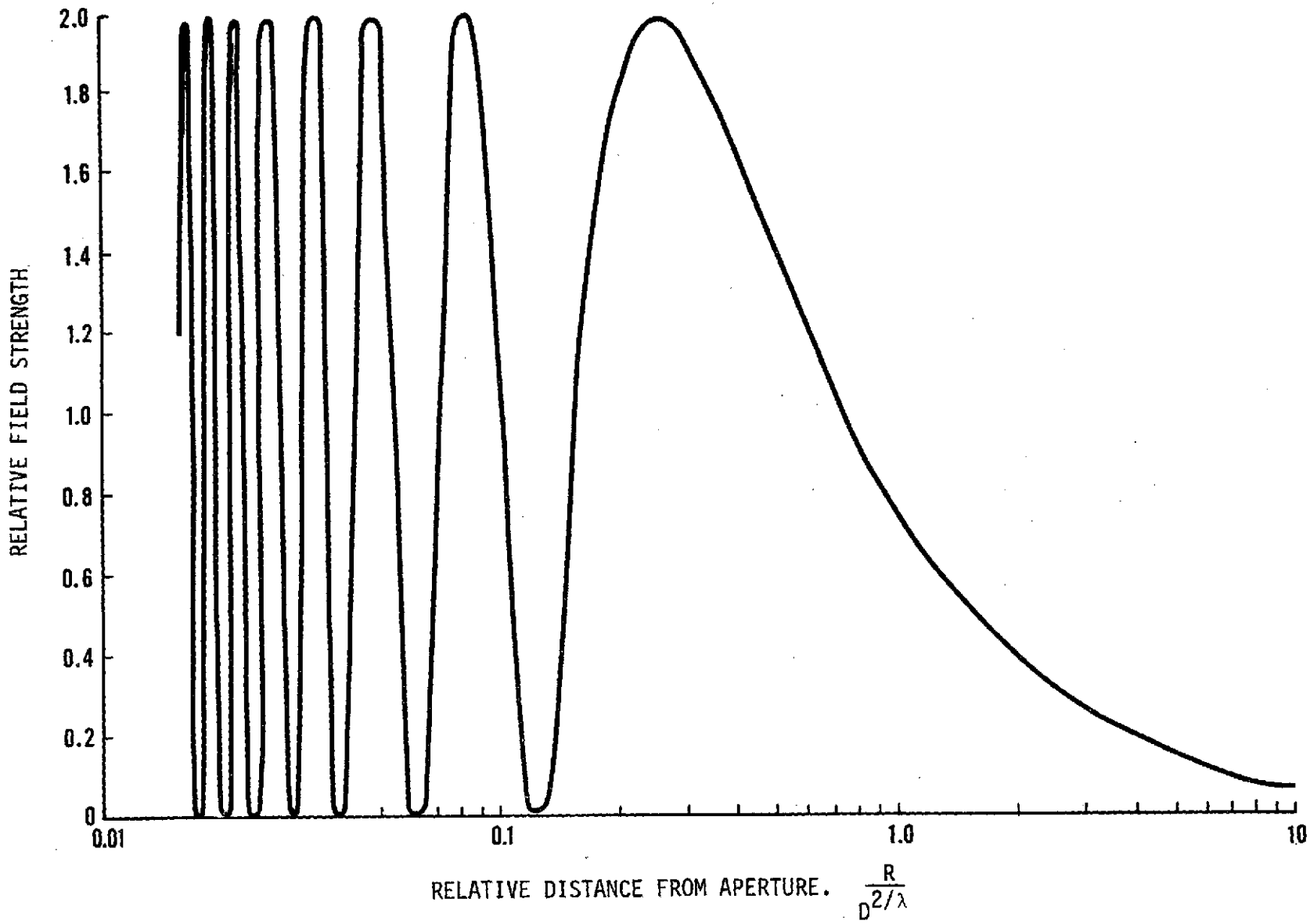

Figure 4-2. Near Field Echo

To avoid dynamic range problems it is necessary to control the radiated laser power. This will have to be done through a feedback loop connected to the laser receiver. On sensing a high power signal near the upper limits of its dynamic range, the feedback loop will generate a control signal which will cause a switchover to reduced output power.

4.4 Power Reduction

There are many possible techniques by which the output power might be reduced. In concept, the simplest method is to drive the main laser mirror piezoelectric transducers (provided for the control of prf and wavelength) to a setting where a very low power output would be generated. The most desirable technique from a power efficiency standpoint, is to turn off the main laser and direct part of the LO power out of the aperture.

Since the peak power of the laser transmitter is 500 watts when seeking a target at 300 nmi range, and the dynamic range of the system is 80 dB, only 125 microwatts of radiated power is required at the point where the high power operation exceeds the system dynamic range. In order to provide a practical operating margin, i.e., an overlap in the dynamic range between high and low power operation, the actual power transfer will be implemented at the 20 milliwatt level. The 20 milliwatt level is well below the detector damage threshold. Nevertheless, there is still enough signal about 30 dB margin, to guarantee suitable operation when transfer is effected. Since the transfer involves mechanical motion of mirrors, it will take about 0.1 second.

Switchover from the main transmitter to the LO is made when the signal has increased 60 dB above threshold. The range would be between 6 and 20 nmi. Where transferring to LO operation a different ranging technique is required, since a CW signal is now being transmitted.

4.4.1 Scan Modulation Effect

To perform ranging in the region between 20 nmi and 200 meters (the final approach distance), it is proposed to take advantage of the modulation inherent in the echo when running the vertical scan mirror at a frequency of 8,333 Hz. Since this mirror deflects the beam ±0.25 milliradian and the transmitted Gaussian beam is ±0.167 milliradian between the peak and the one σ points, there will be 3.8 dB down 2f modulation as the beam is scanned. Near 200 meters the retroreflectors are essentially point targets. Therefore, the phase detector would compare a reference signal derived from the position of the vertical scan mirror to a filtered amplitude response of the echo. The phase angle would give a time difference which would be converted to the range of target.

At the scan rate of 8,333 Hz, the range measurement could be ambiguous. Nevertheless, using the information available at the time of switchover from the main laser, the range would be known unambiguously at the point. (Tracking would also be effected, provided angle tracking and range tracking were maintained continuously.) The high speed vertical scan generates a double frequency echo response, since the mirror is oriented at the target twice during each scan cycle. Thus, the echo frequency would be 16,667 Hz or a period of 60 microseconds. If the phase detector is accurate to 1°, this corresponds to a time accuracy of 1/6 microsecond and a range measurement accuracy of 25 meters. The range accuracy of the phase detection system is limited by the signal-to-noise ratio which, in turn, limits the phase angle increment which can be measured.

4.4.2 Homodyne Operation

The CW mode uses homodyne detection. Homodyne detection tends to be less sensitive than heterodyne detection by 8 to 10 dB. This results from the IF noise of the semiconductor detectors. The sensitivity loss is compensated for when the system is switched from the wideband pulse mode to a narrowband mode of operation.

In CW operation the echo will be an amplitude modulated CW signal wave derived from the sinusoidally scanned antenna pattern. Signal strength will vary from peak value to 3.8 dB down. This is bandpass filtered to extract only the 16.67 kHz frequency component in a 0.1 kHz wide band. Since the 0.1 kHz filter follows a 12 MHz wide IF, the noise in the 12 MHz band is folded over in the ratio of the bandwidths.

The random noise voltages add as the square root of the sum of the squares in each 0.1 kHz interval. The signal voltage however, is unaffected since it exists in only one frequency interval. The result is that the noise bandwidth of a wide band IF, followed by a narrow band video is the geometric mean of the two bandwidths, or

$$B_{eff} = (B_{IF} \times B_{video})^{\frac{1}{2}} = (12 \times 10^6 \times 10^2)^{\frac{1}{2}} \text{ Hz} = 34.7 \text{ kHz}$$

The effective narrowing of the noise bandwidth improves the signal-to-noise ratio by 17.6 dB, compensating for the sensitivity loss when switching to homodyne detection.

When switching over to the LO transmitter, the signal-to-noise ratio would be about 30 dB. As the target is approached, the signal-to-noise ratio increases and range measurements become

increasingly accurate. The accuracy is ultimately limited by the accuracy of the resistors and capacitors used in the phase detection circuits. Component tolerances are expected are to be 0.01%, corresponding to 0.06° phase angle.

Using the vertical scan mirror as the basis, ranging modulation ceases to be effective at ranges of approximately 100 meters and below. At this range the ±0.25 milliradian deflection is equal to ±2.5 meters lateral deflection. The transmitted spot would move within the confines of a single cube corner retroreflector and the return beam would have little or no modulation. At ranges below 200 meters, the ranging technique would be changed into the final approach (docking) phase.

4.5 Final Approach

At a range of 200 meters, the rendezvous ladar resolves an 8 cm diameter spot. With this resolution, the system is capable of scanning the target to search for and recognize the distinguishing pattern which identifies the docking surface.

4.5.1 Maneuvering

The Tug would be brought to nearly zero relative velocity with respect to the target and a series of docking maneuvers would be instituted. The maneuvers would entail taking up of positions with respect to the target and searching for the docking face pattern. When the pattern is found, the rendezvous ladar will be put into a conical scan mode at 5 scans per second. (At this time, the vertical scan sensor operating at 8.333 kHz is turned off.)

4.5.2 Conical Scan

The conical scan gives an amplitude modulated signal whose frequency varies depending on where the beam falls on the docking face pattern. The conical scan angle would be controlled during the final approach in order to illuminate a preferred portion of the pattern, identified by the modulation frequency of the echo. During final approach (between 200 meters and contact) the conical scan angle will gradually increase. The magnitude of scan angle is inversely proportional to range. The angle will vary from about 5 milliradians at 200 meters to about 250 milliradians at contact.

When the Tug and the axis of the target are in line, the return echo will be a pure tone. However, when misaligned, amplitude modulation occurs on the tone, which will be detected and used to furnish a correction signal for the Tug propulsion unit.

During final approach the receiver of the rendezvous ladar will be operating as a photon counter. Because the pattern will consist of a series of alternating light and dark diffuse reflectors the echo will be essentially an incoherent wave.

4.5.3 IR Safety

An advantage of using a low power transmitter during final approach is that the target is protected from the full power of the main laser. If the satellite were using either star trackers or earth horizon sensors, these are protected from damage from the laser beam.

The maximum laser beam intensity on the target occurs at switchover to the low power system. At a range of 10 nmi (18.5 km), the laser beam (which has a divergence of 0.33 milliradian) would distribute its energy over a spot area of

$$\text{Spot area} = \frac{\pi}{4} \times (0.33 \times 10^{-3} \times 18{,}500)^2 = 29.3 \text{ m}^2.$$

This results in a power density of

$$P_d = 6 \div 29.3 = 204 \text{ milliwatts per square meter.}$$

The power density level of 205 milliwatts/m^2at 10.6 microns is below the damage threshold for the human eye and for most (if not all) IR surfaces.

4.6 Tradeoff Evaluation

On the basis of the preceeding values of the various parameters, the signal-to-noise ratio, in dB, was computed for a laser with an average transmitted power of one watt. The results plotted in Figure 4-1 cover reflector sizes from 2 inch (5.1 cm) to 8 inch (20.3 cm).

The information contained on this graph should be interpreted by taking into account that:

a. The S/N required to obtain the specified probability of detection and still remain within the allowable false alarm rate is 12 dB.*

- - - - - - -

*Skolnik, M., *Radar Handbook* pp. 2-19, McGraw-Hill, 1970

b. The graph is obtained by specifying a probability of detection, per pulse, of 0.5 and a probability of false alarm, per channel per pulse, of 10^{-7}. These probabilities are equivalent to an overall probability of detection, per frame, (assuming a minimum of 4 pulses on target) of $1-(0.5)^4 = 0.94$, and a number of false alarms, per frame, of $10^{-7} \times (524)^2$ pulses per frame x 8 channels = 0.22.

c. The minimum practical transmitter power is 2 watts.

Thus, a 300 nmi (555.6 km) system can be implemented with 4 watts of average power and the use of 7 inch (17.8 cm) corner reflectors.

Similarly, a 30 nmi (55.56 km) system can be implemented with a 2-watt laser and 2 inch (5.1 cm) corner reflectors, with an excess S/N of 13 dB.

5. SUBSYSTEM DESIGN CONSIDERATIONS

5.1 Optical System

Infrared laser radiation provides an attractive alternative to conventional radar for space applications. Diffraction effects are smaller with the IR by a factor equal to the ratio of the wavelengths. The 3dB beamwidth of a 10.6μ laser beam, for example, can be held to about 1/3 mrad (3dB) with only a 76 mm (3 in) aperture, whereas an equivalent beamwidth in a radar operating at several millimeters wavelength would require an aperture of many meters.

A system can be designed which emits powerful coherent pulses in a given direction and detects energy which is reflected by a target. This direction can be changed continuously, by mirrors or other means, in order that a section of space may be scanned.

Heterodyne detection is extremely efficient. It can readily be implemented by combining, at the detector, the returning pulse and a constant coherent beam of slightly different wavelength. The interfering coherent waves then produce a "beat" frequency which can be detected. Different pulses can be coded by varying the emitter frequency in a predetermined pattern. Cooperative targets, equipped with retroreflectors, maintain the coherence of the reflected beam and minimize the required transmitter power.

5.1.1 Design Constraints

The laser radiation must be projected in a collimated beam with 1/3 mrad divergence at the half-power (3dB) points. The returning pulses must be brought to focus at the appropriate detector position, where they are combined with the reference beam from the local oscillator (LO). The optics and detection and scanning systems required to achieve this are subject to many constraints; the most important are weight, power consumption, maintenance of coherence, optical efficiency, efficiency of the detector and its cooling system, and efficiency of the scanning system. The design, techniques, components, and materials used are limited to what can be confidently predicted to be technologically feasible in a 1980 time frame.

5.1.1.1 Weight and Power Consumption

It is essential that the system be as light as possible, since it must be launched into orbit and maneuvered through space. Every additional pound of payload represents an enormous expenditure of fuel and an equivalent launch cost of thousands of dollars. Hence, every aspect of the design must be approached from the point of view that system weight must be minimized. Power consumption must also be kept low, in order to reduce the weight of the power supply.

5.1.1.2 Coherence

Since the detection approach is based on optical interference, the system must be designed in such a way that sufficient coherence is maintained in the pulses throughout the entire trip from laser to target to detector. When a single optical channel is used for both transmitting and receiving, beamsplitter and antireflection coatings should be avoided, since they tend to cause backscatter into the detector. This can defeat the heterodyne detection process.

5.1.1.3 Optical Efficiency

The system should utilize as few elements as possible, both to save weight and to minimize losses resulting from absorption, scattering, and undesired surface reflections. Such losses would require greater output power for a given range, thus increasing the weight of both the laser and the power supply.

5.1.1.4 Detector/Cooler Efficiency

A detection system must be incorporated with a compatible cooling system to achieve maximum efficiency and reliability with minimum weight and power consumption. The useful lifetime of the cooling system should be sufficiently long for all proposed missions.

5.1.2 Optical Design

In the system actually designed, careful consideration has been given to all factors discussed above. In order to save considerable weight and reduce alignment difficulties, a single channel (common aperture) is used for both transmission and reception.

5.1.2.1 Single Channel

The attempt to use the same optical channel for both transmitted and received radiation seems at first to run counter to the intention to avoid the large scattering and efficiency losses associated with ordinary beamsplitters. This difficulty is circumvented by utilizing an efficient Brewster angle window to distinguish between incoming and outgoing radiation.

Pulses emerging from the laser are linearly polarized perpendicular to the plane of incidence at the beamsplitter. By orienting the system so that the angle of incidence is Brewster's angle, (about 70° for the material used), approximately 75% of this radiation is reflected. It then passes through a retardation plate (nominally a quarter-wave plate) and emerges circularly polarized. Upon returning, it is further retarded by the plate and becomes linearly polarized in the plane of incidence of the Brewster angle window. Practically all of this radiation then passes through the window, since it is incident at Brewster's angle. The roundtrip efficiency of such a beamsplitter can be conservatively estimated to be at least 75%.

5.1.2.2 Beam Expander Tradeoffs

In order to achieve the desired transmitted beam, divergence must be held to about 1/3 mrad at the 3 dB points. The minimum practical aperture diameter is (for $\lambda = 10.6\mu$) 77.6 mm. Since the requirement is that divergence at the 3 dB beamwidth be 1/3 mrad some margin is allowed for geometrical aberration, and for aperture illumination tapering. The aberrations, however, are held considerably lower than the permissible limit, in order that fabrication tolerances need not cause unacceptable performance.

The need to minimize image aberrations while maintaining high transmission efficiency with as few optical elements as possible, points toward a reflecting system. A single spherical mirror can have far less spherical aberration than a lens of equivalent focal length and diameter. Several lenses might be required to equal the performance of one mirror for small field angles. Surface scatter, reflection losses, and absorption in the lenses also cause much greater inefficiency and loss of coherence than a reflecting surface. It is therefore desirable that the optical system be reflective rather than refractive whenever possible.

Because of the small size of the detector, the returning pulses must be focused to concentrate the energy on the detector. Thus, the beam expander has been designed as a focusing

telescope in order to avoid using additional optical elements. The transmitting system, therefore, will radiate as a point source, rather than emit collimated wavefronts.

In any telescope design, specification of the desired magnification and aperture forces the designer to tradeoff the working relative aperture against the allowable length and complexity of the optics, using image quality as a criterion of acceptability. Since magnification must also be traded off against length and other physical constraints (and since excessive length results in excessive structural weight), the range of simple reflective configurations which can satisfy the system requirements (particularly the field of view) is limited.

5.1.3 Telescope Configuration

The system type chosen is a modification of the classical Gregorian telescope. It consists of two confocal ellipsoidal mirrors of differing focal length and eccentricity. The angular magnification of the telescope is 10 and it works internally at a relative aperture of f/2.8. The solid angle of the image cone is equivalent to a relative aperture of f/13.78 (i.e., the cone angle is 4.16°). The effective focal length of the system is 1.05 meters and its field of view to space is 0.6°. The maximum geometrical aberration is less than 0.1 mrad anywhere in the field. At the 3 dB points the angular spread is reduced to less than 0.05 mrad. The significant optical design parameters are listed in Table I. An exploded view and mechanical layout of the optical train are shown in Figures 5-1, and 5-2, respectively.

A characteristic of reflective designs which cannot be overlooked is that the image is formed in object space. In order to circumvent this problem either direct occlusion is permitted, i.e., some radiation passes through a hole in one or more mirrors, or beamsplitters must be used. In the design, the use of folding mirrors with central apertures has been chosen as the most effective method. The size of the central hole is determined both by the diameter of the converging light cone at the mirror location (this is dominant for the pointing mirror) and by the angular field within the system (this dominates for the folding mirror at the telescope focal plane, where the primary mirror forms an image). The field of view is therefore limited by the efficiency which is accepted for these mirrors. The latter can be estimated approximately by the ratio of usable mirror area to its total area including the hole. In the design chosen the field of view is ±0.3°. The efficiency of each mirror is at least 83%, since each central aperture represents no more than 17% of the area of its associated mirror.

Table I. Optical Design Parameters

SURFACE	RADIUS OF CURVATURE (mm)	AXIAL THICKNESS (mm)	INDEX OF REFRACTION	FREE APERTURE (mm)	HOLE DIAMETER (mm)
1	OBJECT	∞	1 (VACUUM)		
2	∞	135.	-1 (POINTING MIRROR)	107. (AXIS)	36.5 (AXIS)
3	-420.	-210.	1 (PRIMARY MIRROR)	76.3	
4	∞	-25.2	1 (FOCAL PLANE MIRROR)	7.7 (AXIS)	1.1 (AXIS)
5	30.48	25.2	-1 (SECONDARY MIRROR)	13.3	
6	IMAGE				
CONIC CONSTANTS SURFACE 3 -0.82 SURFACE 5 -0.45					

5.1.4 Materials

5.1.4.1 Mirrors

An important decision in the design was the choice of beryllium for the mirrors. This enables the production of extremely light but rigid elements which can have very high reflectivity (>98%) even when uncoated, or which can be coated to yield 99.4% reflectivity. The weight of such elements can be less than 1/3 that of conventional lightweight glass mirrors; by 1980, this discrepancy may be even wider. Even with the factor of 3, however, the weight of all mirrors in the system is less than 0.3 kg rather than about 0.9 kg for glass.

5.1.4.2 Mounting Structure

Mounting and housing for the entire system is also envisioned to be of beryllium, both to minimize weight and to keep thermal expansion as uniform as possible. The mechanical housing must be constructed in such a way that, in spite of thermal expansion or contraction over the expected

Page intentionally left blank

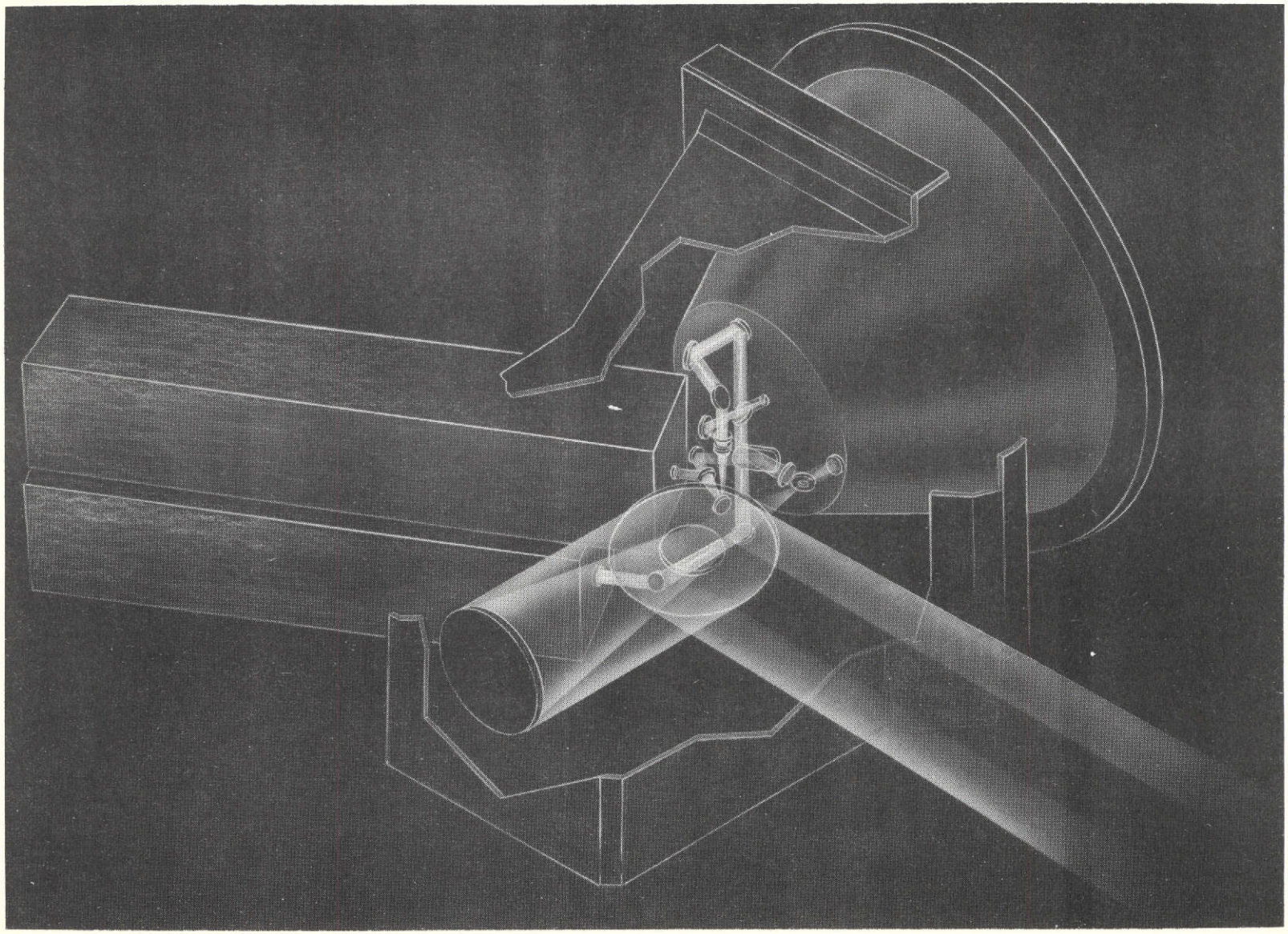

Figure 5-1A. Ladar Package (Artist's Conception)

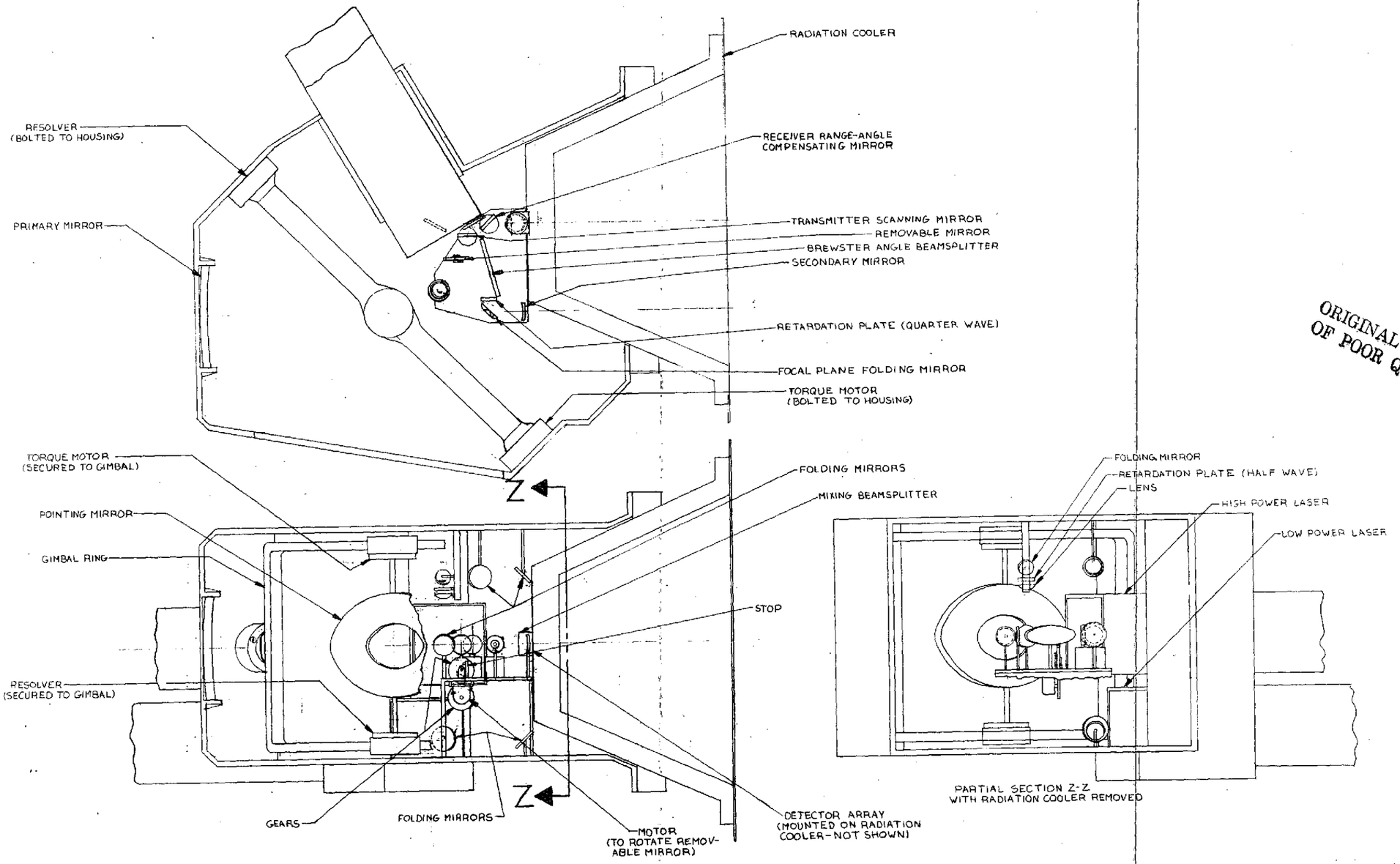

Figure 5-2. Mechanical Layout of Optical Train

temperature range, the two converging mirrors will remain confocal and the laser source and detector positions will remain at the focus of the entire system.

5.1.4.3 Thermal Properties

Unfortunately, raw beryllium is known to have anisotropic thermal expansion properties, largely as a result of its hexagonal crystal structure. Several years ago, this drawback alone could have excluded the element for consideration in the optical system. Today, however, enormous progress has been made towards more uniform characteristics and research and development are continuing at a strong pace. It is confidently expected that the manufacture and working of beryllium with nearly isotropic thermal properties will shortly become routine. Even today, in fact, similar housings for optical systems have been made and qualified for space.

5.1.4.4 Reflection Efficiency

A more fundamental difficulty, however, lies with the manner in which linearly polarized radiation is reflected from metallic surfaces. Unless the polarization direction is either parallel or perpendicular to the plane of incidence, slightly elliptical polarization is produced. A similar effect occurs for circularly polarized light. This in turn leads to a loss of transmission efficiency when a returning pulse arrives at the Brewster angle window, since the retardation plate then transforms nearly circularly polarized radiation to nearly linearly polarized radiation. In the present design, however, the incidence angles are sufficiently small that this effect is acceptable. The round-trip efficiency of the Brewster angle window is estimated to be at least 80% of that which it would exhibit for perfectly linearly polarized radiation. In order to avoid this loss, all mirrors must be coated with dielectric reflection coatings, rather than be left bare, or coated with metals such as aluminum or gold.

5.1.4.5 Quarter-Wave Plate

Not many materials are available for 10.6μ retardation plates. Cadmium sulfide is one of these, and its internal transmission is acceptable (>99%) for short optical paths up to 3 or 4mm.

5.1.4.6 Brewster Angle Element

It is desirable that the Brewster angle window have a high refractive index, since this is the condition for high reflectivity of perpendicularly polarized radiation at the Brewster angle. On the other hand, germanium and silicon, which have very high indices, are subject to thermal runaway; i.e., their transmissibility is reduced significantly when their temperature rises too high. The material chosen for this design is gallium arsenide. Its thermal stability and transmittance at 10.6μ are good, and its refractive index of 3.25 is high enough to allow 75% reflection of perpendicularly polarized light incident at Brewster's angle.

5.1.5 Detector

The choice of detector is constrained by the necessity for high sensitivity, high quantum efficiency at the wavelength of interest (10.6μ) and fast response (in order that high Doppler frequency can be detected), and an operating temperature that can be attained without heavy, power consuming equipment. At present, these requirements are satisfied by mercury-cadmium-telluride detectors that can be cooled by radiation into space. Such detectors can be operated at temperatures of 120°K, and will provide quantum efficiencies of over 50%. They respond to frequencies in the region of 10^9 Hz, which is considerably higher than necessary for this ladar. Research and development are continuing, both on this detector and on lead-tin-telluride detectors which can be made with similar properties.

5.1.6 Optical Train

Figure 5-3 shows in schematic diagram the system components, consisting of the LO situated near the main laser (both nominally 10.6μ wavelengths), all necessary optics including a complex beamsplitter with an associated retardation plate, and a detector array in a radiation cooler. The components are discussed in the following sections.

5.1.6.1 Main Laser Output Path

Both the high power transmitting laser and the LO laser are located on a heat sink and are, therefore, relatively close together. They are kept at a temperature below 20°C, which is required for efficient operation.

The beam emerging from the transmitting laser is directed from a small removable folding mirror, A, onto the vertical

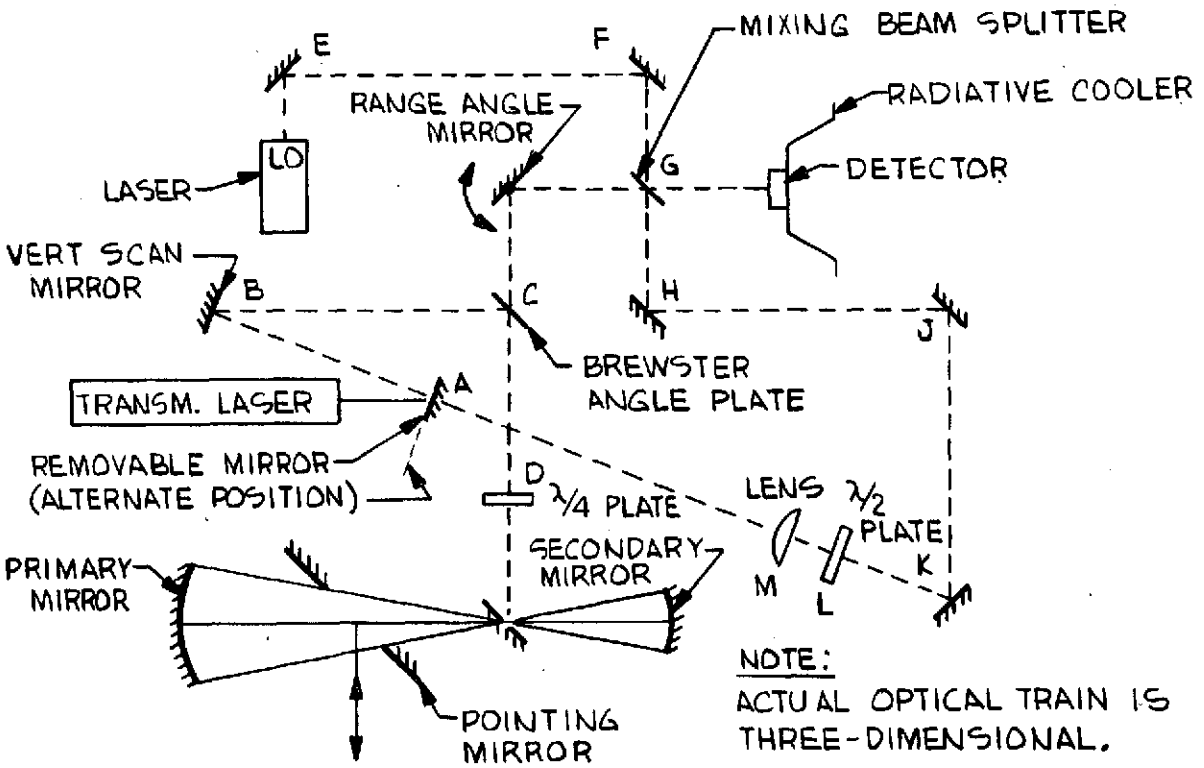

Figure 5-3 Optical Train, Schematic

scanning mirror, B, which generates the four-line pattern described in Section 5.2. From the vertical scan mirror, the transmitting laser beam is directed onto the Brewster angle beam splitter, C, and then is reflected to the telescope.

5.1.6.2 Telescope

The telescope optics are essentially unchanged from the design described in the previous report. An improvement is that the pointing mirror has taken over part of the scan function and is to be moved somewhat more rapidly than before.

Within the telescope, improvements in efficiency have been obtained because the field of view has been reduced from 1° to 0.6°. This enables the holes in the pointing mirror and the small mirror to be smaller and results in improved optical efficiency. Also, it has been possible to reposition the pointing mirror much closer to the focus of the primary mirror. This permits the hole in the pointing mirror to be smaller without occluding the passage of the focused beam.

By reducing the hole sizes in the two mirrors the optical efficiency is improved by about 25% each way or about 50% round trip. The efficiency improvement, however, is partially cancelled by the increased losses in the mixing beam splitter in front of the detector.

5.1.6.3 LO Output Path

The LO beam is diverted through mirrors E and F to a mixing beam splitter, G, which divides the 60 milliwatt LO beam into a 52-milliwatt through component and an 8 milliwatt reflected component which illuminates the four-quadrant detector.

The 52-milliwatt beam is steered by mirrors H, J, and K to the back of mirror A where, in normal (long range) operation, the beam would be absorbed. A small lens, M, is provided to bring the beam to a focus with an f number of 13.6:1 giving a ray geometry equivalent to that of the main transmitting laser. The location of the focal point is a corresponding point behind mirror A. When mirror A is removed from the optical train, the 52 milliwatts of energy from the LO will appear with identical ray geometry in the mainbeam path.

Since the LO beam has to be polarized for mixing with the received signal and since the transmitted beam is polarized at right angles to the received signal, it is necessary to insert a half-wave plate, L, to rotate the plane of polarization of the

LO beam prior to transmission. The rotator can be inserted at any point after the beam has passed through the mixing beam splitter, G. In the design, the rotator is inserted in front of the converging lens, M.

5.1.6.4 Mixing Beam Splitter

The mixing beam splitter in front of the detector, as originally designed, had a 0.99 transmission factor; i.e., only 1% loss. At present, a loss of 16.7% is required as explained below. The reason for the change in the design is to conserve power. In order to use a 1% mixing beam splitter it would have been necessary to use a 1-watt LO, requiring at least 10 watts of excitation power. In the present design a 60-milliwatt LO is used, which will require only 2 watts of excitation power. A considerable saving results in the size, weight, and overall power drain of the package.

5.1.6.5 Detector Signal Levels

The reduction to the 60 milliwatt level was also implemented in order to prevent saturation and the possibility of damage during close approach and/or docking, when the transmitted beam could be returned by a corner cube reflector on the target with little or no loss.

The 60-milliwatt power level arrives at the detector as a 12-milliwatt signal after going through round-trip losses in the optical train. If a 1 watt LO power level were used, it would present a 250 milliwatt signal at the detector, resulting in a large increase in temperature. Damage to the detector would probably occur, particularly since the received spot is focused down to only 0.167 millimeters in diameter on the 0.72 mm square array.

5.1.6.6 Angle Lag Compensation

A movable mirror, K, located after the Brewster angle beam splitter but before the detectors is used to take care of the angle lag between the echo and the transmitted beam. The mirror, using a galvanometer drive, is driven in a step function as the scan reverses from left to right and vice versa.

5.1.6.7 Dichroic Coating

Both the pointing mirror and the flat angled mirror will be dichroic, with an absorptive backing. Thus, the possibility of damage from the Sun's rays is eliminated by limiting the system optical bandwidth to 1000Å (This eliminates more than 99.9% of the power in the Sun's rays).

5.1.7 Shaping of Main Beam

The 18% geometric loss from the large hole in the center of the pointing mirror would be prohibitively high for a Gaussian beam taper (40-50%). To prevent this loss the laser beam is shaped, by a device illustrated in Figure A-1, to concentrate the energy into a conical shell which illuminates the annular pointing mirror. The optical efficiency of this mirror, in the high-power transmit mode, will therefore be approximately 90% (instead of the geometric factor of 82% which applies to cases of uniform illumination).

The above considerations do not apply to the LO transmit mode, since uniform illumination of the detector array is desired and since strong signal conditions will prevail.

5.2 Scanning Mechanism

5.2.1 Summary of Improvement

The scanning mechanism is the portion of the system which has undergone the most improvement since publication of the first quarterly progress report. At that time, the baseline scanning system consisted of a resonant mirror which scanned in one dimension with a peak-to-peak beam deflection of one degree. The beam was then deflected in the other dimension by the large scanning mirror. The distribution of pulses was not uniform and, subsequently, the average power was not being utilized in an optimum fashion. In addition, a linear detector array was required. Since this type of array was not commercially available, it would have required a development program.

Further study of the scanning pattern has been accomplished in order to investigate possible improvements in efficiency. The result is a new and substantially improved scanner. The search throughout the 5 by 5° field of view will now be uniform (i.e., each element of the area will be searched once, with an equivalent amount of overlap in each of the many thousands of elemental areas). In addition, the present scanner utilizes a single four-quadrant detector array for search, acquisition, and track. The detector array will be readily available as a modified commercial device and will lend itself readily to heterodyning.

5.2.2 Techniques Considered

In the course of the contract, numerous scanning techniques have been considered for the scanning function. These techniques ranged from counter-rotating refractive wedges to optoacoustic devices and galvanometer and resonant driven mirrors. At the present time, it appears that most of these techniques are limited in either optical power efficiency, drive efficiency, or angular deflection.

5.2.2.1 Mirror Scans

The possibility of using only scanning mirrors was also investigated. The first approach considered the possibility of generating the entire raster scan by moving the large pointing mirror (Item A in Figure 5-1) at the required rate. It was found that an interpulse period of 30 microseconds (33,333 pulses per second) with a beam deflection step of 0.167 milliradian between pulses resulted in an angle deflection rate of 5.55 radians per second. At this angle rate, scanning the 5 by 5° field of view

(5° = 87.2 milliradians) requires 15.67 milliseconds per scan line. Assuming the scan is to reverse in 4 milliseconds, * an overall scan efficiency of approximately 80% results; i.e., the scan would be operating for approximately 16 out of every 20 milliseconds. Further angular deceleration, which is required to occur in 2 milliseconds, corresponds to about 2800 radians per second squared. Likewise, 2 milliseconds of acceleration at 2800 radians per second squared are required at the start of each scan line.

Based on the above assumptions, computations were made and it was found that motor requirements preclude the use of this approach. Accordingly, methods of reducing the power required to drive the large mirror were investigated.

5.2.2.2 Sinusoidal Scans

The scan technique that has been selected as optimum uses a sinusoidal scan in the vertical axis and a linear scan in the horizontal axis. It is similar to the technique discussed in the earlier progress report.

5.2.2.2.1 Two-Line Scan

The scan is sinusoidal at one-half the PRF of the laser with one scan line width (1/6 milliradian wide) generating two scan lines on one pass of the pointing mirror. The technique is depicted in Figure 5-4. With this technique each scan line pair takes 31.3 milliseconds. Assuming a 4-millisecond turnaround time at the end of each scan line pair, the operation results in 31.3 ÷ 35.3 = 88.66% scan efficiency.

Because the optical train has a magnification of 10:1, the small mirror must scan an angle of $\theta = 0.167 \times 10/2 = 0.833$ milliradians peak-to-peak in order to generate a two-line scan with 0.167 milliradian separation at the output. Note that the laser pulses must occur at the alternate peaks of the sine wave.

- - - - -

* Assuming the 4-millisecond period between successive scan lines consists of 2 milliseconds of deceleration followed by 2 milliseconds of acceleration, since the scans are alternating from left to right and from right to left.

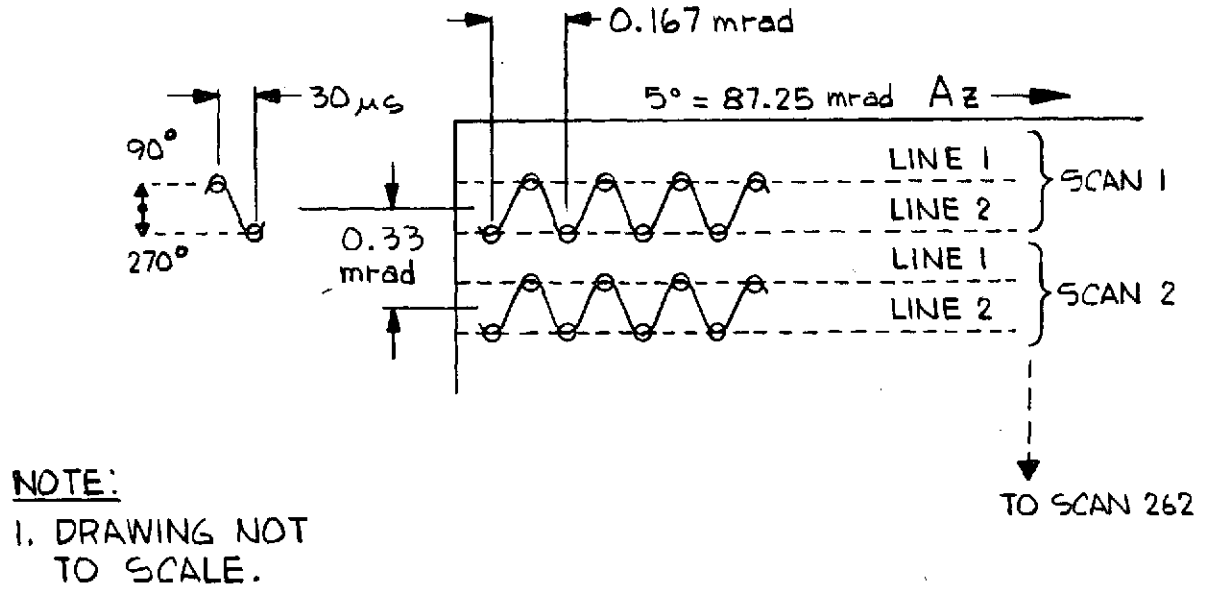

NOTE:
1. DRAWING NOT TO SCALE.

Figure 5-4 Two-Line Scan of Field of View

In the improved design the angular rate of the pointing mirror is cut in half. Furthermore, the number of reversals in scanning the field of view is likewise cut in half. Consequently the average power required for reversing the large mirror is reduced by a factor of 8. (The average power to reverse the scan mirror as it is driven through the field of view varies inversely as the cube of the number of lines being scanned in one pass.) This results from the combined effect of reducing the motor I^2R losses and the duty cycle.

Upon further investigation, it was found that it is also possible to generate three or four lines simultaneously, by using a modified sinusoidal scan technique. These are shown in Figures 5-5 and 5-6.

5.2.2.2.2 Three-Line Scan

The three-line scan technique would require a sinusoidal scanning mirror drive at 1/3 the frequency of the laser PRF or 11,111 scans per second. The laser pulses would have to be synchronized every 120° with respect to the sinusoidal scan angle of the scanning mirror. As seen in Figure 5-5, one pulse occurs at zero crossing whereas the other two occur at the $\pm$ 0.866 relative amplitude points of the sine wave.

With this technique the power required to drive the scanning mirror is reduced to 1/27 of the power required to generate the entire raster scan on a line-by-line basis. Assuming the same millisecond turnaround time, the angular velocity is only 1/3 as great. Therefore, only 1/3 as much current (1/9 I^2R losses) would be required in the servo motor to decelerate and accelerate the scanning mirror. In addition, as noted earlier, there are only 1/3 as many mirror reversals. A three-line scan requires 47 milliseconds to complete and the overall efficiency (with 4 milliseconds between scans) would be 92.1%.

5.2.2.2.3 Four-Line Scan

A four-line scan can also be synthesized as shown in Figure 5-6. In this case it is necessary to synchronize the laser pulse starting at a mirror angle of 18° 26' with respect to the zero crossover and every 90° thereafter. Thus four lines are generated as the large pointing mirror scans 5°. With the four-line scan technique the mirror speed is reduced to 1.39 radians per second. This method reduces the required servo drive power by a factor of 2.37 with respect to the three-line scan technique. It appears now to be the most suitable for the rendezvous ladar and is, therefore, the scan design chosen. The corresponding scan efficiency for the configuration is 94%.

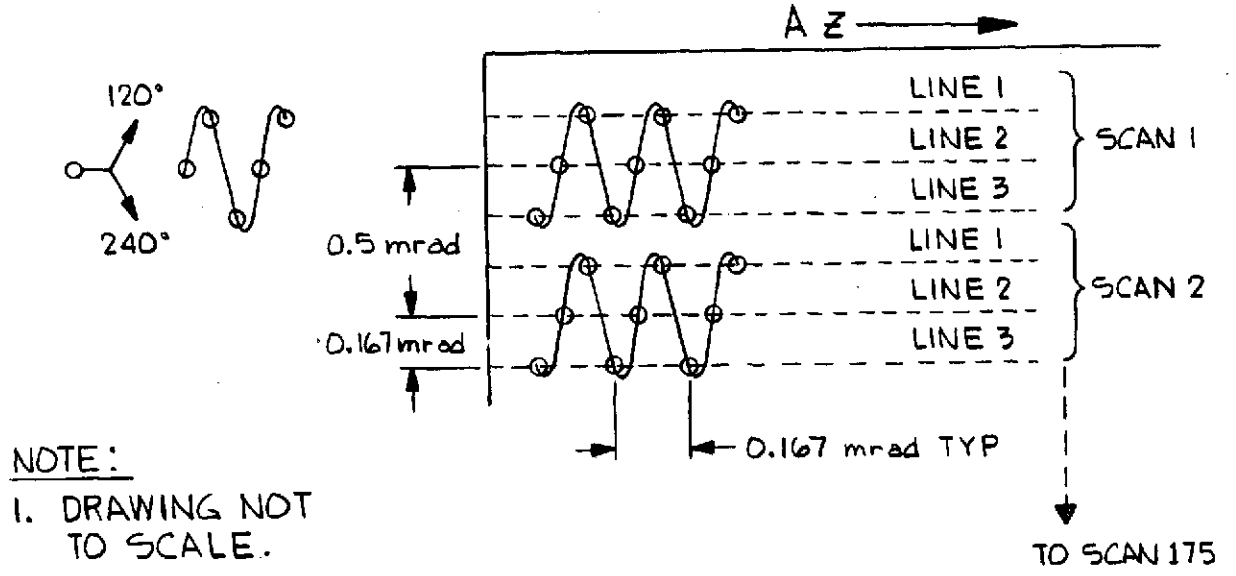

Figure 5-5. Three-Line Scan of Field of View

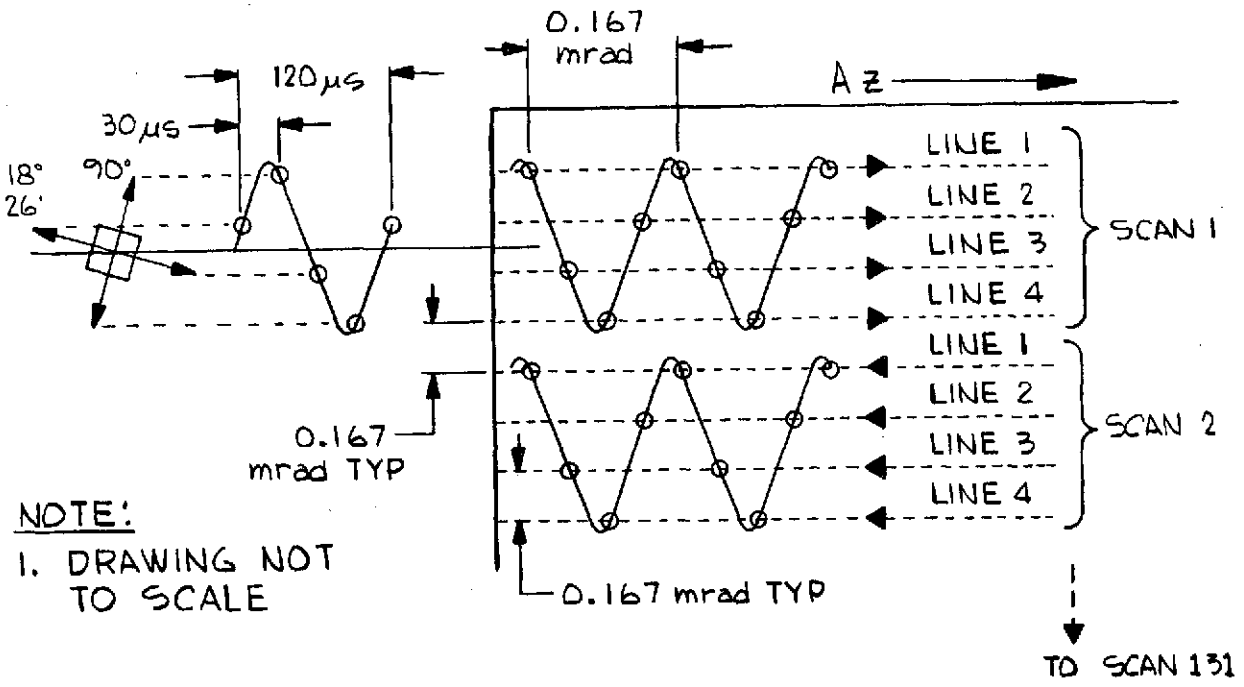

Figure 5-6 Four-Line Scan Synthesis

A further study was made of the possibility of simultaneously generating more than four lines. Within the constraints of a sinusoidal scanning mirror, however, it appears to be impossible if the scan lines are to be equally spaced.

The optoacoustic scanning technique (mentioned earlier) can synthesize scans with as many as 10 lines per scan, or more. However, the losses and auxiliary power requirement of the optoacoustic scanning technique exceed the power and weight requirements of the four-line scan technique.

5.2.3 Elemental Areas

Since the field of view is being scanned by a pulsed ladar, it is essentially divided up into a number of elemental areas with each area being covered by a specific pulse. Since the ladar beam has a Gaussian taper and is approximately 0.33 milliradians wide between the 3 dB points, the areas should overlap in order to prevent excessive loss should the target happen to fall between two successive pulses.

Whereas there would be full response on the peak of each beam, the response would be down 3 dB should the target fall in between two successive beams. If the two scan points overlap at the 50% point, however, then the power loss will be only 1 dB. Dividing the 87.25 milliradian angular extent of each scan line into 1/6 milliradian increments we have 524 elements per line.

Since the field of view is square, there are as many scan lines required as there are elements within one scan line (the adjacent elemental areas are to be equally spaced in elevation and azimuth). Since there are 524 elements in a scan line, 524 scan lines will be required. The field of view can be covered in 131 passes of four lines each.

The number of elements in the total field of view is $524 \times 524 = 274{,}576$ elements per $5° \times 5°$ field of view.

5.2.4 Scan Time And Efficiency

At the interpulse period of 30 microseconds, the time required to cover the field of view is

$$30 \times 10^{-6} \times 274{,}576 = 8.22 \text{ seconds},$$

the actively useful time of the scan. The time spent in reversing the scan is in addition to this period. The period required to scan one group of four lines (with an interpulse period of 30 microseconds) is

$$30 \times 10^{-6} \times 524 \times 4 = 62.88 \text{ milliseconds}.$$

With a turnaround time of 4 milliseconds the total time efficiency of the scan is

$$62.88 \div 66.88 = 94\%.$$

The time required to make a complete scan would then be

$$8.22 \div 0.94 = 8.74 \text{ seconds.}$$

This is well within the 10-second period desired for scanning the field of view.

5.2.5 Echo Angle Lag

For a target at the maximum range of 300 nmi, the echo will arrive approximately 3.75 milliseconds after the pulse is transmitted. As a consequence, there will be an angle lag in the received signal between the direction in which the mirror was pointing when the pulse was transmitted and the direction where it is pointing when the echo is received. The magnitude of this error is computed as follows:

$$\text{angle error } (\Delta\theta) = 0.00375 \times 1.4 \text{ radians per second}$$
$$= 5.25 \times 10^{-3} \text{ radians or } 0.3°.$$

Since the range uncertainty is equal to 5% of the maximum range, this represents a period of

$$\Delta T = 12.5 \times 10^{-6} \times 0.05 \times 300 = 187.5 \text{ microseconds.}$$

The range uncertainty corresponds to an angle spread of

$$\Delta\theta = 187.5 \times 10^{-6} \times 1.4 \text{ rad/s} = 2.625 \times 10^{-4} \text{ radians.}$$

5.2.5.1 Mirror Compensation

As noted in the earlier progress report, the angular error from the delayed arrival of the target echo requires a mirror to be offset. With a telescope magnification of 10, the angular error correction in the small mirror is 52.5×10^{-3} milliradians, or approximately 3°. Within the field of of view (between the primary mirror and the target) this represents only 0.3° of offset.

Since the scanning mirror velocity is constant, the angular error will be constant throughout each scan line. As a result, when the scan is from left to right, the received echo will lag to the left. When the scan is from right to left, the echo will lag to the right.

To compensate for the angular error, a small mirror in the received signal channel has to be provided that alternately changes its angle depending on the direction of the scan. The angle difference is constant throughout the scan. However, during the 4-millisecond period when the scan direction reverses, the small angle compensating mirror has to switch from left to right.

At the present time there are scanning mirror drives available commercially which will change direction by as much as 10° within approximately 1.2 milliseconds, and still be within 0.01% of their correct angle. The angular error of these mirror drives is well within the angle ambiguity of 2.62×10^{-4} radians resulting from the initial range uncertainty.

5.2.5.2 Detection Compensation

The range uncertainty of 187.5 microseconds (corresponding to the angle of 2.62×10^{-4} radians) requires a detector only 0.262 millimeters long in the focal plane of the receiving optics. This is comparable to the received spot size and could conceivably be accommodated by one detector element.

The detector array will have sufficient size to cover the angular uncertainty of the target echoes. Uncertainties are in both azimuth and elevation across the width of four scan lines which are 1/6 milliradian each. In elevation there is a total of 0.667 milliradians. As noted previously the angular uncertainty is 0.262 millimeters long in the focal plane of the receiving optics. This is comparable to the received spot size and could conceivably be accommodated by one detector element.

Because the detector array will be used in angle tracking of the target after acquisition, it was decided to use a four-element array giving two elements in azimuth and two elements in elevation as illustrated in Figure C-2. Each element of the array will be 0.35 millimeter square and the spacing between each element of the detector will be 0.02 milliradians in azimuth and 0.72 milliradians in elevation. This will accommodate four lines of scan plus 100% greater angle ambiguity than the previously reported technique.

The receiving pattern of the optics (i.e., the diffraction limit) is 0.167 milliradians between the 3 dB points. This is computed from

$$\theta = 1.22 \frac{\lambda}{D}$$

$$= 1.22 \times 10.6 \times 10^{-6} \div 77.6 \times 10^{-3} = 0.167 \text{ milliradian.}$$

The elevation dimension of the detector array allows for the spot size plus the spacing of the four-line scan, which constitutes a total of 0.667 milliradian. The 0.72-milliradian wide detector array will encompass some additional energy within the main lobe of the receiver pattern, since the receiver spot size is 0.33 milliradian between the nulls. Most of the energy, however, is within the 0.167 milliradian half-power points.

The width of the four-quadrant array will actually allow for range uncertainty substantially greater than 5%. The primary reason for using the four-quadrant array, however, is to implement amplitude comparison angle tracking after acquisition. Each of the four elements of the detector array will be coupled to a summing amplifier (Figure 5-7). Thus the signal will be received irrespective of the angle in elevation or azimuth from which it is received, within the limits of angular uncertainty in each direction.

The four-element array will also be connected in two azimuth groups of two and in two elevation groups of two, to appropriate sum and difference amplifiers; amplitude difference signals will be derived and fed to the vehicle computer to generate error correcting signals. The computer will control the pointing mirror to equalize received energy in each of the four quadrants.

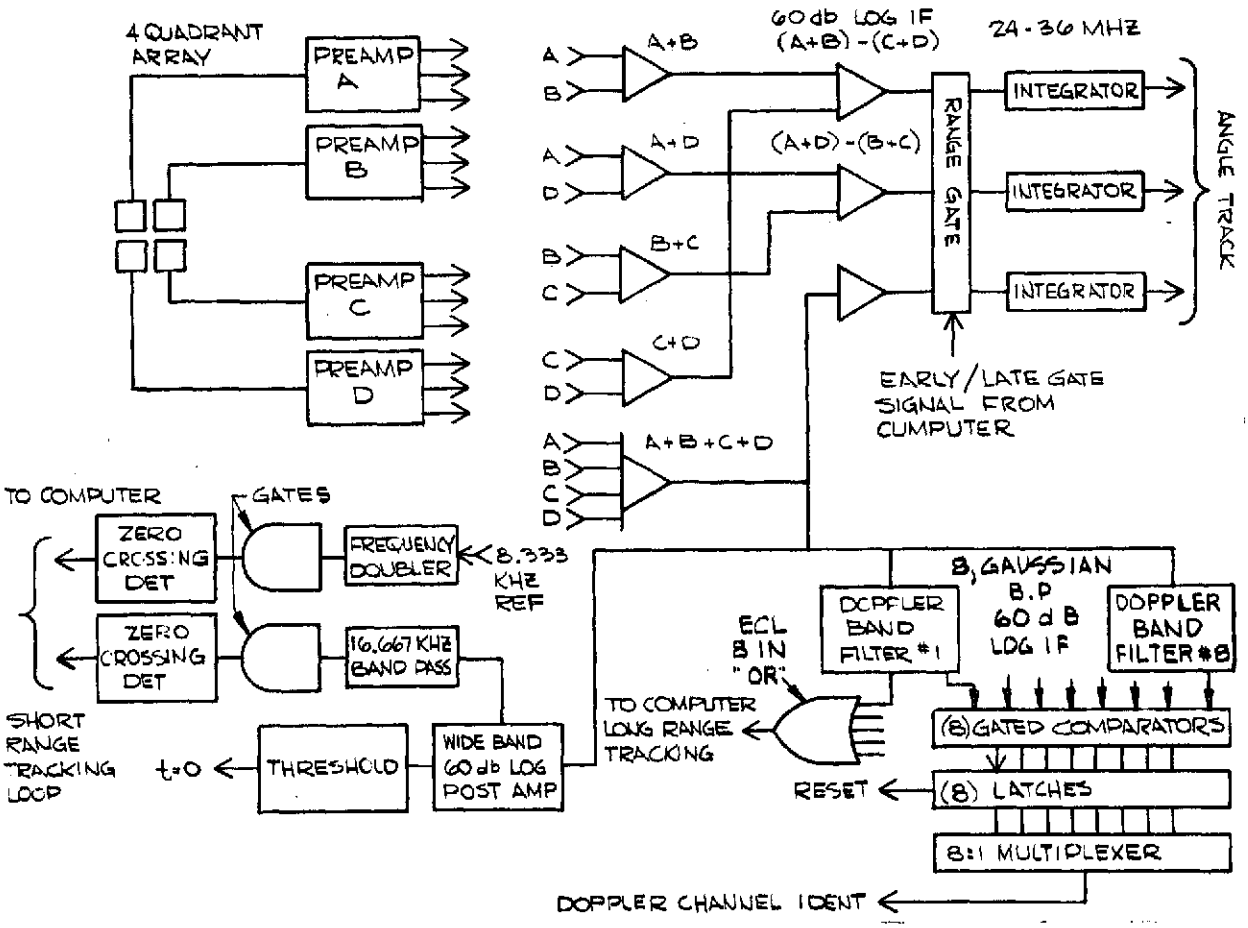

Figure 5-7. Signal Processor System

5.3 Signal Processor

The signal processor converts the electrical output of the coherent detector array into data which indicates the presence or absence of a valid target, and which will permit the target to be tracked in angle and range. In addition to the dedicated circuitry and logic in the signal processor, much of the required computation is handed off to the vehicle computer. (A block diagram of the signal processor is shown in Figure 5-7.)

5.3.1 Background Considerations

The most significant advantage of optical heterodyne detection is that the LO can be set at a power level to ensure it is significantly higher than the detector internal noise. The dominant noise energy is, therefore, the quantum noise mechanism in the LO.

5.3.2 Target Detection

The targets are restricted to cooperative objects in or near synchronous orbits. As such, any valid target will be configured with a pattern of passive retroreflectors. The deployment and characteristics of the passive, cooperative target are discussed in Section 4. The results of the analysis indicate that the mean cross section can be as much as 64.4 dB above a square meter. Since the range interval which is being searched is restricted in magnitude to 5% of the maximum system range (15 nmi), the target return amplitude will be used as the initial basis for rejecting spurious targets, which will have signigicantly smaller cross sections. In addition, the cooperative retroreflectors will reflect the energy in the same polarization as it was transmitted, while the spurious target will be randomly polarized.

If a very high order of discrimination against spurious targets is desired, an optically cross-polarized detector channel can be implemented. Thus, the ratio of the in-phase to the cross-polarized component of return can be measured. This can furnish an additional pulse basis for discriminating against false echoes, minimizing the possibility of locking on false targets.

5.3.3 Corner Cube Reflector Considerations

When the rendezvous ladar is being used on a cooperative target in orbit, the target could conceivably have a single corner cube reflector with its optic axis oriented tangential to the orbit. The Tug would be in a nearly coplanar orbit with the target. The off-axis look angle of the rendezvous ladar will be nearly the same as the off-axis angle with respect to the corner cube (Figure 5-8).

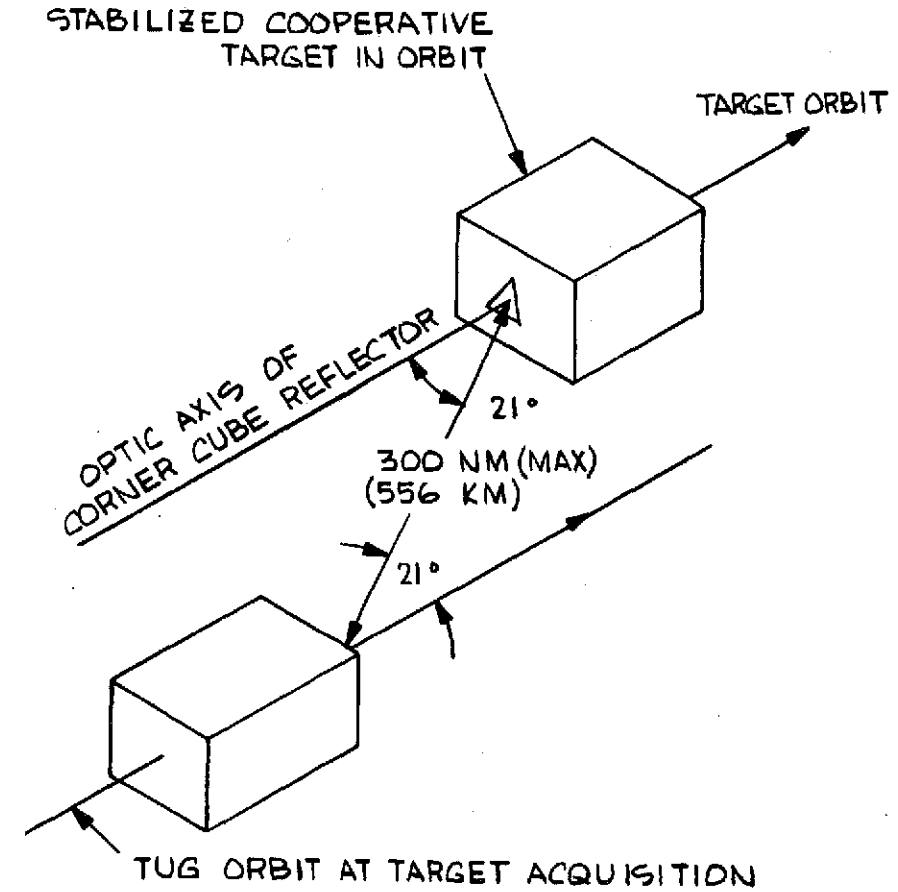

NOTE: THE ORBITS ARE CURVED, WITH A RELATIVELY LARGE (22000 NM) RADIUS. AT THE 300 NM (556 KM) DISTANCES THE GEOMETRIC RELATIONSHIPS CAN ALL BE CLOSELY APPROXIMATED BY STRAIGHT LINES AS SHOWN.

Figure 5-8. Off-Axis Look Angle

Using data from Skolnik's "Radar Systems Handbook," (Section 27-18) it is seen that +70 dBm effective cross section corner cube is 18.1 cm on edge, ideally, or 21.5 cm on edge, assuming 50% optical efficiency. At off-axis angles of 21°, the radar cross section of the reflector is about 5 dB down. This gives +65 dBm effective cross section for the target when the total off-axis angle is less than 21°, corresponding to the total angle (i.e., 15 by 15°) of the 30 by 30° field of view (Figure 5-9).

The typical geometry of a corner cube reflector is shown in Figure 5-10. The off-axis angular response is the same at all wavelengths. The radar cross section, however, rises rapidly as the wavelength, λ, decreases, provided the surfaces of the corner cube reflectors are flat and aligned to one-quarter wave or better.

5.3.4 Signal/Noise Considerations

The transmitted pulse shape of the rendezvous ladar is determined by the Q-switching mechanism; it will be a Gaussian shaped pulse, 350 nanoseconds wide at the one sigma points.

The Fourier transform of the pulse gives a Gaussian spectrum with one sigma (in the frequency domain) of 909 kHz, or a double-sided bandwidth of 1818 KHz*. The matched filter for this waveform is a Gaussian bandpass of $B\tau = 0.44$ ** where

B = Bandwidth and

τ = Pulse width = 350×10^{-9} s

giving $B = 1.3$ MHz

- - - - - - - - - - -

*Reference Data for Radio Engineers, Fifth Edition p. 42-6, 1968.

**Lawson & Uhlenbeck, "Threshold Signals," *MIT RADLAB* Series, Volume 24, p. 208, 1950

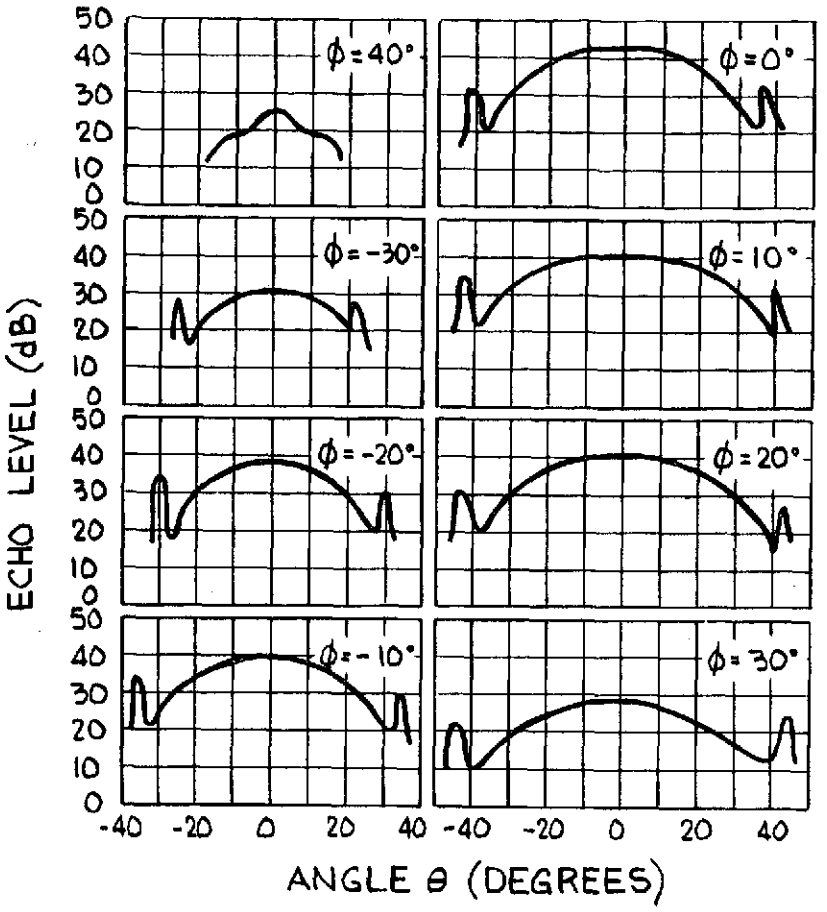

Figure 5-9 Echo-Response of a Corner Cube Reflector

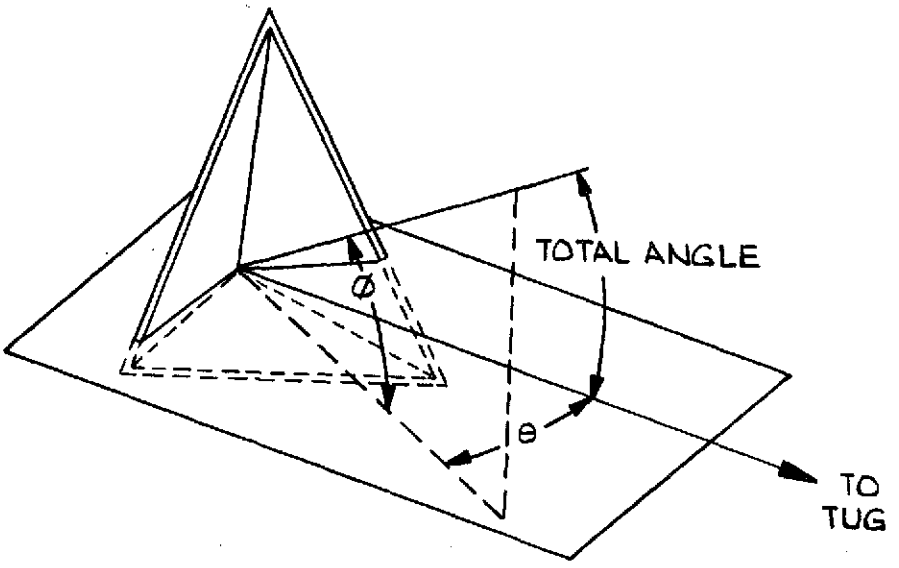

Figure 5-10 Corner Reflector

In this system, however, there is a Doppler uncertainty based on an unknown closing velocity between 0 and 61 meters per second, giving a Doppler bandwidth of

$$f_d = \frac{2V}{\lambda} = \frac{2 \times 61}{10.6 \times 10^{-6}} = 11.51 \text{ MHz}$$

The total bandwidth required to pass any signal at any Doppler is the sum of the Doppler plus the required Gaussian spectrum as shown in Figure 5-11.

Since the quantum noise is proportional to the noise bandwidth, the signal processor will divide this total bandwidth into a series of subbands. The pass bands must necessarily overlap, since a signal which falls between two bands should be detectable with minimum performance degradation. A parametric study of the response of Gaussian filters of various bandwidths and with off-center (detuned) signals was made. The result showed that a set of 2 MHz wide filters spaced 1440 KHz apart, would be within 1 dB of optimal performance and would have only 0.5 dB performance variation for any signal within the Doppler band. This showed that eight filters were required. Each filter defines a Doppler band of 1.44 MHz, giving a one-pulse Doppler measurement to that accuracy.

To minimize cost, it was decided to include a low-noise, 12-MHz bandwidth, 30 dB gain, preamplifier, thus permitting each 2-MHz filter section to be noncritical and low cost. The preamplifier will have a 2-dB noise figure. This is followed by an eight-channel distribution amplifier (see Figure 5-7).

The filter amplifiers will be logarithmic with 80 dB dynamic range. They will take a -60 dBm signal and provide two outputs compatible with ECL (emitter coupled logic) and/or CMOS logic, respectively.

The eight channel outputs are thresholded and used to drive an eight-input ECL (emitter coulped logic) OR gate. ECL is used for its short time delay, to preserve range information accuracy. The OR gate output goes to the vehicle computer.

The CMOS is used for a logic system of gates and latches to identify the Doppler channel within which a signal has been received. This provides velocity information to ±4 meters per second.

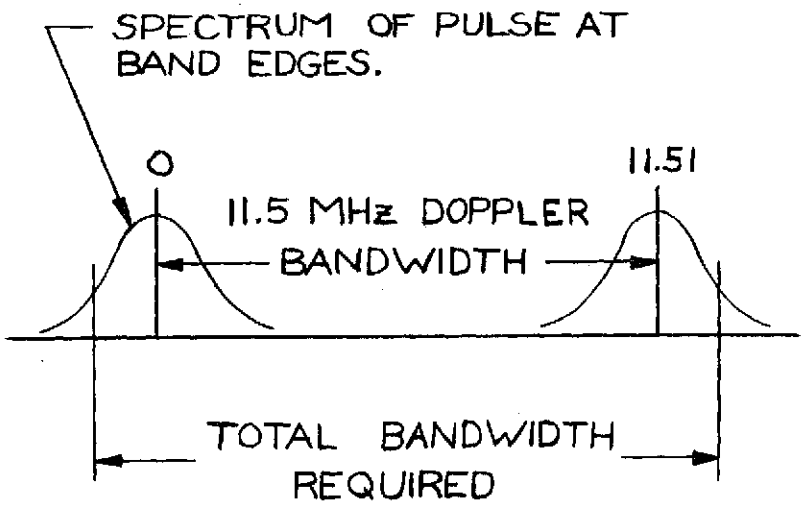

Figure 5-11 Bandwidth Requirements

A computer-adjustable threshold will provide a minimum threshold control to effectively discriminate against small amplitude echoes; i.e., AGC action.

The individual channels are coupled to differential comparators and AND/NAND gates to discriminate the largest amplitude response. The output of the gates is latched and coupled to an 8:1 multiplexer to provide the computer with the information; i.e., the strongest Doppler channel. To avoid the (small) possibility of two equally strong channels, the comparators will be given a hysteresis bias so that their outputs will be in a clearly defined state. The hysteresis will be not more than 0.05 filter bandwidth.

If the system, as described, were to encounter tumbling or spin stabilized spacecraft then the Doppler return would be broadened in proportion to the circumferential velocity of the target about is own axis. This would not be significant unless the Tug was skin tracking and the circumferential velocity of the skin was above 4 meters/second, corresponding to a Doppler of 750 kHz and a 76 RPM for a 1 meter diameter spacecraft (Figure 5-12).

If the spacecraft had a group of corner cube reflectors distributed at regular angular intervals (e.g., 20°) about the skin axis, then the significant portion of the target return would be from the corner reflector whose optic axis was facing the rendezvous ladar. The motion of the ladar is essentially translational, and the Doppler smear would be proportional to the sine of the off-axis angle. (e.g.,: sin 20° = 0.35 and the Doppler smear effect would be reduced to ± 258 kHz for a 1 meter diameter spacecraft spinning at 76 RPM.)

If the corner reflector were spinning around its optic axis, or around an axis at a small angle to the optic axis of the reflector, the effect would be an amplitude modulation of about 1 Hz and result in some narrow-band Doppler, well within the 2.0 MHz filter bandwidth.

5.3.5 Ranging

After the rendezvous ladar finishes its search mode and a target is selected, it will be aimed (at the direction of the vehicle computer) at the target and precision ranging will be performed. The purpose of this precision ranging is to resolve remaining range ambiguities.

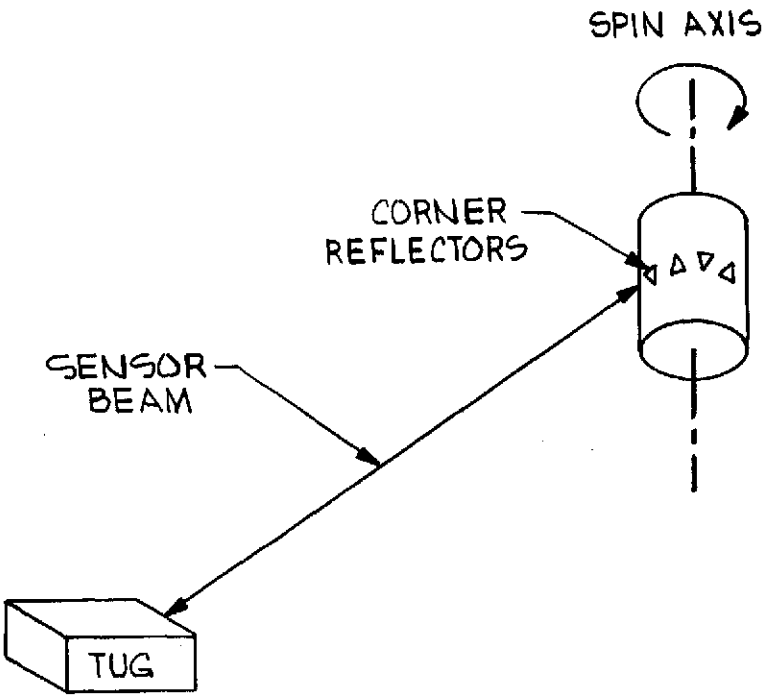

Figure 5-12 Spin Stabilized Spacecraft with Corner Reflectors

Preliminary range has been determined since the offset mirror was searching only a small range interval. When a return indicates a valid target, either the scan can be stopped or the target location can be stored. The telescope will then be pointed at the target, scanning will cease, the target will be tracked in angle, and the precision ranging sequence will commence. This procedure will be directed from the vehicle computer.

During the precision ranging process, the PRF is set at its nominal value, and the range is ambiguously determined. The PRF is then varied until the target return falls into a set of predetermined values, and the values of these secondary PRF intervals are used to compute the unambiguous range. The range accuracy will have a variance of 0.5 meter. Range rate is derived from successive range measurements.

5.3.6 Blind Ranges

The pulse rate of the transmitting laser can be varied from 30 to 50 kHz. Each transmitted pulse has to decay by 50 to 70 dB for the received echo to be visible and/or unaffected by backscatter of the transmitted pulse. Since the transmitted pulse is Gaussian, this corresponds to the 4 sigma limit or about ± 0.70 microsecond about the pulse peak (i.e., a total of 1.4 microseconds). The backscatter of the transmitted pulse will be about 80 dB down at the detector. Each transmitted pulse will blind the rendezvous ladar about 1.4 microseconds. The data processing system will keep track of the relative position of the transmitted pulse within the interval between transmitted pulses and make adjustments to the PRF to prevent the prolonged coincidence of the echo and the received pulse. An adjustment range of ± 5 microseconds in the interpulse interval will, in all cases, be more than sufficient to avoid interference with signal processing. Prior to target acquisition, the time occupied by the transmitted pulse will be 4.7% of the 30-microsecond interpulse interval, reducing the probability of detection by a factor of 0.95.

Each of the eight Doppler channels in the signal processor has its own statistically independent probability of false alarm. Since the overall false alarm probability is 8×10^{-7}, each channel requires a false alarm rate of 10^{-7}. The system requires an overall probability of detection of 0.5.

If the overall probability of detection is to be 0.5, then taking the blind zone factor of 0.95 into account, the probability of detection with respect to random noise must be greater: i.e.,

$P_d' = 0.95 \times P_d$
$= 0.52,$

where

P_d = Probability of detection and

P_d' = Probability of Detection with respect to noise.

This requires a signal-to-noise ratio of 12.0 dB* to provide the necessary signal-to-noise ratio for the combined P_{fa} and P_d.

In this analysis target fluctuation has not been considered. Target fluctuation would be a factor in skin tracking where the echo would be a random sum of scattering centers on the target. For a cooperative target, the corner cube reflector provides a single dominant coherent echo. Fluctuations have been allowed for by assuming +60 dBm target cross section in the worst case (off-axis). On-axis, +70 dBm cross section will be realized. The average probability of detection will be greater than the worst case value computed above.

5.3.7 Precision Ranging

The true range, R, and the observed range, α, are related by an expression of the form

$$R = m\left(\frac{cT}{2}\right) + \alpha$$

where:

m is an interger,

$\frac{cT}{2}$ is the maximum unambigous range,

T is the pulse repetition period,

c is the velocity of light.

In other words, the true range is the observed modulo $\left(\frac{cT}{2}\right)$. Additional information is required to determine the integer m. Two measurements are therefore performed, corresponding to observation of α and β, at respective pulse repetition periods

---

*Skolnik's "Radar Handbook," page 2-19, Figure 4.

T_1 and T_2, for the same value of m. This yields

$$R = \tilde{m}\left(\frac{cT_1}{2}\right) + \alpha = \tilde{m}\left(\frac{cT_2}{2}\right) + \beta$$

Solving for $\tilde{m}$, one obtains a number very close to the integer m (as the following error analysis shows). The value found for m can then be used to evaluate R by means of the equation.

$$R = m\frac{cT}{2} + \alpha.$$

This measurement is implemented by varying the PRF, between 30 kHz and 50 kHz, until the target return is made to fall at a set of predetermined values with respect to the main bang. These are the values of α and β. The predetermined values are set by generating early and late gates which are used to close a loop around the PRF. The timing is shown in Figure 5-13, and the control logic in Figure 5-14.

Subsequently, the echo signals passed by the early and late halves of the split gate are separately integrated. The difference of the integrated signals is used as an error signal to vary the pulse repetition period in a direction such as to cause the echo pulse to exactly straddle the 25 μs point. The value of T_2 is measured by counting the output of a nonsynchronous 10-MHz clock during one hundred radar pulses. The procedure is then repeated for a value α corresponding to 5 μs on the time scale, and yields a count for T_1.

Initially, the split gates are wide and fill most of the unambiguous interval from 0 to T, in order to supply a correct error signal to the pulse-repetition-period control loop. When the echo signal is approximatley centered (i.e., when the error signal has fallen below some predetermined value) the halves of the split gate are narrowed to 0.7 times the pulse width. They are symmetric, which minimizes the effect of noise.

5.3.8 Error Analysis

The error analysis (see Appendix F) shows that:

a. Where $\hat{m}$ is computed, the value obtained differs from the true value of m by a quantity very small compared to unity, so that there is no possibility of an error in the selection of the integer m.

b. The range R is determined with a standard deviation σ_R = 0.42 m.

c. The range rate R, obtained by taking the difference of two range measurements spaced 10 seconds apart, has a standard deviation σ_R = 0.06 m/s.

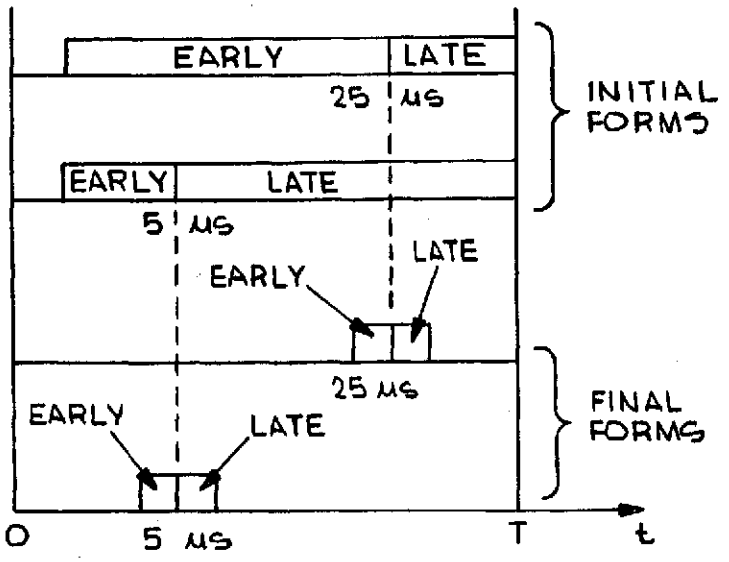

Figure 5-13 Split-Gate Timing

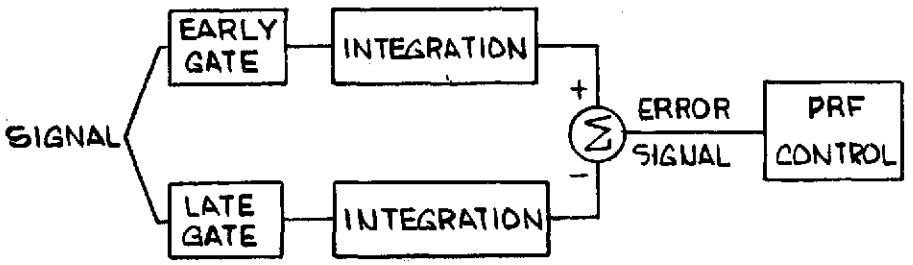

Figure 5-14 PRF Control Loop

5.4 Docking Implementation

The accurate alignment of the Tug and the satellite prior to docking, is implemented by the following:

a. The ladar, powered by the low-power LO, performs a conical scan, of semicone angle β. The scan is performed by a motion of the pointing mirror, under control of the vehicle computer.

b. A special circular target, shown in Figure 5-15, centered on the mating face of the satellite.

5.4.1 Docking Surface

The target consists of two concentric sections. The main section is an annulus, A, whose reflectivity depends only on the distance, r, from the center of the target, being a maximum for small values of r and a minimum for larger values. Specifically, the reflectivity η (r) can be written

$$\eta(r) = ke^{-ar}$$

This effect can be achieved by a series of narrow concentric annular zones, alternately of very high and very low reflectivity. The ratio of the widths of two adjacent zones is appropriately tapered as a function of r. The maximum width of a zone is such that it constitutes a small fraction of the diameter of the light spot on the target.

The second section, B, is a circular area whose surface has a low-level peaked backscatter pattern, which is a function of the angle of incidence only. A possible design of such a special reflector is described in some detail below.

The reflector consists of a sheet, transparent to the wavelength of the CO_2 laser, with identical patterns of black opaque pigment deposited on both sides in a precisely matching relationship. One of the sides is backed by a white surface whose roughness makes it a good light scatterer (see Figure 5-16a).

The operation is as follows. Light incident in a direction normal to the reflector surface passes through the two layers of black pigment, seen in perfect register, and illuminates the exposed white surface. The light scattered by the white surface is returned to the direction of incidence. Light incident at an oblique angle illuminates a portion of the white scattering surface. The portion of the white scattering surface is smaller as the angle of incidence increases, which results in a decrease of backscattered energy.

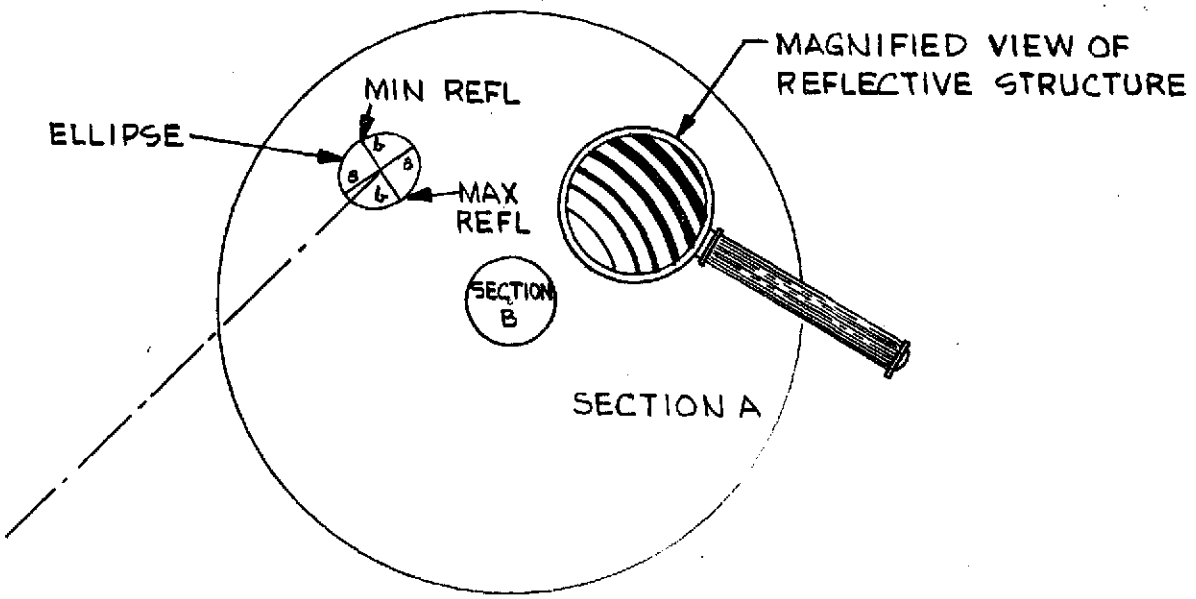

Figure 5-15. Docking Target and Scanned Ellipse

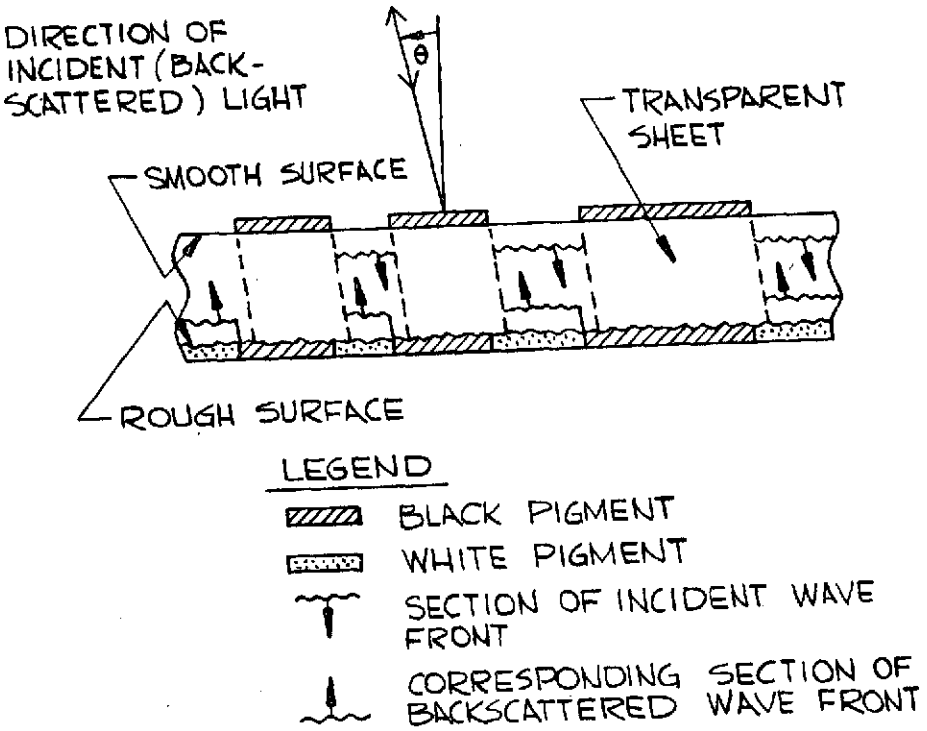

Figure 5-16a. Detail of Cross Section

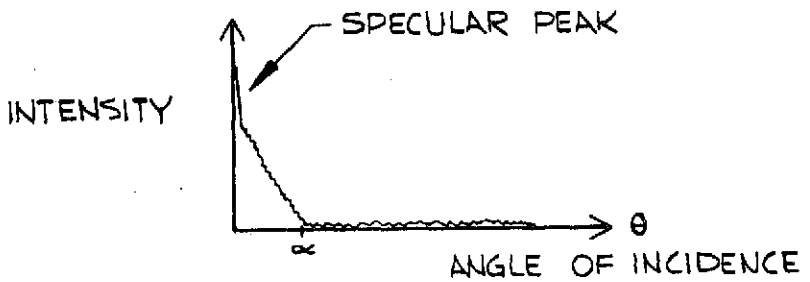

Figure 5-16b. Backscatter Diagram of Random Pattern

In general, if the black pigmented pattern has circular symmetry or exhibits a randomness which gives it an isotropic property, then the amount of back scattered energy is a function of the angle of incidence only.

In can be shown that the backscattering diagram is related to the autocorrelation function of the black pigmented pattern. This fact makes it possible, given the desired back scattering, to compute the required pattern.

In the case of interest here, the pigment pattern is random and isotropic. The backscattering diagram resulting from such a configuration is shown in Figure 5-16b. The width, α, of the peak is inversely proportional to the spatial frequency (average number of spots per mm of the random pattern). The spike at the center of the peak is a result of the specular reflection on the front surface at normal incidence.

Three possible methods are suggested for the generation of the random pattern.

a. Microscopic pigmented resin particles are dispersed in a chamber and allowed to settle on a clean glass plate until they cover approximately 50% of the glass surface. They then are fixed by heating of the glass substrate. The pattern is photographically reproduced, with suitable change of scale.

b. A photographic plate is exposed to laser "speckle," developed, and suitably scaled in size.

c. The pattern can be generated by a computer program and printed by a suitable computer peripheral device (plotter or CRT and photographic camera).

Figure 5-17, illustrating the docking geometry, shows three quantities which are to be reduced to acceptably small values prior to docking. They are:

(1) The radial misalignment r,

(2) The angle θ between the axes of the two spacecraft (not necessarily coplanar),

(3) The distance, or range, R, between the mating surfaces.

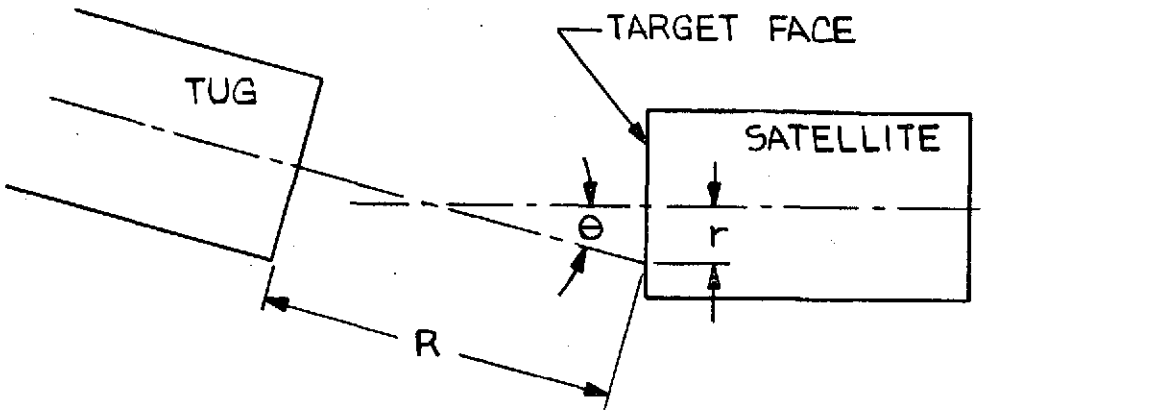

r : RADIAL MISALIGNMENT
θ : ANGULAR MISALIGNMENT
R : RANGE

Figure 5-17. Docking Geometry

5.4.2 Sensing of Range

If, as a result of a conical scan of semi-cone angle β, (see Figure 5-15) the light beam paints a circle of radius r^1 on section A of the target ($r \neq o$, $\theta = o$), the reflected power will fluctuate between a maximum and a minimum value, corresponding to distances from the center of the target $r-r^1$ and $r+r^1$ respectively. The ratio of the maximum and minimum reflected powers will be

$$\frac{ke^{-a(r-r^1)}}{ke^{-a(r+r^1)}} = e^{2ar^1},$$

a quantity independent of the radial misalignment r, but dependent on the radius r^1 of the painted circle.

The range, or distance between the sensor and the target, can now be sensed by adjusting the scan angle β so that the ratio of maximum and minimum reflected powers equals a known value A

$$A = e^{2ar_o}$$

i.e., so that the radius of the painted circle equals r_o.

From the geometry, the range, R is given by

$$R = \frac{r_o}{\beta \text{ (radians)}}.$$

In general, the figure painted on the target will be an ellipse of small eccentricity (for an angular misalignment $\theta = 15°$, the ratio of the semiminor and semimajor axes a and b equals $\cos 15° = 0.966$) so that the value of range obtained from the above measurement will be in error by a few percent. The accuracy of the measurement improves, however, as

a. the angular misalignment θ decreases, which decreases the eccentricity of the ellipse; and

b. the range R decreases, since the required cone angle β will be larger, while the noise or uncertainty in β remains a constant.

5.4.3 Sensing of Radial Misalignment

The direction and sense of the radial misalignment are dervied from a knowledge of the scan coordinates ϕ_{max} or ϕ_{min} (the scan spin angles at the moments of maximum or minimum reflected power) (see Figure 5-18.)

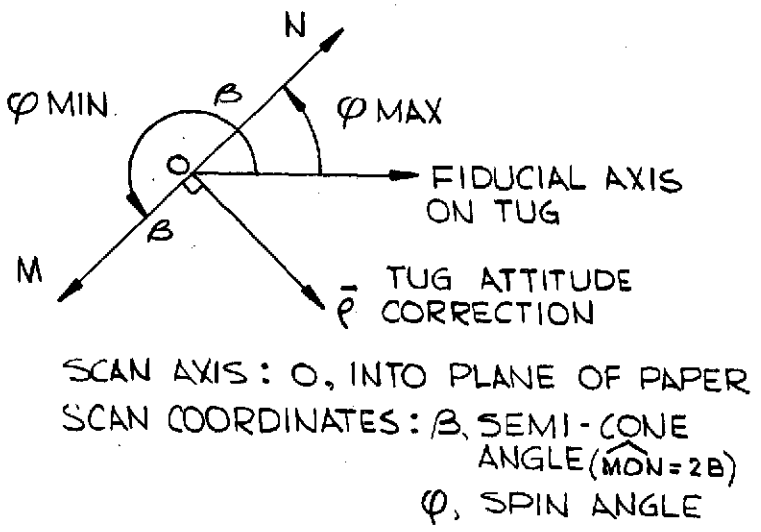

Figure 5-18. Correction of Radial Misalignment

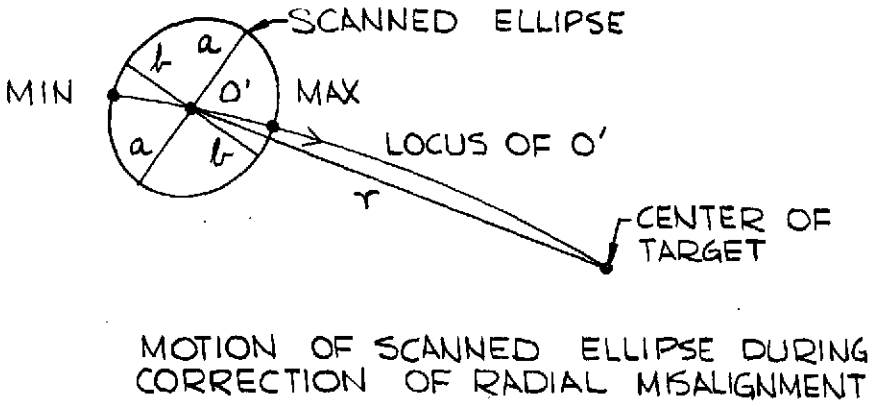

Figure 5-19. Motion of Scanned Ellipse During Correction of Radial Misalignment

The required correction is a rotation of the tug about the axis ρ, in a right-hand screw convention.

In general, a sequence of such corrections will cause the center of the painted ellipse to approach the center of the target not in a straight line, but in a very slightly curved line, as shown in Figure 5-19.

The magnitude of the required correction is not known. As the radial misalignment r is reduced to a small value, the ladar illuminates increasing portions of the central circular area of the target face, section B. The low reflectivity of section B causes increasingly long dips to appear at the output of the light detector, signalling the approaching end of the radial correction phase. That phase is ended when the entire conical scan falls into section B.

5.4.4 Sensing of Angular Misalignment

Here again, in each scan period, there will be a point of maximum and a point of minimum backscattered light power, as illustrated in Figure 5-20. For a given angular misalignment, θ, the ratio of maximum to minimum outputs will be larger at smaller ranges, which is desirable. As the value of θ decreases, the fluctuations in output decrease and finally vanish.

The required correction is known in direction and sense, as was the case for the correction of radial misalignment; it is a rotation of the Tug about an axis Ψ in the plane of the target. In addition, the magnitude of the required rotation can be approximately calculated from the known backscatter pattern of the surface of section B.

5.4.5 Sequencing of Corrections

As the alignment proceeds, the three sensing modes and the subsequent corrections can be sequenced or performed simultaneously; initially, the sensing of R and r, and finally, the sensing of R and θ. This latter sequence is obtained by deliberate offsets of the scan axis to alternate between conical scans in sections A and B.

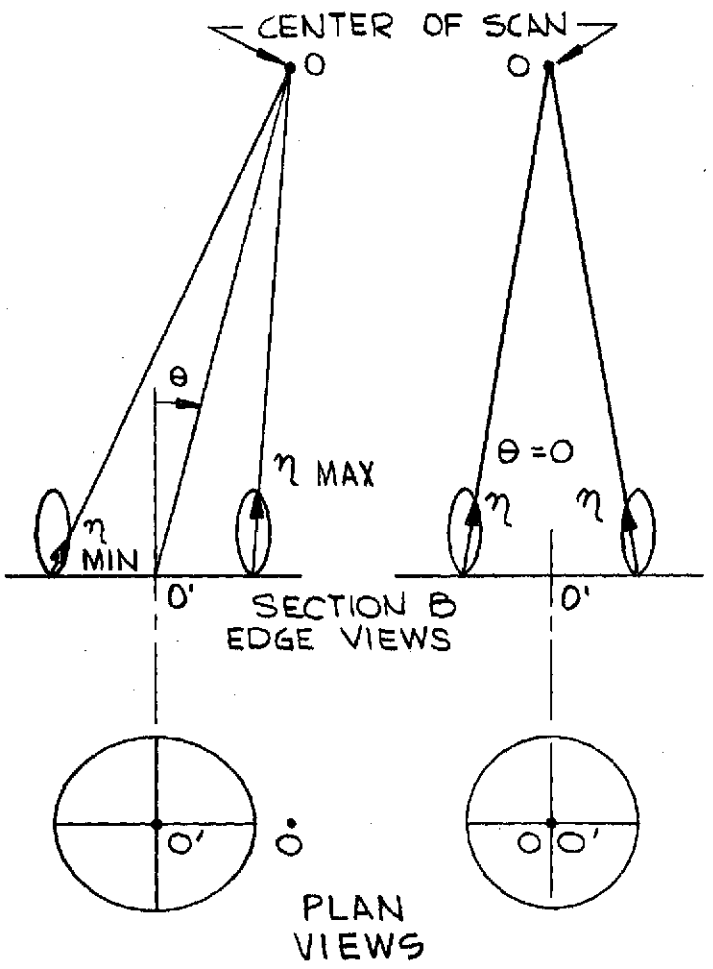

θ≠O: POWER FLUCTUATES ; θ=O: POWER IS CONSTANT

Figure 5-20. Backscattering Pattern at Two Opposite Points of Scan

5.5 Power Supplies

The DC power supplies for the rendezvous sensor will be designed for high efficiency and easy implementation.

5.5.1 High Power Section

5.5.1.1 Main Laser

The excitation of the main laser will be the single largest load on the system. The laser is essentially a negative resistance plasma discharge, requiring a characteristically high voltage and low current. The plasma discharge is anticipated to require 11 mA at 5500 volts. The laser also requires about 11,000 volts to initiate the discharge.

The negative resistance of the discharge requires that a stabilizing impedance be used. An inductor is to be used in conjunction with a high frequency switching regulator set to regulate the plasma current in a current limiting mode. The main laser will be set to hold the beam current with ± 10% limits about its mean value. The LO high voltage drive will be derived using the same type of circuit. However, the current will be more closely regulated to ± 3% within its cyclic limits.

A simplified schematic of the proposed laser power supply is shown in Figure 5-21. A single high power transistor is used to perform the combined functions of a DC DC converter and a current regulator. The operation of the circuit is as follows.

The current through the laser is sensed by R1. When the current is too low, amplifier A1 turns on the driver transistor Q1. The collector voltage on the drive transistor goes low. The voltage is used to provide a hysteresis latching effect required for the proper operation of the switching regulator.

When the driver is turned on, a high positive voltage is applied to the rectifier and inductor filter, causing the current to the load to increase. When the current exceeds a certain value, the driver is shut off. The current through the inductor L1 will decrease until the driver turn-on threshold is reached and the process is repeated.

Amplifier A2 senses the current in resistor R2. When the current in R2 exceeds a threshold, A2 triggers the one shot which switches off the driver via A1 for the pulse period of the one shot.

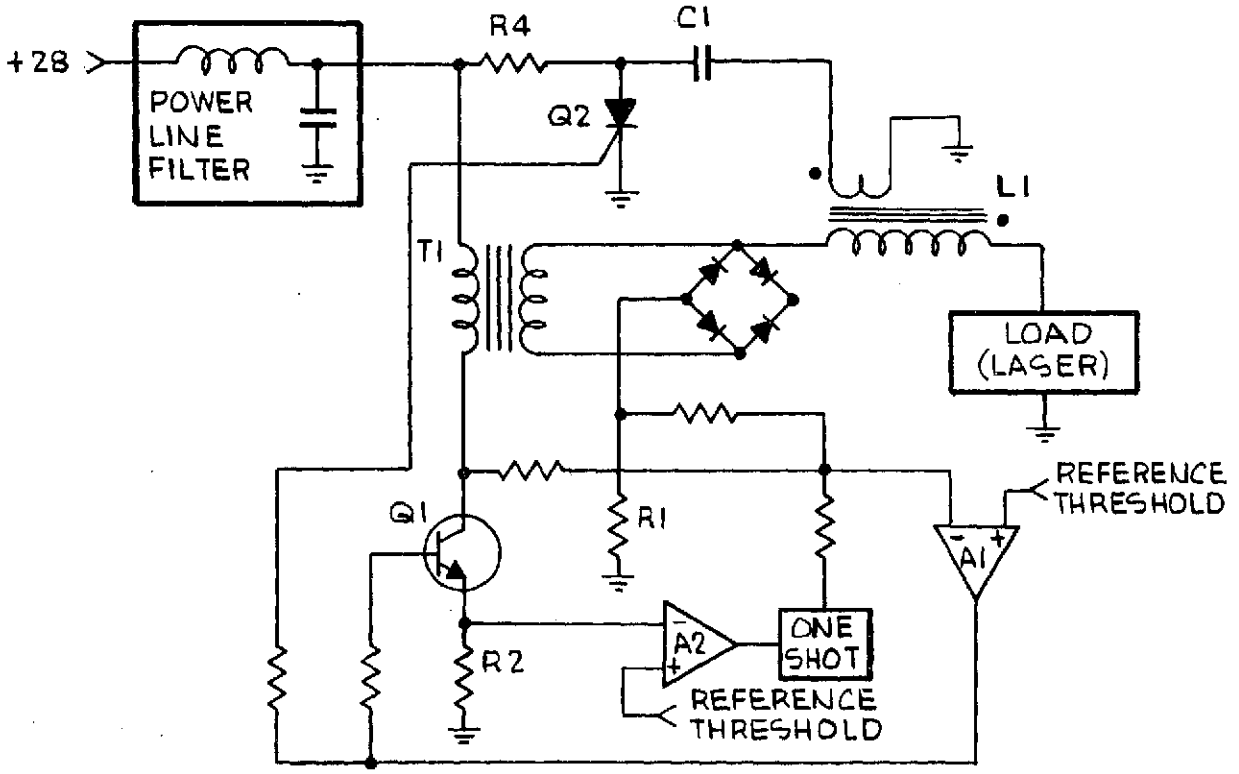

Figure 5-21. Laser Power Supply

The loop is also used for start-up. The load current in L1 builds up slowly, since transformer T1 will saturate if the driver transistor is left on too long. The load current will require 10 cycles to reach its operating value, at which point the feedback loop through amplifier A1 controls continuous operation.

A full wave rectifier is used to damp the backswing of T1, diverting the energy to the load.

Inductor L1 is also used to couple an ionizing pulse to the laser tube by transformer action. Q2 is an SCR pulse generator which is automatically triggered by the turn-on signal to Q1. Q2 fires only once, discharging C1 through the auxiliary winding on L1 to generate the starting pulse. R4 limits the DC current drawn to a low value, since Q2 is always in the ON STATE during operation.

The system will operate at 68 kHz nominal frequency. L1 and T1 will be ferrite core inductors of the E1-375 size. Each will weigh about 75 grams and be 4.0 by 3.7 by 2.6 cm in size. The efficiency of the high power supply will be 67%, comprising switching, I^2R, and other losses.

5.5.1.2 LO Laser

The LO power supply will be similar except that it will be smaller in size and in power rating. The estimated size of L1 and T1 is EI-187; 2.2 by 2 by 1.5 cm with a weight of 10 grams each.

The LO inductor and transformer sizes are disportionate because of wire size limitations. The nominal operating frequency will be 57 kHz. The LO will operate with 1000 volts at 2 mA. The LO supply will be about 60% efficient.

The LO inductor and transformer sizes are disportionate because of wire size limitations. The nominal operating frequency will be 57 kHz. The LO will operate with 1000 volts at 2 mA. The LO supply will be about 60% efficient.

The CO_2 laser has the property of filtering the current ripple. Fluctuations of ± 10% in current will induce less than a ± 0.5% change in optical output. Correspondingly, the LO current regulation of ± 3% will hold the optical output changes to a negible value.

5.5.2 Low Voltage Section

The low voltage supplies for the amplifiers in the signal processor and the mirror drive units will be ±5 volts, and ± 10 volts derived from a square wave DC-DC inverter (Figure 5-22).

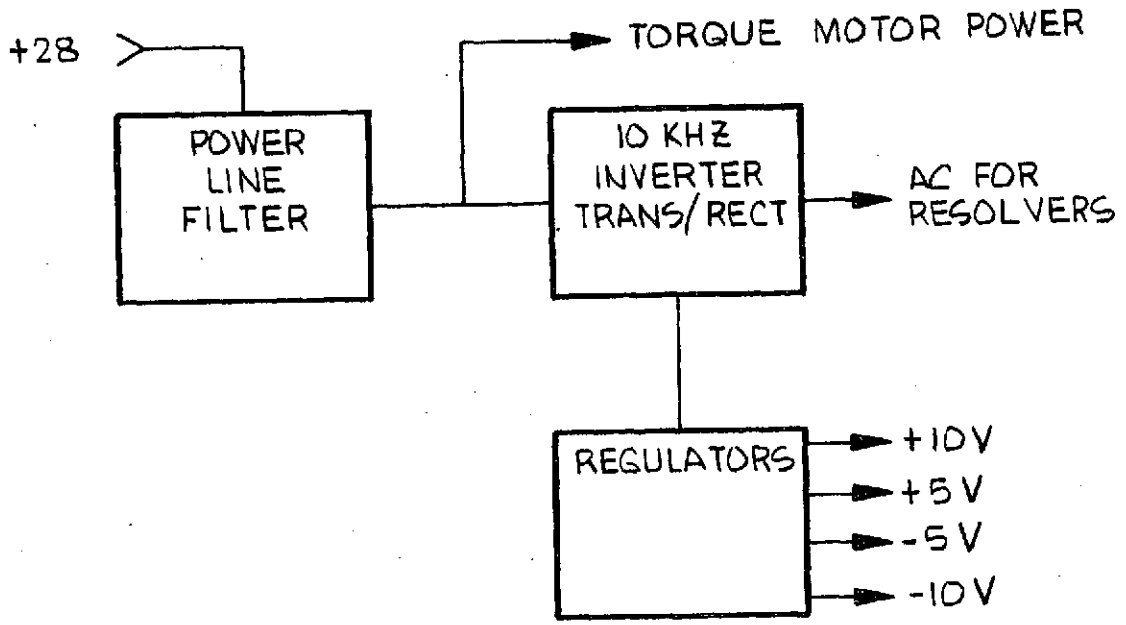

Figure 5-22. Low Voltage Power Supplies

The inverter would also derive an AC voltage for the resolvers. The operating frequency will be 10 kHz.

The 5-volt supplies will be for the digital circuits. The 10-volt supplies will be closely regulated and will serve as reference voltages for analog control functions. The voltages will be regulated at the supply. Separate reference voltage lines will be required for accurate reference voltages without IR drops from OP-AMP loads.

Torque motor drive power will come directly from the 28-volt line.

All the auxiliary loads are estimated to be less than 30 watts. The auxiliary power supplies will average 50% efficiency.

5.5.3 EMI

Primary power line filters will be used to suppress EMI generated by the switching regulators and inverters. Because of the high frequencies and fast rise times, shielding will be required to suppress radiated noise.

In the low voltage section, output voltages will be filtered at the point of use; e.g., on the circuit card, to control EMI problems.

5.5.4 Size and Weight

The power supplies will fit into a 10 by 10 by 20 cm (2 liters) volume and will weigh 1000 grams. Heat sinking will be required on a 10 by 20 cm (200 cm^2) face.

6. INSTALLATION CONSIDERATIONS

6.1 Mechanical

From a mechanical viewpoint, the laser system consists of two lasers; two gimballed pointing mirrors; a series of folding mirrors, beamsplitters, lenses and optical hardware; a primary detector array with a radiation cooler; and an electronics package.

The many elements are mounted in a housing designed to provide the required functional support; a window opening for light passage; internal thermal isolation for the detector array and radiation cooler; and a thermally conductive path from heat sources to the heat sink within the spacecraft.

The main and LO lasers are functionally mounted into the housing. Extending outward, they are supported by cantilevered shelves. The shelves also serve to conduct most of the heat dissipated into the main housing, and then into the spacecraft.

Two degrees of freedom, $\pm$ 7½° in azimuth and $\pm$ 7½° in elevation, are provided for the pointing mirror, which is moved and controlled by torquers and resolvers in the two axes.

The receiving range-angle compensating mirror and transmitter scanning mirror oscillate on resonant vibrators.

The one removable mirror is mounted on bearings; it can be moved in and out of the line of sight by energizing a motor and gear train.

The stationary optical elements are pin mounted with provision for both linear and angular adjustments.

6.2 Heat Dissipation

6.2.1 Detector

The most critical of all heat to be dissipated is 10 milliwatts from the detector. The heat dissipation by the radiation cooler is well within the capability of the unit selected.

The detector array with its radiation cooler is designed for the mission requirements. Detector temperatures of 90 to 100 K will be maintained by radiation to outer space. The particular cooler selected is presently utilized in several space applications.

6.2.2 Heat Sinks

The remaining parts of the system will be designed for conductive cooling to the spacecraft and then radiation to outer space. Heat dissipators will be conductively mounted to appropriate heat sinks. Heat sinks will be aluminum bus bars, possibly reinforced with heat pipes when the power levels are high enough to justify their use. Since the spacecraft provides the ultimate heat sink for the system, the final design will minimize path lengths and shape factor problems so that minimum material will be required.

6.2.3 Power Dissipation

Preliminary estimates of power dissipation indicate that direct conduction to heat sinks will be adequate for all functions. The power to be dissipated, for a typical ladar is estimated to be as follows:

OUTPUT LASER POWER	MAXIMUM RANGE (8" REFLECTORS)	PROCESSING & LOCAL OSC.	MAIN LASER	TOTAL DISSIPATION
2W	300NM	63W	30W	93W
4W	350NM	63W	60W	123W
10W	500NM	63W	150W	213W
20W	600NM	63W	270W	333W

6.2.3.1 Transmitter

The majority of heat in the optical assembly is associated with the transmitter (main laser). The power to be dissipated can be directly coupled to a heat sink in the package. An alternative is to mount the laser directly to a heat sink in the spacecraft, which would require the addition of a folding mirror for orientation. Although somewhat more difficult to implement, the latter approach would reduce the weight by about 500 grams. The small laser (LO) and torquer motor account for only 4 watts which can readily be dissipated without special consideration.

6.2.3.2 Electronics

The electronics account for 36 watts while the power supply will dissipate about an additional 60 watts. These functions can be installed in a single 10 x 15 x 20 cm box or can be fabricated in two separate boxes. The circuit boards will

be conductively designed to carry component heat to conductive slides. The slides in turn will carry the heat into the box walls and eventually into spacecraft heat sinks. This type of design is common and does not present any special problems. There will be sufficient flexibility for the box housing to be sized and shaped to meet the requirements of the space vehicle.

6.3 Weight

CO_2 Ladar Weight Breakdown

MAIN COMPONENTS	WEIGHT (grams)
Case and Hardware	5800
Radiation Cooler	1360
Optical Train	536
Mounts	268
Local Oscillator	450
LOPS	100
Circuitry	1000
LVPS	425
Main Laser and Power Supply	
2 watt	2232
4 watt	2965
10 watt	4113
20 watt	5831
TOTAL SYSTEM WEIGHT	
2 watt	12,171
4 watt	12,904
10 watt	14,052
20 watt	15,770

7. COMPARISON WITH ALTERNATIVE SYSTEM (GaAs)

As a portion of the study, the CO_2 ladar has been compared with an existing sensor. This is a laser sensor that uses a pulsed Gallium Arenside injection laser as the transmitter, and an image dissector as the detection/tracking device. The GaAs laser system has been developed by NASA/Marshall Space Flight Center under several previous contracts. The parameters of the GaAs laser system were supplied by NASA in the course of this program. In order to provide meaningful tradeoff data, the comparison was made on two distinct bases.

a. Assuming that each laser has an equal peak power available, what are the theoretical performance limitations relating to each technique?

b. Assuming that each laser is capable of utilizing typical existing laser transmitter powers, what is the performance?

The CO_2 ladar uses a passively Q-switched laser, with a PRF on the order of 32 kHz. The pulse width is fixed by the Q-switching mechanism, and is about 350 nanoseconds. The detector is a four-quadrant photodiode device, which is radiation cooled to 110° Kelvin. The detector is used with a laser local oscillator (LO) to effect coherent heterodyne detection. The single four-quadrant detector is used for both acquisition and track. Average powers of about 20 watts are readily realizable with this type of laser.

The pulsed GaAs laser system operates at 0.9 microns. At the present time, the typical peak power realizable from a practical laser transmitter is about 500 milliwatts. The laser pulse rate is typically 1 kHz. Pulse widths are about 50-100 nanoseconds. The receiver utilizes an image dissector, and a wideband amplifier.

The comparison between the two systems centers on the basic radar equations. For either system, it is possible to calculate the level of the signal returned from the target. The peak power re-radiated from the target is given by

$$P_s = \frac{P_t G_t \sigma}{4\pi R^2},$$

where

P_t = peak transmitted power

G_t = transmit optics gain with respect to an isotropic radiator

σ = target cross section with respect to an isotropic radiator

R = range to target

The power density of the reradiated energy at the receive aperture is

$$P = \frac{P_t G_t \sigma}{(4\pi)^2 R^4}$$

The power captured by the receive aperture is, therefore, given by

$$P_r = \frac{P_t G_t \sigma A_r}{(4\pi)^2 R^4}$$

where

A_r = the receive aperture area

The received signal-to-noise ratio is given by

$$S/N = \frac{P_r}{P_n} = \frac{P_t G_t \sigma A_r}{(4\pi)^2 R^4 P_n L}$$

where

P_n = the noise power

L = system losses

This expression can also be related to receive-optics gain since

$$A_r = \frac{G_r \lambda^2}{4\pi}$$

where

G_r = receive optics gain.

The beamwidth (3 dB) is

$$BW = 2\sqrt{\frac{\pi}{G}}$$

The above parameters are derived from basic physical constants and can be used to predict the performance of either system. The basis of system comparison is a tradeoff of the achievable parameters for each of the systems.

The most interesting and most salient parameter is the effective noise power, P_n. The theoretical limit for heterodyne detection with a photodiode detector is

$$P_n|CO_2 = \frac{h\nu\Delta f}{\eta\rho_o\rho_A} = \frac{hc\Delta f}{\eta\lambda\rho_o\rho_A},$$

where

h = Planck's constant = 6.6256×10^{-34}

ν = laser frequency = c/λ

Δf = noise bandwidth

η = quantum efficiency of detector

ρ_o = optical efficiency

ρ_A = detector efficiency

For the image dissector (which is essentially a beam-steerable photomultiplier) the limiting, or best possible performance, is obtained when the dark current is very small. Therefore, the significant noise is the quantum noise in the received energy. The quantum noise limit (a theoretical performance bound which is seldom realized in practice but which will be used for purposes of comparison) is

$$P_n|GaAs = \frac{h\nu\Delta f}{\eta\rho_o\rho_A} = \frac{hc\Delta f}{\eta\lambda\rho_o\rho_A}$$

7.1 Effective Receiver Noise

Typical values of the parameters that relate to effective noise power are listed in Table 7-1. Relative values have been determined on the basis of best available information and tabulated for comparison.

Table 7-1. Effective Noise Power Parameters

	CO_2	GaAs	$P_n \mid CO_2$
h	6.6256×10^{-34}	same	-
c	3×10^{8} m/s	same	-
Δf	2 MHz	40 MHz	-13 dB
η	0.5	0.02	-14 dB
λ	10.6×10^{-6}m	0.9×10^{-6}m	-10.7 dB -37.7 dB

The effective noise for the CO_2 system is therefore 37.7 dB lower than the equivalent noise for the GaAs system.

7.2 Peak Power

The existing GaAs system uses a 1 kHz PRF, 500 milliwatts peak power, and a pulse width of 100 nanoseconds. Because of the narrow pulse width and low duty cycle, the average laser power is very low.

$$P_{av} = P_t(PRF)(\tau) = 0.5 \times 10^{3} \times 10^{-7} \text{watts} = 0.05 \text{ milliwatts}$$

The CO_2 laser has a 350 nanosecond pulse and a nominal PRF of 40 kHz. For a peak power of 500 milliwatts, the average power is

$$P_{av} = (0.5)(4 \times 10^{4})(0.35 \times 10^{-6}) \text{ watts} = 7 \text{ milliwatts}$$

The CO_2 laser, with a passive Q-switch is designed to be capable of providing 20-watt average power at 10% efficiency. For this case

$$P_t = \frac{20}{4\times10^{4}\times0.35\times10^{-6}} = 1428 \text{ watts.}$$

The ratio $[P_t\ (CO_2)]/[P_t(GaAs)] = \frac{1428}{0.5}$ or 34.6 dB

is the typical peak power advantage of the pulsed CO_2 laser compared to the existing Gallium Arsenide device.

7.3 Transmit Gain

The gain of the exit aperture, relative to an isotropic radiator is given by

$$G_t = \frac{4\pi}{(BW)^2},$$

where BW is the beamwidth in radians.

For the CO_2 system, the 3 dB beamwidth is 0.32 milliradians, and the transmit gain is

$$G_t = \frac{4\pi}{(0.33\times10^{-3})^2} \quad \text{or 80.6 dB.}$$

For the GaAs system, the beamwidth is 0.10°, and the transmit gain is given by

$$G_t = \frac{4\pi}{(0.1)^2} \times (57.3)^2 \text{ or 66.2 dB}$$

7.4 Equivalent Cross Section

The equivalent cross section of a passive retroreflector relative to an isotropic radiator is a function of $1/\lambda^2$. Therefore, the cross section for GaAs (0.9 microns) is greater than that at 10.6 microns by an amount

$$(\frac{10.6}{0.9})^2 \text{ or } 21.4 \text{ dB.}$$

The above equation assumes a diffraction-limited corner reflector at each wavelength. In practice, the diffraction limit -3 dB can be achieved at 10.6 microns, and the diffraction limit -8 dB at 0.9 microns. As a result the 21.4 dB advantage of the GaAs system is reduced to 16.4 dB.

7.5 Receive Aperture

The equivalent receive aperture is given by

$$A_r = \frac{\lambda^2}{(BW)^2}$$

The GaAs system receive aperture is

$$A_r = \frac{(0.9\text{x}10^{-6})^2 \ (57.3)^2}{(0.1)^2} = 2.7\text{x}10^{-7}\text{m}^2$$

For the CO_2 system the receive aperture is

$$A_r = \frac{(10.6\text{x}10^{-6})^2}{(0.167\text{x}10^{-3})2} = 4.05\text{x}0^{-3}\ \text{m}^2$$

Note: The receive beamwidth is one-half the transmit beamwidth for the same physical aperture. The reason is that in receive the aperture is uniformly illuminated, yielding the diffraction limited beamwidth, while in transmit the aperture is illuminated by a Gaussian cross section laser beam, which leads to a wider beam.

Therefore, the CO_2 system with a 3-inch (76mm) physical aperture has an equivalent aperture, which is,

$$\frac{4.03\text{x}10^{-3}}{2.66\text{x}10^{-7}} \quad \text{or 41.8 dB}$$

greater than that of the GaAs system.

7.6 Conclusions

The results of this discussion are summarized for both cases of equal peak powers and respective typical powers in Table 7-2. The range factor clearly shows the superiority of the CO_2 system.

Table 7-2. Equal Peak Powers and Respective Typical Powers

	$\frac{S/N\ (CO_2)}{S/N\ (G_A A_S)}$	
	EQUAL PEAK POWER (dB)	TYPICAL AVAILABLE POWER (dB)
P_t	0.0	34.6
G_t	14.4	14.4
σ	-16.4	-16.4
A_r	41.8	41.8
P_n	37.7	37.7
TOTAL	77.5	112
RANGE FACTOR	86.6:1	631:1

8. TECHNOLOGY IDENTIFICATION AND MEASUREMENTS PROGRAM

8.1 Technology Identification

The CO_2 rendezvous ladar has been configured to be consistent with existing technology. The present configuration can be constructed at this time without any additional basic technology development. The only development that will be required relates to the deployment of the system in a spacecraft environment. There are, however, several areas that should be investigated in order to determine the feasibility of improved performance and/or improvements in size, weight, and accuracy.

8.1.1 Detectors

The detectors may be enhanced by improvements in manufacturing technology of detector arrays. By closely spacing the various individual detectors in an array, the signal energy that would fall on the spaces between the detectors is minimized and the signal-to-noise ratio is optimized.

Present day detectors are spaced from 50 to 70 microns. A substantial gain in efficiency would result in a reduction of the spacing from 10 to 20 microns.

In particular, a closely spaced, quadrantal array for optical monopulse (10 to 20 micron spacing) would be a tremendous improvement over the performance factors achievable with 50 to 70 micron spacing. The 167 micron spot size with most of its energy concentrated near the center is particularly vulnerable. Falling in the middle of a 50 to 70 micron gap may cause power losses up to 6 to 8 dB. A 10 to 20 micron spacing would reduce these losses to the order of 1 dB.

8.1.2 Docking

As presently configured, the rendezvous ladar will depend on corner cube reflectors for (1) long-range acquisition and track, and (2) for a special geometric pattern for use in guidance from 200 meters down to docking.

The rendezvous ladar, as it approaches the target, does not know its relative orientation with respect to the target, since one corner cube reflector is effectively equivalent to another. Reflector brilliance exceeds the skin track return to such an extent that the rest of the target will not be visible. The Tug, in our present plans, would have to execute certain maneuvers, circling about the target in order to ascertain the location of the docking face.

A reduction in docking time as well as corresponding fuel economy (removing the necessity for certain search maneuvers to determine the docking face) might be achieved, if the corner cube reflectors could be put into a predetermined three-dimensional pattern about the surface of the target. The three-dimensional pattern would not be a regular pattern, though of necessity the individual corner cubes would have overlapping coverage. (For example, the angle between their axes would probably have to be less than 28°.) In addition, the pattern would have to be irregular in some controlled manner.

When such a pattern is viewed by a raster scan, one corner cube would appear relatively bright. The other corner cubes would appear to have less brightness and the relative magnitude of the signals could be determined in the signal processor.

It might be possible to recognize (from the angular spacing of the three or four brightest corner cubes in the pattern) the approach angle to the target with respect to the target's own coordinates. The approach angle would be with respect to the docking face and could result in minimum energy and minimum expended maneuver time to align the Tug and the target in the docking position.

For this technique to be implemented, a study of computer pattern recognition techniques should be performed to determine which patterns might be employed and their appearance to the Tug ladar as it approaches in any relative attitude.

It is also possible that the corner cubes might, in themselves, be used to form a pattern suitable for guiding the Tug down to contact. The tradeoff is essentially one of the weight of the fuel saved vs the weight and cost of the corner cubes and the computer size for performing the pattern recognition as opposed to the computer size necessary for executing the various acquisition, tracking and, docking maneuvers. It is believed, however, that the system could be improved by this technique; should it prove simple, it would be very beneficial.

8.1.3 Homodyne Detection Technique

The homodyne detection technique for radar signals is well known. Its use in optical radars such as the rendezvous ladar has, so far, not been implemented. The homodyne technique is used in microwave radars for altimeters and other devices that have problems similar to docking; i.e., an altimeter essentially has to have a wide dynamic range down to a few feet when the aircraft is landed.

Homodyne detection is more noisy than the regular heterodyne detection process because of 1/F noise, both in the detector and in the amplifier following the detector. This is a consequence of the flicker in the laser LO and in the various semiconductors, detectors, and amplifiers. Precise data is lacking, however, it is estimated that the 1/F noise generated by the flicker effect would not degrade performance more than 10 dB.

Homodyne detection is also recommended for an experimental investigation. The object of the investigation should be to derive data based on (1) current LOs, and (2) current detectors vs current targets.

8.1.4 Holographic Applications

In the rendezvous ladar, mixing beamsplitters with losses up to 17% are employed in order to superimpose the LO beam and the received signal with the proper phase fronts on the detector. A suitable reflection hologram might accomplish the process more efficiently. The holographic technique may also be of use in the forming and control of hollow laser beams, circumventing losses resulting from the holes in the plane mirrors in the optical train.

8.1.5 Manufacturing Technology

It is very desirable to investigate methods for the economic fabrication of lightweight corner cube reflectors. In this application there might be as many as 24, or even more, corner cube reflectors on an unstabilized target. The need exists for both a lightweight and a relatively low-cost corner cube reflector of high optical performance.

The application of graphite epoxy with glass or metallic facing to the corner cube reflector manufacturing problem should also be investigated; this is an area which promises to pay very high dividends.

The use of graphite epoxy in the manufacture of the optical train also merits investigation. The graphite epoxy material can be molded to have a wide range of coefficients of expansion and structural strengths. A material is required for the optical train, which is both structurally and thermally stable, since we are dealing with angles typically on the order of 0.167 milliradians. Maintaining the angle tolerances requires that the parts remain in close alignment. However, the requirement for space use also requires that the materials be light and stable in vacuum over time.

8.1.6 Power Supply Technology

The laser load is a negative resistance with a very high impedance characteristic. Present day techniques usually involve either a current-regulated supply or a high-voltage constant-voltage supply, each followed by a ballast resistor wasting up to 50% of the primary power.

The switching-regulator current-type power supply recommended for this application should be experimentally studied to determine the effects of driving negative resistance loads. Data on the actual magnitude of the negative resistance load can be taken and a design formula generated for future use.

An additional item for study would be the self-smoothing effect of the laser vs the frequency of the ripple being applied in the drive current.

8.1.7 Acoustic or Mechanical Modulation

The rendezvous ladar and other airborne lasers are affected by motions of only a few microns. Such motions which may be acoustically induced or which may be induced from other motions (e.g., the scanner, the mirror drive, other machinery, or the engines of the Tug) will induce a modulation on the signal return to the ladar. A measurements program to study the effects of controlled acoustic or mechanical vibration on the ladar is recommended in order to determine the extent of such problems, and to study the techniques for preventing modulation effects from affecting the detectability and lock-on to the target during track.

8.1.8 New Materials Technology

During the study the use of carbon-filament epoxy-bonded composite materials in the optical train was considered. The purpose was to consider an alternative to the beryllium construction. Interest is high in the possibility of saving weight and/or cost, and the possible advantages with respect to beryllium.

The carbon-filament epoxy-bonded material is highly recommended. It is possible to synthesize the material properties by appropriate layering of the carbon-filament woven fabric in such a manner as to generate, literally, any desired coefficient of expansion, including zero. The material is also very rigid with respect to its weight, and is very strong.

The epoxy graphite material was found to be very suitable for structural members of the telescope and maintaining elements in alignment. The epoxy graphite material was also considered for such optical surfaces as the primary mirror, the pointing mirror, or any of the various smaller mirrors.

Presently available data indicates that the material does not have the surface stability for use in the various optical surfaces. Overnight measurements of creep or deformation induced by humidity testing, vacuum cycling, or thermal cycling has shown deviations from flatness of up to 12 microns (which is greater than one wavelength).

The mirrors require flatness to about 1/20 of a wavelength in order for all of the wavefront components of the received signal and the transmitted signal (as they are distributed over the various surfaces) to be essentially in phase. If the elements of the wavefront are not in phase, there is a loss of signal strength varying from a few percent to total extinction when substantial amounts of the wavefront are 180° out of phase. If the transmitted and received radiation does not have a uniform phase front, the beam will broaden and the optical system will lose efficiency. The radiation patterns can become asymmetric, causing a loss in angular accuracy; sidelobe level will also increase. In extreme cases echoes could be received on the sidelobes, generating false target indications.

One fabrication technique that provides the desired surface stability is a thin glass or metal shell optical surface backed by graphite epoxy laminate. The laminate would be suitably fabricated to have a matching coefficient of expansion with the optical surface. The technology is relatively new at this time. Data indicate that a glass thickness of about 0.5 millimeter bonded to a graphite epoxy substrate gives excellent results. The graphite epoxy substrate supports the mirror during launch and absorbs the stresses during scan. The pointing mirror is reversed during scan at the end of each scan line, or 16 times per second.

The mirror material should have a high stiffness-to-mass ratio in order to minimize the forces acting on the mirror. Simply increasing the mass of the mirror to make it strong is self defeating, because the forces are proportional to the mass of the mirror. The scan accelerations are about 1500 centimeters per second squared (1.5g) at the fastest moving edge of the pointing mirror. The greatest stresses are where the driving torque is applied. The torque levels will be in the order of 0.021 newton-meters during scan reversal and zero during the unaccelerated (linear) part of the scan. It is, therefore, only necessary that the mirror deflect elastically and return to its previous shape without residual deformation. The high stiffness-to-mass ratio of graphite epoxy structures appears ideal for this purpose.

The use of epoxy graphite material as a simple structural member (for the telescope) and for holding the optical elements in alignment appears to be readily implementable with current technology. The stability is well within the depth of field and allowable focus of the optical system and angular shift of the mirror mounts.

One of the very attractive features of the graphite epoxy material is the possiblity of molding it into shape.* If quantities of ladars are to be built, this will be reflected in production exonomies and the reproducibility between units. The freedom from toxicity and the ability to control the thermal expansion coefficient of the material during the fabrication process is also advantageous. The use of the material in the ladar in the 1980s would also benefit from the research currently in progress for its use in aircraft structures. The materials tecnnology of graphite epoxy, which is relatively new, is expected to be quite advanced by the 1980's. The material should be more highly developed for the rendezvous and docking ladar application.

8.2 Measurements Program

8.2.1 Detectors and Detection Technology

The saturation effects in mercury-cadmium-telluride detectors can be measured. Data on temperature, signal level, and the recovery period as well as operating conditions (i.e., back bias) can be very beneficial in the development of future rendezvous and docking ladars.

8.2.2 Homodyne Detection

The noise equivalent power of homodyne detection can be measured using existing UAC facilities. The data is vital since the midcourse guidance and docking of the Tug will be controlled through a homodyne detection process.

---

* "Advanced Composite Missile & Space Design Data," *Air Force Materials Laboratory Report* No. AFML-TR-73-33. Air Force Systems Command, Wright Patterson AFB, Ohio 45433

8.2.3 Corner-Cube Reflector Cross Section

The effective radar cross section of corner cube reflectors under a variety of conditions should be measured. The corner cube reflectors would be developed in accordance with the manufacturing technology referred to earlier. A solid metal corner cube reflector could also be constructed to serve as a reference. The reference corner cube could be investigated over a wide variety of angles, with respect to the effectiveness of coatings and surface finishes, and deliberately induced errors in its alignment.

The data would give some idea of what to expect when deploying such reflectors in space on cooperative targets in particular, since the corner cube reflectors could be in space for long periods of time.

8.2.4 Docking

A check of the effects in the near field of a corner cube reflector as it is being approached by the rendezvous ladar should be made. This can be done on the antenna range at Norden, or at a comparable range at UARL. Near field effects when viewing the proposed docking surface should also be checked to determine the equivalent amplitude of the return and any problems which might occur from the interaction of the complex scatterers.

A docking simulation could be investigated on the antenna range by mounting a simulated reflecting surface on a small vehicle and moving the vehicle towards a simulated front end of a ladar. The front end would consist of a transmitter and receiver plus measuring equipment that would indicate signal amplitude and doppler. A dynamic test such as this is very feasible, because there would be low ground clutter return from the 10.6 micron wavelength. It would also derive dynamically the effects to which the system would be subject.

9. PASSIVE ACQUISITION SYSTEMS

9.1 Introduction

Passive acquisition systems, particularly TV and FLIR (forward looking infrared), have been considered for detection and tracking of target satellites. Each approach, however, appears to have serious drawbacks which dictate the requirement for an active system.

The greatest difficulties with the passive system arise when:

a. distinguishing the desired target from spurious objects in the field of view,

b. acquiring targets at long ranges.

Spurious objects will be in the vicinity of the target satellite. When illuminated by the sun, the objects will provide their own signal to the detection mechanism. Therefore, a method must be provided to distinguish false signals from that of the target. The target must also be distinguished from stars, planets, etc, within the field of view. Spurious target rejection is readily accomplished via range discrimination in the active case.

9.2 Television (TV)

The concept of using a simple television camera for detection in the visible or near-visible spectral region will depend upon the target being illuminated by the sun.

9.2.1 Earth Shadow Considerations

For geosynchronous orbital distances (42,138 km from the center of the earth), the diameter of the earth's shadow is 12,354 km, as shown in the following calculations (see Figure 9-1).

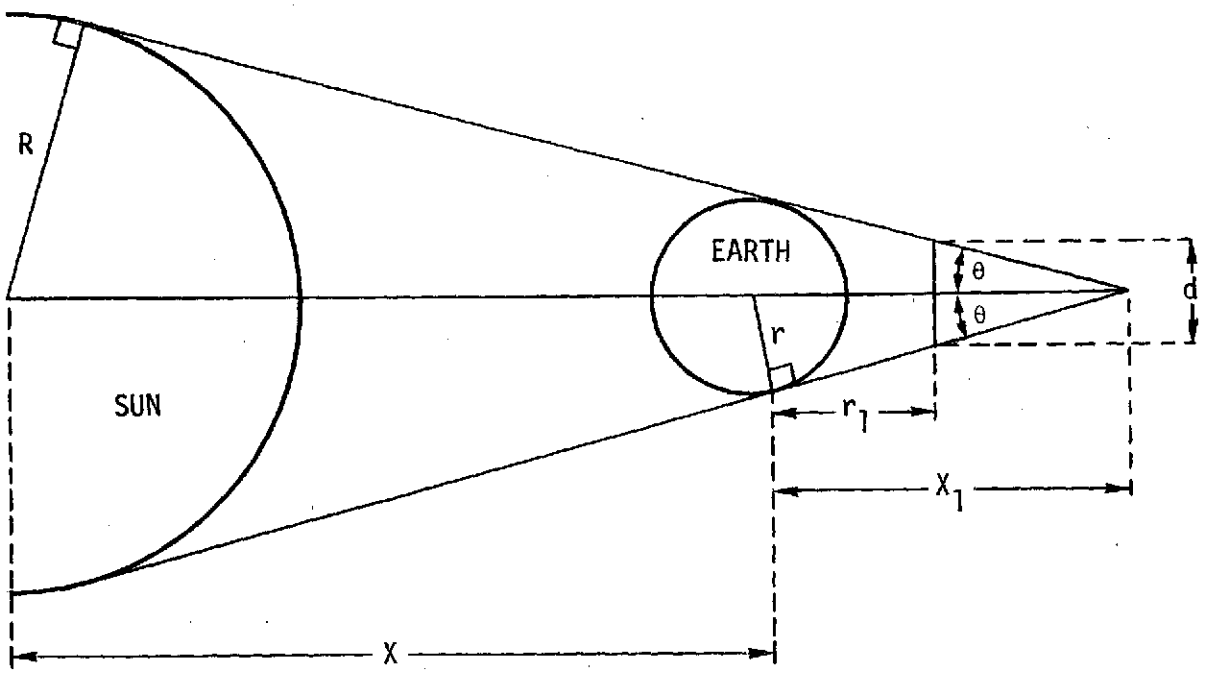

r = 6371 km

R = 6.96×10^5 km

X = 1.496×10^8 km

r_1 = 42138 km

Figure 9-1. Length of Earth's Shadow

$$x_1 = \frac{6371}{\sin \theta} \quad \text{and}$$

$$\sin \theta = \frac{6.96 \times 10^5}{1.496 \times 10^8 + x_1}$$

Solving these equations,

$x_1 = 1.382 \times 10^6$ km

and

$\theta = 0.00461$ rad

Since θ is so small, we can assume $\tan \theta \simeq \sin \theta$ and

$$\frac{x_1}{2r} \simeq \frac{x_1 - r_1}{d}$$

therefore,

$$d = \frac{2r(x_1 - r_1)}{x_1} = 1.235 \times 10^4 \text{ km}$$

The orbital arc through which a geosynchronous satellite travels while in the earth's shadow is 0.2943 radians, which is 4.7% of its orbit. As shown in Figure 9-2,

$$\frac{r+a}{\sin\beta} = \frac{x_1}{\sin\gamma} = \frac{x_1}{\sin(\pi-\alpha-\beta)}$$

$$\frac{r+a}{\sin\beta} = \frac{x_1}{\sin(\alpha+\beta)}$$

$$\beta \simeq \sin \beta = 0.00461 \text{ rad}$$

$$\sin(\alpha + 0.00461 \text{ rad}) = \frac{1.382 \times 10^6 \times 0.00461}{42138} = 0.1512$$

therefore

$$\alpha = \sin^{-1}(0.1512) - 0.00461 = 0.14717 \text{ rad}$$

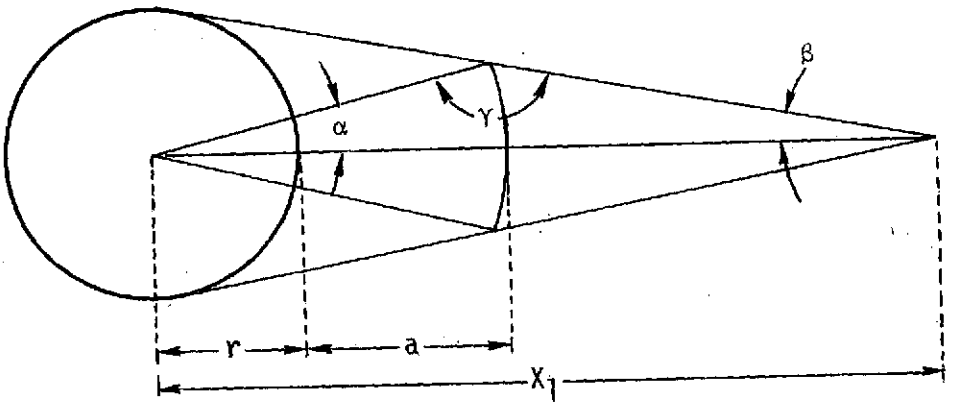

Figure 9-2. Length of Eclipsed Orbit

and

$$2\alpha = 0.2943 \text{ rad}$$

Since reflected sunlight is the only source of illumination, the system cannot be used during the time the target is in the earth's shadow. A full orbital period is 24 hours so the length of time is slightly more than 1.12 hours. Unless the non-functioning time can be accepted, a passive acquisition system based solely on television detection of reflected sunlight cannot be considered.

Because of the 23.45° inclination of the earth's equator to the plane of its orbit, the calculation of "dead time" is valid only at the vernal and autumnal equinox, when the polar axis of the earth is perpendicular to the line joining the centers of the earth and sun. At other times, the time spent by the satellite in the earth's shadow will be less than 1.12 hours per orbit; during periods centered about the summer and winter solstices, the entire orbit will be outside the shadow.

When the equator is tilted at the angle $\alpha = 8.43°$ to the axis of the shadow cone, the satellite orbit intersects the cone at only a single point. The satellite does not enter the cone again until α (again) becomes smaller than 8.43°. Since the time required for α to reach its maximum of 23.45° is 1/4 year (from equinox to solstice), the time required to travel from -8.43° to +8.43° twice a year is

$$t = 4\left(\frac{8.43}{23.45}\right)\frac{365.25}{4} = 133 \text{ days}$$

Thus, it may be tolerable to accept the loss of detection capability from the presence of the satellite in the earth's shadow, since this can happen only 133 days per year and most of the days correspond to shadowed periods less than an hour in duration.

9.2.2 Beacon Considerations

Some consideration might be given to requiring the satellite to have a beacon, which would allow the use of coded signals. This would provide a means of distinguishing the satellite from stars, planets, and space debris. It is clear, however, that the beacon would be required to radiate omnidirectionally, since no a priori information would be available to define the relative direction of approach. The power required to provide an acceptably strong

detected signal at any range would, therefore, be enormously greater than that required by an active system of similar wavelength, since the beam spread of the latter can be tightly controlled. The advantage gained by concentrating all radiated power in a narrow beam can be readily seen by comparing the detector irradiance at a given distance, r, from two transmitters. The first is an omnidirectional radiator of power P_1 and the second is a laser of 0.35 mrad beam divergence and transmitted power P_2. The former spreads its power over 4π steradians, and the illumination at a detector of unit area, a, is

$$E_1 = P_1 \frac{a}{4\pi r^2}$$

For the active system, however, the solid angle through which the power is transmitted is only $3.0625\pi \times 10^{-8}$ steradians, and

$$E_2 = P_2 \frac{a \times 10^8}{3.0625\pi r^2}$$

The ratio of the illumination from the two systems is, therefore,

$$\frac{E_1}{E_2} = \frac{P_1}{P_2} \left(\frac{a/4}{10^8 a/3.0625}\right) = \frac{3.0625}{4 \times 10^8} = 7.656 \times 10^{-9} \frac{P_1}{P_2}.$$

Thus, in order to yield the same illumination the "passive" approach would require 1.3×10^8 as much power. This is clearly unacceptable.

It must be assumed, therefore, that a passive TV system will rely solely on the reflection of sunlight from the target satellite, and that the non-functional period of up to 1.12 hours per day must be accepted.

9.2.3 Signal Strength Considerations

If the cooperative target would reflect the sun's radiation in the form of a plane wave, the energy received at the TV would be of optimum brightness, and the satellite would be easily detectable. This is impractical, since it would require plane

mirrors at over 184,000 locations on a spherical satellite, with the normal to each surface displaced 0.53° from its neighbors (0.53° is the angle subtended by the sun from the vicinity of earth's orbit). For a satellite of one meter radius, each mirror facet would have to have an equivalent cross sectional area of 68 mm^2, and it would be necessary to cover the entire satellite.

It is nearly impossible to satisfactorily align such a system. Furthermore, the deflection of so much solar energy could seriously impact the internal temperature control of the satellite and make the use of solar energy cells difficult or impossible, unless partial obscuration of the reflectors is tolerated. It is possible to use partially reflective or "cold mirror" coatings to allow a specified portion of the energy to pass through the mirror; however, the complexity of an already dubious design would increase.

Most probably, the reflectivity of the target satellite would simply be dictated by the requirements of good thermal design. A reasonable assumption might be that the satellite would be approximately spherical, with an average spectral reflectivity of 80% over the spectral range to which the TV is sensitive. In this case, the reflected light will appear to diverge from the focal surface of the sphere, and the irradiance at the detector will be subject to the inverse square law. Since the solar irradiation, E_s, in the vicinity of earth orbit is 135 mw/cm^2, the irradiance, E_o, at the detector location is less than 8 nanowatts/cm^2 for a satellite of one meter radius and 80% reflectivity at a distance of one nmi as the following calculation shows. (See figure 9-3).

$$\frac{0.8\ (0.135)}{E_o} = \frac{R^2}{r^2/4}$$

therefore

$$E_o = 0.108\ \frac{r^2}{4R^2}$$

when R = 1 nmi = 1852 m, and r = 1 m, $E_o = 7.87 \times 10^{-9}$ w/cm^2.

At 300 nmi, E is reduced to 8.75×10^{-14} w/cm^2 for the same system.

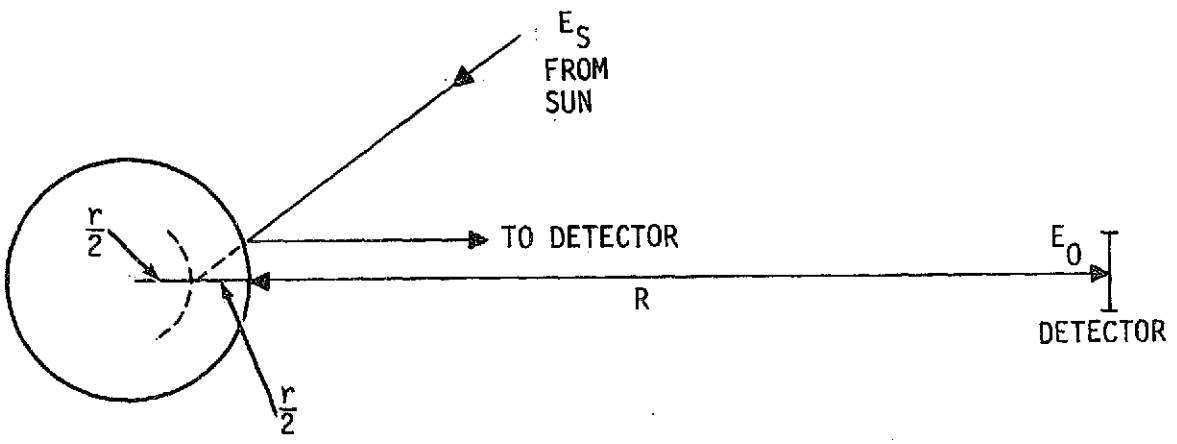

Figure 9-3. Reflected Illumination

For the rendezvous acquisition system, a field of view of 30° is required. Assuming a 1-inch vidicon, a lens of 67 mm focal length would be required. Thus, even with an advanced optical system, the entrance aperture could hardly be more than 70 mm in diameter, which corresponds to an area of 38.5 cm^2. If this system were assumed to be 80% efficient, then the power incident on a point image at the vidicon face for the previously described satellite, at 300 nmi, would be

$$E = 8.75 \times 10^{-14} \times 38.5 \times 0.8 = 2.7 \times 10^{-12} \text{ watts.}$$

In the absence of selective spectral reflection, the irradiance would be spectrally proportional to the radiance of the sun. By Planck's law, the radiant energy of a black body, $W(\lambda)$, at any wavelength, λ, (in microns) is related to the absolute temperature, T, (in degrees Kelvin) of the body by

$$W(\lambda) = \frac{37405}{\lambda^5} \left[\exp\left(\frac{14387.9}{\lambda T}\right)-1\right]^{-1},$$

and the total radiated power is equal to $5.6697 \times 10^{-12} T^4$ w/cm^2. The proportion of this energy within any wavelength interval $[\lambda_1 \lambda_2]$ is equal to

$$\frac{\int_{\lambda_1}^{\lambda_2} W(\lambda)\,d\lambda}{5.6697 \times 10^{-12}\ T^4}$$

Since the sun radiates as if it were a black body at 5776°K, the fraction of its output within the sensitive region of the camera tube (which may be assumed to between 0.3μ and 1.1μ for silicon-target vidicons), is calculated to be about 73.4%. Furthermore, the relative spectral response of the camera is such that the total response to radiation over the bandwidth is about 50% of what it would be if it were spectrally uniform.

The net result of the calculations is that the effective irradiance of the camera resolution element because of sunlight reflected by the satellite is

$$E_{eff} = 2.7 \times 10^{-12} \times 0.734 \times 0.5 = 9.91 \times 10^{-13} \text{ watts}$$

Since the response of a silicon-target vidicon is about 0.22 amperes/watt (averaged over the spectral region of 0.3μ-1.1μ) and careful preamplifier design can limit noise to about 5×10^{-9} amperes, a signal-to-noise ratio of 1 can be provided for power levels as low as 2.3×10^{-8} watts. Unfortunately, even this noisy signal is more than four orders of magnitude larger than the actual power incident upon the camera face. Silicon-intensifier target tubes can provide an additional two or three orders of magnitude in sensitivity. However, even this improvement is insufficient, since about 5 orders of magnitude would be required. Even then, the extremely optimistic assumptions made throughout the previous calculations make realization of a usable system problematical at best.

The difficulties are compounded when it is realized that the irradiance levels being considered are smaller than those from many stars. A star of zero visible magnitude, for example, corresponds to a visible irradiance (outside the atmosphere) of 3.1×10^{-13} w/cm^2 (or 1.19×10^{-11} watts for the 38.5 cm^2 lens). Sirius, which has a visible magnitude of -1.6, provides a visible irradiance of 1.35×10^{-12} w/cm^2, (which corresponds to 5.2×10^{-11} watts). Thus, the task of distinguishing the actual target from stars and other spurious targets becomes even more formidable, particularly since nearby debris may appear even brighter.

9.3 Forward Looking Infrared (FLIR)

In an attempt to avoid some of the problems associated with TV acquisition, the use of a long wavelength FLIR system was also considered. In this case, the significant assumption is that the target satellite is maintained in thermal equilibrium at a temperature of about 300°K and will appear as a black body radiating at the temperature. The target's appearance to a passive infrared sensor would be essentially constant whether is sunlight or shadow, since internal thermal management during the time in earth's shadow would provide the equivalent of solar heating and any required regulation.

9.3.1 Black Body Radiation

A perfect black body at 300°K emits infrared radiation according to Planck's law. At 9.66μ, the peak output, a perfect black body emits 3.13×10^{-3} watts per square centimeter. The total power emitted is 0.0459 w/cm^2, of which 46% or 0.02113 w/cm^2 is within the band between 4μ and 13μ.

9.3.2 Detector Considerations

Mercury-cadium-telluride detectors can be obtained which provide an average signal-to-noise ratio of unity throughout the band of 4-13μ for incident power levels as low as 3.5×10^{11}w. (Of course, signals several orders of magnitude weaker may be detected with heterodyne detection, but this would require an active system, rather than a passive FLIR.) In order to achieve this performance, however, the detector must be cooled to approximately 77°K. (When heterodyning, detectors can be used at temperatures up to 130°K, since quantum efficiency is then the critical parameter. For passive detection, however, considerably lower temperatures are required for adequate suppression of detector noise.) Such temperatures are presently beyond the capability of simple radiation coolers, and would require a considerably more complex and heavier cryogenic system.

Since less than 0.2% of the total power emitted by a black body at 300°K corresponds to wavelengths below 4μ, the detector is responsive (with S/N=1 and the peak response set at about 10μ) to 46% of the emitted power up to its cutoff wavelength of 13μ, for power levels of 3.5×10^{-11}w.

9.3.3 Signal Strength Considerations

The area of a spherical satellite of one meter radius is approximately 4π m^2. A perfect black body of that size would, therefore, emit 0.02113 w/cm^2 x 4π m^2 = 845π watts into 4π steradians. If an optical aperture 7 cm in diameter (as was considered for the TV system) were employed, the 38.5 cm^2 area would subtend a solid angle of 1.25×10^{-14} steradians at a distance of 300 nmi (555.6 km). Thus, the intercepted power, P, from the black body (a point source at that distance) would be

$$P = \frac{845}{4} (1.25 \times 10^{-14}) = 2.63 \times 10^{-12} \text{ watts}$$

Because of the requirements for thermal control, it is unlikely that the emissivity of the target spacecraft, can even approach unity, as for a black body. If a value of 0.5 is assumed for the emissivity, the power intercepted by the FLIR aperture will be just half that from the black body described above, or less than 1.32×10^{-12} watts. Since the detector would respond satisfactorily to only 46% of this power, the usable IR signal strength would be about 6.06×10^{-13} watts.

This would be only about 1/60 of the signal required for a signal-to-noise ratio of unity, therefore, the system could not perform satisfactorily over the required range. In fact, under the assumptions made for these calculations, the usable range of the system would be less than 40 nmi but still better than the range calculated for the TV system.

9.3.4 Spurious Signals

As with the TV system, the problem of distinguishing the actual target from spurious objects remains extremely difficult. Debris which reaches thermal equilibrium at or near 300°K could be mistaken for the target, if it were closer to the detector. For example, a 1/2 meter diameter sphere radiates 1/16 as much power as a two meter diameter sphere of similar emissivity and temperature. It will, therefore, provide the same irradiance if the range of the latter is four times that of the former.

On the other hand, certain types of debris (particularly dark bodies with high absorptance) may stabilize at temperatures even higher than 300°K. Such bodies could appear as bright or brighter than the target satellite, even at the same range, depending upon their relative sizes. Obviously, a passive FLIR system of relatively broad spectral range, such as the one described, would have no way of distinguishing the true target from the spurious targets, without range information. Two narrow-band detectors might be employed, in an attempt to isolate the 300°K target by comparing the relative power levels at two different wavelength regions, but this would require considerably more sensitivity.

False detection of stars may be even more troublesome than in the case of the TV system, because of the greater sensitivity of the FLIR system to this type of target. It must also be remembered that bright stars of low effective temperature (such as Arcturus, Betelgeuse, and Antares) will radiate a much higher percentage of their power in the infrared regions than will high temperature stars of bright visual magnitude. When adjusted for the spectral region of FLIR sensitivity, therefore, additional stars of bright stellar magnitude will be found to exist.

9.4 Range Error

A basic problem associated with any passive system is that of determining the range to the target. The only reliable method is triangulation; i.e., observing the target from two different positions separated by a known distance, d, and measuring the difference between viewing angles, θ. When

the range, R, to the target is large, it can be calculated from $R = d/\theta$. For accurate ranging, of course, the value of θ must be known very precisely. The range error corresponding to any error in θ is found by differentiating the above equation with respect to θ; i.e.,

$$\frac{dR}{d\theta} = -d/\theta^2$$

or, since $\theta = d/R$,

$$\frac{dR}{d\theta} = -R^2/d$$

When R = 300 nmi, a system which could measure θ to within an accuracy of one arcsecond (4.85×10^{-6} radians) would yield a range error equal to $\frac{1.5 \times 10^6}{d}$ meters. Thus, a baseline, (d), of nearly 27 meters would be required to hold the ranging error to ±30 nmi. In order to achieve the same ranging error with a one meter baseline, the required accuracy in measurement of the angle θ would be 0.18 microradian, or 1/27 of an arcsecond. This is practically impossible for such a system.

The tracker would, therefore, be required to change its position by a considerable baseline distance in order to allow $\frac{dR}{d\theta}$ to take on reasonable values. The very act of doing this, however, affects the attainable baseline accuracy and causes an uncertainty in the measured value of θ. Furthermore, in the time taken to move and realign the tracker (e.g., with a known star) the target changes its relative position, both in range and angle. Attempting to make accurate range measurements with this approach would be futile.

A similar approach would be to align the target with a known point on the celestial sphere (a known star or at a known angle to a star), and move the tracker at a known velocity perpendicular to the line joining it with the target. Since $d = \theta R$, then,

$$\frac{d(d)}{dt} = R\frac{d\theta}{dt} + \theta\frac{dR}{dt}$$

It must be assumed that $\frac{dR}{dt}$ is sufficiently small because of the perpendicular direction of $\frac{d}{dt}$ (d) and that no significant error is introduced by assuming

$$\frac{d}{dt}(d) = R\frac{d\theta}{dt}$$

It is then possible to measure $\frac{d\theta}{dt}$, and knowing $\frac{d}{dt}(d)$, to calculate R. Rewriting the equation, with $v = \frac{d}{dt}(d)$ and $\omega = \frac{d\theta}{dt}$

$$v = R\omega$$

This can be differentiated to show the range error associated with inaccuracies in the measurements of ω or v as follows:

$$\frac{dR}{d\omega} = -v/\omega^2 = -R/\omega = -\frac{R^2}{v}$$

$$\frac{dR}{dv} = \frac{1}{\omega} = \frac{R}{v}$$

It can be seen both v and ω must be measured rather precisely, and v should remain constant. Furthermore, ω should be known to be zero when v is zero. The time spent in making the measurements should be small, in order to be confident of the validity of the assumption that $\theta\frac{dR}{dt}$ is relatively small. Thus, the entire procedure is fraught with sources of inaccuracy and inefficiency in spacecraft maneuvering.

9.5 Conclusion

In conclusion, therefore, the passive acquisition systems considered are inferior to active systems on many counts; the most serious drawbacks being acquisition range, reliability of target detection, ranging ability, and basic feasibility.

APPENDIX A
DERIVATION OF THE RADAR EQUATION AS RELATED TO 10.6 MICRON LADAR

A.1 Signal-To-Noise

If a transmitter radiates isotropically a power P_T, then the power density at a distance R is equal to the transmitted power divided by the surface area $4\pi R^2$ of an imaginary sphere of radius R, or

$$\text{Power density} = \frac{P_T}{4\pi R^2}$$

If the transmitter, instead of radiating isotropically, radiates directively, then the power density at the distance R will be increased by the factor G_T, the transmit antenna gain. From antenna theory the gain is given by

$$G_T = \frac{4\pi A_T}{\lambda^2} \quad ,$$

where A_T is the effective antenna area. A target of cross-sectional area σ will intercept, and reradiate in the direction of the radar, the power given by

$$P_{\text{reradiated}} = \frac{P_T G_T}{4\pi R^2}$$

The power density at the receive antenna, assuming that the target reradiates isotropically, is then given by

$$P_{\text{density at receive antenna}} = \frac{P_{\text{reradiated}}}{4\pi R^2} = \frac{P_T G_T}{(4\pi R^2)^2}$$

The power intercepted by a receive antenna of effective aperture A_R is then

$$P_R = \frac{P_T G_T A_R \sigma}{(4\pi R^2)^2}$$

Defining a receive gain G_R, analogous to the transmit gain

$$G_R = \frac{4\pi A_R}{\lambda^2}$$

and expressing A_R in terms of G_R, the received power finally can be expressed as

$$P_R = \frac{P_T G_T G_F \lambda^2 \sigma}{(4\pi)^3 R^4 L} \quad ,$$

where the factor L has been added to account for the composite effects of a variety of system losses.

The signal-to-noise ratio, S/N, is the ratio of the received power, P_R, to the noise power P_n, an expression for which is given in 4.1.2.

The final form of the signal-to-noise ratio when expressed in decibels, is

$$S/N = 10 \log_{10} \left[\frac{P_T G_T G_R \lambda^2 \sigma}{(4\pi)^3 R^4 L \, P_n} \right]$$

A.2 Effective Aperture and Beamwidth

If the two previously mentioned expressions for the antenna gain G are equated,

$$G = \frac{4\pi}{\beta^2} = \frac{4\pi A}{\lambda^2} \quad ,$$

it is possible to express the beamwidth as

$$\beta = \frac{\lambda}{\sqrt{A}} \quad ,$$

where A is the effective antenna (or aperture) area.

When the aperture is uniformly illuminated (as is the case in receive), the effective area equals the actual area, and

$$\beta = \frac{1.06 \times 10^{-5}\text{m}}{\left(\frac{\pi(0.075\text{m})^2}{4}\right)^{1/2}} = 0.16 \text{ milliradian}$$

It is planned to transmit a "hollow" beam, where the energy is concentrated in an annulus, to match the useful area of the pointing mirror. This effect can be achieved by the use of two conical mirrors in the optical path (see Figure A-1).

To a first approximation, the distribution of energy will be uniform over the useful area of the pointing mirror. The resulting beamwidth will be less than 0.16 milliradian (the figure for a full aperture). By means of judicious defocusing, however, the transmit beamwidth will be increased to 0.33 milliradian.

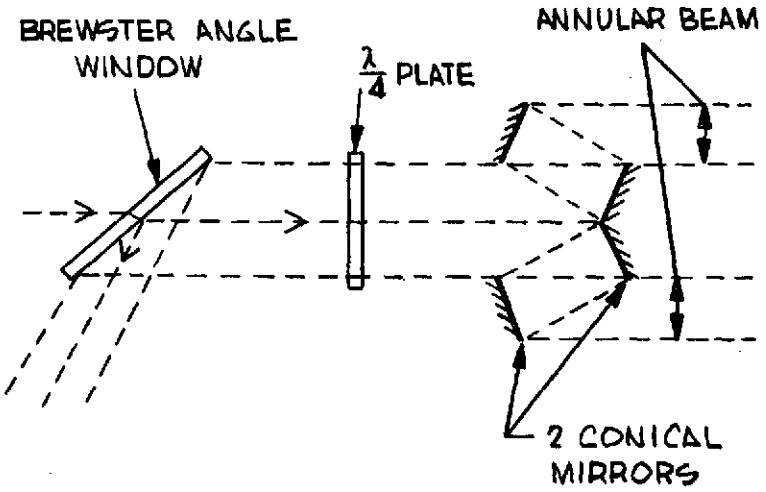

Figure A-1. Annular Beam Former

APPENDIX B
OPTICAL EFFICIENCY

Changes in the optical design since the quarterly report was issued have modified the overall efficiency of the optical train. The reflectances and transmittances of the various elements are tabulated below:

Transmit

Folding mirror	.99
Vertical scan mirror	.99
Brewster angle window (reflection)	.76
$\lambda/4$ plate	.96
Small mirror, with hole	.94
Secondary mirror	.99
Primary mirror	.99
Pointing mirror	.90*
Product	.593

Receive

Pointing mirror	.82
Primary mirror	.99
Secondary mirror	.99
Small mirror with hole	.94
$\lambda/4$ plate	.96
Brewster angle window (transmission)	.99
Range track mirror	.99
Mixing beamsplitter	.667
Product	.4741

Total two-way efficiency: 0.281 or -5.5 dB

Corresponding loss factor: $\frac{1}{0.281} = 3.56$

---

*Includes effect of hollow or annular beam.

APPENDIX C
SCANNING AND GEOMETRIC LOSSES

C.1 Scanning Loss

In the scan raster, the beams are arranged in a square lattice as shown in Figure C-1.

The target will, in general, not be located at the peak of a beam, and is assumed to be equally likely in any position in the raster. The effective power density can be obtained by averaging the power density over the cross-hatched area in the figure. Conservatively, the power outside a square of side $2\theta_0$ is neglected.

The power density g, assuming a Gaussian beam, is of the form

$$g(\theta) = e^{-\alpha\theta^2}$$

To average over the cross-hatched area, one may write,

$$\bar{g} = \frac{1}{\theta_0^2} \int_0^{\theta_0}\int_0^{\theta_0} g\ (x,y)\,dxdy$$

where

$$g(x,y) = e^{-\alpha(x^2 + y^2)}.$$

This integral is separable, and can be written

$$\bar{g} = \frac{1}{\theta_0^2} \left[\int_0^{\theta_0} e^{-\alpha x^2} dx\right]^2$$

If the variable of integration is changed to $X=\sqrt{\alpha x}$, then the integral becomes

$$\frac{1}{\sqrt{\alpha}} \int_0^{\sqrt{\theta_0}} e^{-X}\, dX = \frac{1}{2} \left(\frac{\pi}{\alpha}\right)^{\frac{1}{2}} \text{erf}\ (\sqrt{\alpha\theta_0})$$

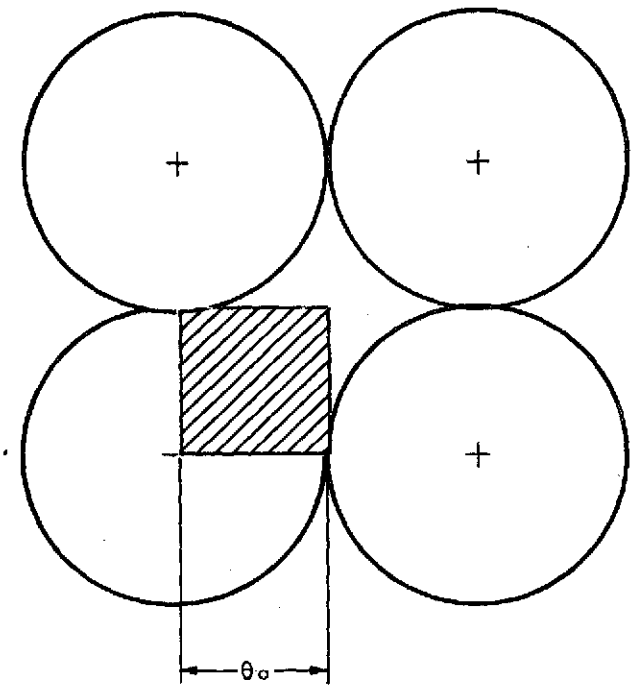

Figure C-1. Scanning Loss Geometry

The average power density is now expressed as

$$\bar{g} = \frac{\pi}{4\theta_o^2 \alpha} [\mathrm{erf}(\sqrt{\alpha}\theta_o)]^2$$

The value of the coefficient α can be obtained from the following considerations:

The beamwidth at the half-power density point is β and

$$g(\beta/2) = \frac{1}{2} = e^{-\alpha(\beta/2)^2}$$

Taking natural logarithms on both sides and solving for α yields

$$\alpha = \frac{4\ell n2}{\beta^2}$$

Substituing this expression in the expression for the average power density finally yields:

$$\bar{g} = \frac{\pi\beta^2}{16\ell n2\theta_o^2} [\mathrm{erf}(\frac{2\sqrt{\ell n2}\theta_o}{\beta})]^2$$

Evaluating for

$\beta = 3.33 \times 10^{-3}$ radian and

$\theta_o = 8.333 \times 10^{-4}$ radian

one obtains

$\bar{g} = 0.891$, and the corresponding loss factor is 1.15.

C.2 Geometric Loss of Detector Efficiency

The geometry of the 4-quadrant detector is shown in Figure C-2. By a straightforward numerical integration it is found that the power intercepted by a median strip of the detector, when exactly straddled by the spot, is approximately 10% of the total power in the spot. The worst case, namely that of a spot at the center of the detector, would correspond to a power loss of 20%. Since the spot is equally likely to fall anywhere within the detector, the losses are averaged by the following technique.

49 discrete positions are allowed for the spot, arranged in a uniform 7 by 7 square lattice to fill the detector area. The 49 positions are broken down as follows:

	Losses
12 positions straddling a strip (12 x 10%)	1.2
1 position in the center	.2
36 positions elsewhere	0
Total	1.4

The total loss, averaged over 49 spots, is 1.4/49 ≈ 0.03, correspond to a loss factor of 1.03.

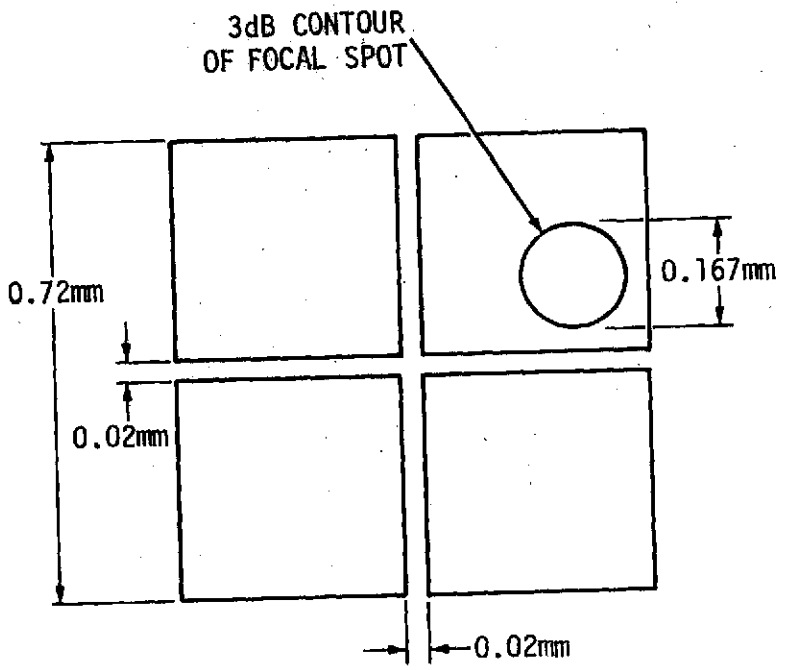

Figure C-2. Four-Quadrant Detector Geometry

APPENDIX D
DEPLOYMENT OF CORNER REFLECTORS ON THE TARGET VEHICLE

A deployment of fourteen corner cube reflectors is analyzed. The reflectors are located at the extremities of seven intersecting lines, which define optic axes. Figure D-1A shows one view of the configuration.

The axis of reflectors 1 and 2 is perpendicular to the plane of the page. Three planes, each perpendicular to the plane of the page, contain reflectors number 3, 4, 9, 10; 5, 6, 11, 12; and 7, 8, 13, 14, respectively. One of the three planes is illustrated in Figure D-1B.

There are experimental curves for corner cube reflector cross sections in directions forming various angles in two mutually perpendicular planes.* This information, reproduced in Figure 5-9 of this report, was used to average the cross section over a solid angle approximating a cone of a semiangle of 30°. This is somewhat conservative, since the configuration described is not isotropic and corresponds to a slightly smaller coverage per reflector.

The result of this computation indicates that the average cross section of a corner cube is 5.2 dB below the value calculated on the optic axis. The corresponding loss factor is 3.31.

---

*Robertson, Sloan D., "Targets for Microwave Radar Navigation," *Bell System, Technical Journal*, Vol. 26, pp. 852-869 Oct. 1947.

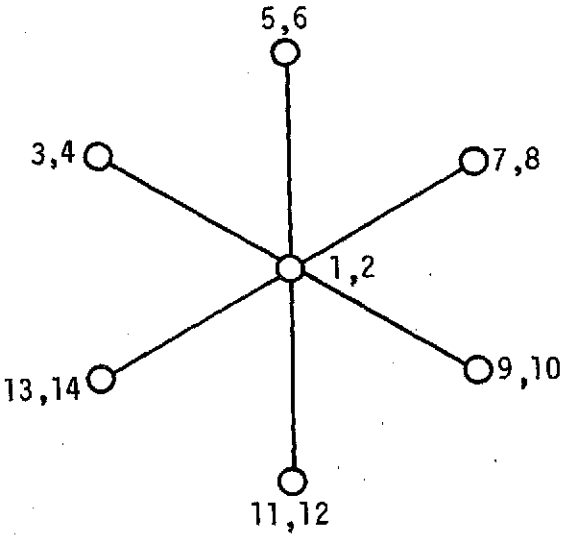

A) PLANE PROJECTION

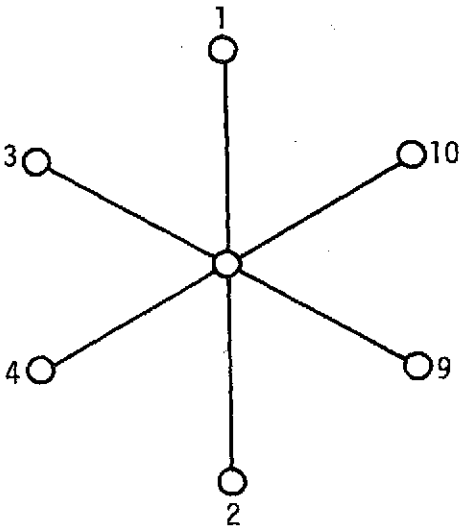

B) VIEW OF ONE PLANE

Figure D-1. Corner Cube Retroreflector Geometry

APPENDIX E
ANGLE SERVO DESIGN CONSIDERATIONS

E.1 The peak requirements on the angle servos occur during the search interval, when the mirrors are moved up and back in order to scan the required interval. The scan dynamics require maximum rates and accelerations, respectively, as follows:

$$\dot{\theta}_{max} = 1.4 \text{ rad/s}$$

$$\ddot{\theta}_{max} = 350 \text{ rad/s}^2$$

In order to avoid unnecessary gearing in space, it is preferred to use a direct-drive pancake torquer as the prime mover in each axis. These motors are readily available, and have been previously qualified and used in several spaceborne applications. The torque requirements are dictated by the maximum acceleration demand

$$T_{max} = \ddot{\theta}_{max} J$$

where J is the moment of inertia of the beam steering mirror, which is estimated at $8.5 \times 10^{-5} = 0.03$ ft/lb

therefore $T_{max} = 350 \times 8.5 \times 10^{-5} = 0.03$ ft/lb

$= 5.7$ oz/in

A 1.6-oz torque motor with these characteristics is readily available.

E.1.1 Angle & Range Tracking

In order to provide the necessary guidance signals for rendezvous, the target will have to be continuously tracked in angle and range. Monopulse angle error signals will be used to drive the pointing mirror servos with the direction of the target. Resolvers will then indicate the position of the target with respect to the vehicle. Range tracking will be accomplished by first varying the PRF to resolve the range ambiguities, and then tracking such that the position of the target is always known. During track, the relative motion of the target and the Tug would furnish an additional criterion for the identification of the correct target as compared to a false target.

E.2 Angle Track Loop

Elevation and azimuth angle error signals will be obtained by comparing the relative signal strength in each of the four quadrants of the detector array. A block diagram of the angle tracking loop is shown in Figure E-1. After the error signals are analyzed in the vehicle computer, commands will be fed to the drive servos of the pointing mirror to drive the echo return to the center of the detector array.

E.3 Range Tracking

Range tracking will be implemented by means of an early/late gate, which will be positioned about the target echo. In order to implement the early/late gate, it will be necessary to discontinue the random dither interpulse interval feature and change to a stabilized interpulse interval. The 30-microsecond interpulse interval is now adjusted over 20 to 33 microseconds in order to position the received signal between the transmitted pulses. The computer will adjust the interpulse interval in a programmed sequence in order to derive the unambiguous range. The target will then be tracked, and the range rate measured by determining the change of range over a period of time.

As the target is tracked in range, its apparent position will move through the interpulse interval towards a blind range. At this point will be necessary to readjust the interpulse interval in order to set the target echo between the blind periods defined by the transmitted pulse intervals. (Since the interpulse interval of 30 microseconds is equivalent to 4500 meters in range, a target with a 61-meter per second closing velocity would enter a blind range every 75 seconds.) Once target tracking is initiated, the computer will recognize the blind range condition and, within 1/10 of a second, reset the target echo within the interpulse interval to allow tracking to continue with minimum perturbation.

E.4 Loop Accuracies

As desired in the mission requirements, the rendezvous ladar should be capable of accurate range and angle measurements in order to give precision guidance to the target with a minimum expenditure of fuel and time. Angular measurements will be within $\pm$ 0.167 milliradian in elevation and azimuth corresponding to a distance error of 93 meters at 300 nautical miles. The one sigma range error, after measuring and integrating 100 pulses, is 0.42 meters at 300 nautical miles. (See Appendix F.) The range-rate accuracy will depend on the length of time during which the range can be measured and accurately tracked. Assuming a 10-second time base, the one sigma range-rate error would be 0.06 meters per second. (See Appendix F.)

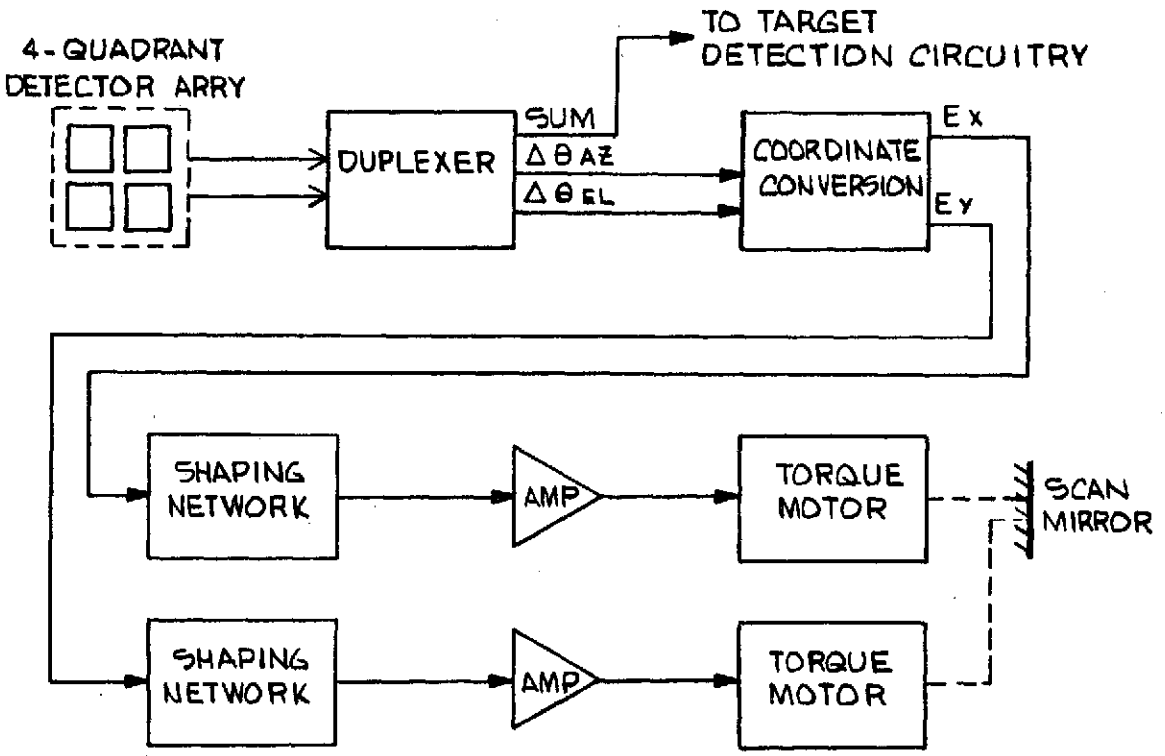

Figure E-1. Angle Tracking Loop Block Diagram

APPENDIX F
ERROR ANALYSIS FOR RANGE AND RANGE RATE

F.1 Error in m (defined in Section 5.3.7)

The error $| \tilde{m} - m |$,

where

$$\tilde{m} = \frac{2}{c} \frac{\beta-\alpha}{T_1-T_2},$$

must be small compared to unity so that the value of the integer m can be obtained without error.

The variance of the error is estimated from the expression

$$\text{Var } (m) = \left(\frac{\partial m}{\partial \alpha}\right)^2 \text{Var } (\alpha) + \left(\frac{\partial m}{\partial \beta}\right)^2 \text{Var } (\beta)$$

$$+ \left(\frac{\partial m}{\partial T_1}\right)^2 \text{Var } (T_1) + \left(\frac{\partial m}{\partial T_2}\right)^2 \text{Var } (T_2)$$

Since Var (α) = Var (β)

and Var (T_1) = Var (T_2), this reduces to

$$\text{Var } (m) = \frac{4}{c^2} \frac{2 \text{ Var } (\alpha)}{(T_1 - T_2)^2} + \frac{2 \text{ Var } (T_1) \cdot (\beta-\alpha)^2}{(T_1 - T_2)^4}$$

Var $(T_1) = 10^{-18}$ s^2, from the fact that 100 periods are measured to the nearest 10^{-9} s.

Var (α) is obtained from Barton's* equation

$$\sigma_t = \frac{\tau}{2.5\sqrt{2 \text{ S/N}}},$$

and the fact that

$$\sigma_\alpha = \frac{c}{2} \sigma_t$$

Substituting for S/N the value 12.5, corresponding to 11 dB, and for τ, the value 0.35 μs, yields a value of σ_α = 4.2m on a single pulse basis. Integrating over 100 pulses reduces this value to T_α = 0.42 m. This yields Var $(\alpha) = (0.42)^2 = 0.18$ m^2.

Barton, David K., *Radar System Analysis*, Prentice-Hall, p.364, 1965

T_1 is taken as 30 μs

β = 3750 m

α = 750 m

$T_1 - T_2$ = 0.18 μs

The value obtained for the variance of m is 2×10^{-12}, and $\sigma_m = 1.4 \times 10^{-6}$, which is negligible.

F.2 The variance of the range measurement is given by

$$\text{Var}(R) = \text{Var}\left(\frac{mcT_1}{2} + \alpha\right)$$

$$= \left(\frac{mc}{2}\right)^2 \text{Var}(T_1) + \text{Var}(\alpha)$$

The first term turns out to be negligible and the result is

$$\sigma_R = \sigma_\alpha = 0.42 \text{ m.}$$

In addition there will be a range bias due to system delays and to range rate. The bias is small and is canceled in computation of range rate from differences of consecutive range measurements.

F.3 Measurement of Range Rate

Over a 10-second interval, the measurement of range rate obtained from the difference of two separate range measurements has an error of

$$\sigma_{\dot{R}} = \sigma\left(\frac{R_2 - R_1}{\Delta t}\right) = \frac{\sqrt{2}\sigma_R}{10}$$

$$= 0.14 \times 0.42 \simeq 0.06 \text{ m/s.}$$